CEOG COMBUSTION ENGINEERING OWNERS GROUP

CEN-604
Revision 01

EVALUATION OF LOW UPPER SHELF ENERGY

FOR

COMBUSTION ENGINEERING
NUCLEAR STEAM SUPPLY SYSTEMS
REACTOR PRESSURE VESSELS

Final Report

prepared for the

C-E OWNERS GROUP

September 1993

ABB Combustion Engineering Nuclear Power

LEGAL NOTICE

This report was prepared as an account of work sponsored by the Combustion Engineering Owners Group and ABB Combustion Engineering. Neither Combustion Engineering, Inc. nor any person acting on its behalf:

A. makes any warranty or representation, express or implied including the warranties of fitness for a particular purpose or merchantability, with respect to the accuracy, completeness, or usefulness of the information contained in this report, or that the use of any information, apparatus, method, or process disclosed in this report may not infringe privately owned rights; or

B. assumes any liabilities with respect to the use of, or for damages resulting from the use of, any information, apparatus, method or process disclosed in this report.

Combustion Engineering, Inc.

Table of Contents

NOMENCLATURE

a	=	flaw depth which includes ductile flaw growth (in.)
a_e	=	effective flaw depth which includes ductile flaw growth and a plastic-zone correction (in.)
C_p	=	Specific Heat (Btu/lb-°F)
C_1, C_2, C_3, C_4	=	material constants used to describe the power-law fit to the J-integral resistance curve for the material
(CR)	=	cooldown rate (°F/hour)
E	=	Young's modulus (ksi)
E'	=	$E/(1-\nu^2)$ (ksi)
F_1, F_2, F_3	=	geometry factors used to calculate the stress intensity factor (dimensionless)
h	=	Convective film coefficient (Btu/sec-in^2-°F)
J	=	J-integral due to the applied loads (in.-lb./in.^{2})
J_{Ic}	=	J-integral fracture resistance for the material at onset of crack initiation (in.-lb/in.^{2})
J_D	=	J-integral fracture resistance for the material (in.-lb/in.^{2})

k	=	Thermal Conductivity (Btu/sec-in-°F)
K_I	=	mode I stress intensity factor (ksi $\sqrt{\text{in.}}$)
K_{Ip}	=	mode I stress intensity factor due to internal pressure, calculated with no plastic-zone correction (ksi $\sqrt{\text{in.}}$)
K'_{Ip}	=	K_{Ip} including plastic-zone correction (ksi $\sqrt{\text{in.}}$)
K_{It}	=	mode I stress intensity factor due to a radial thermal gradient through the vessel wall, calculated with no plastic-zone correction (ksi $\sqrt{\text{in.}}$)
K'_{It}	=	K_{It} including plastic-zone correction (ksi $\sqrt{\text{in.}}$)
M_m	=	correction factor for membrane stress
P	=	internal pressure (ksi)
Q	=	flaw shape correction factor
q	=	heat flux (Btu/sec-in^2)
r	=	radial distance through wall (in)
R_i	=	inner radius of the vessel (in.)
(SF)	=	safety factor (dimensionless)
t_i	=	time (sec)

t	=	vessel wall thickness (in.)
T_c	=	Coolant Temperature (°F)
T_s	=	Vessel Surface Temperature (°F)
$T(r,t)$	=	Temperature in the vessel wall (°F)
υ	=	Poisson's ratio (dimensionless)
σ_y	=	yield strength for the material (ksi)
ρ	=	Mass Density (lb/in^3)

1.0 EXECUTIVE SUMMARY

This report has been prepared for the Combustion Engineering Owners Group (CEOG) as part of an industry effort to address the NRC request for a generic bounding analyses which demonstrates equivalent margins of safety for low Charpy upper-shelf energy material. This report provides the description of both Phase 1 and Phase 2 activities, and the overall results.

Currently, 10 CFR 50 Appendix G requires that the minimum end-of-life upper-shelf energy be at least 50 ft-lb. Materials used in the fabrication of reactor vessels for Combustion Engineering (CE) Nuclear Steam Supply Systems (NSSS) are not expected to drop below the 50 ft-lb. requirement. However, strict application of the methods in Regulatory Guide 1.99 Revision 2 yield a bounding value of 48.5 ft-lb for SA 302 Grade B Modified plate material.

To demonstrate equivalent margins of safety, the methods and criteria provided by ASME Code, currently Code Case N-512, have been employed. The key analysis input parameters were identified as transient loading conditions, reactor vessel geometry and irradiated vessel material properties.

Transient loading conditions were identified for Level A/B and Level C/D events. These were selected based upon expert judgement and consideration for Technical Specification requirements, ASME Code requirements and Final Safety Analysis Report accident analysis chapter. The bounding Level A/B transient analyzed was a 100°F/hr cooldown with a pressure corresponding to 110 percent of design pressure. The bounding Level C/D transient analyzed was a steam line break. These transients were restricted to temperatures which remain on the upper-shelf.

The material properties, specifically the J-integral fracture resistance (J_d) of SA 302 Grade B Modified plate, were estimated using the methods described in NUREG/CR-5729. An upper-shelf energy value of 45 ft-lb was considered adequate to encompass the 48.5 ft-lb minimum predicted upper-shelf energy. A Charpy upper-shelf energy of approximately 38 ft-lb was identified to be limiting for an axially oriented flaw which conservatively bounds the projected limiting CEOG material.

The analysis methods and criteria employed for Level A/B and Level C/D evaluation were consistent with the recommendations provided by the recently approved ASME Code Case N-512. The ASME Code Case methodology was employed directly to calculate the applied J-integral due to Level A/B loadings. The method used to calculate the applied J-integral for the Level C/D transients was based on Linear Elastic Fracture Mechanics with a plastic correction using NUREG/CR-0744 and accounted for all realistic loads.

The result of the analysis were judged against the recommended ASME Code Case criteria. The criteria was satisfied in all instances, therefore equivalent margins of safety to ASME Code Section III Appendix G have been shown for CEOG reactor vessels.

2.0 INTRODUCTION

Currently, 10 CFR 50 Appendix G, Fracture Toughness Requirements (Ref. 1), has explicit requirements regarding reactor vessel beltline material upper-shelf energy. As stated by the requirements, "reactor vessel beltline materials must have Charpy upper-shelf energy of no less than 75 ft-lb initially and must maintain upper-shelf energy throughout the life of the vessel of no less than 50 ft-lb, unless it is demonstrated in a manner approved by the Director, Office of Nuclear Reactor Regulation, that lower values of upper-shelf energy will provide margins of safety against fracture equivalent to those required by Appendix G of the ASME Code".

10 CFR 50 Appendix G was first published in the Federal Register in July 1973 (Ref. 2). At that time, the minimum initial upper-shelf energy required was 75 ft-lb. Although the minimum end-of-life upper-shelf energy was not explicitly defined, the minimum was implicit in the method used to establish the adjusted reference temperature (ART). The shift in RT_{NDT} used to establish the ART was required to be measured at the 50 ft-lb level or 35 mils lateral expansion, whichever resulted in a greater shift. In May 1983, Appendix G to 10 CFR 50 was revised and published in the Federal Register (Ref. 3). The requirement for vessel beltline materials maintaining a minimum upper-shelf energy of 50 ft-lb was explicitly stated. Furthermore, the criteria for establishing the ART was modified to establish the shift at a 30 ft-lb energy level "to make the definition (of adjusted reference temperature) applicable to test data over a broader range of severity of radiation damage" (Ref. 4). This modification was introduced into ASTM E-185-79 (Ref. 5) to reflect the fact that shifts measured at the 50 ft-lb level for low upper shelf materials may be greatly exaggerated compared to those at the 30 ft-lb level.

To date, ASME Code provides no guidance or requirement regarding the minimum upper-shelf energy. ASME Code does provide for a minimum of 50 ft-lb Charpy impact energy, inherent in determination of the reference nil ductility temperature

(RT_{NDT}). Prior to 1972 Summer Addenda to Section III of ASME Code, an initial Charpy energy of 30 ft-lb was the requirement when establishing the NDT.

Historically, low-upper-shelf energy (LUSE) materials have been identified and predominantly limited to light water reactor vessel welds fabricated with Linde 80 flux. Concern has also been expressed regarding A302-B plate material based on testing performed by Oak Ridge National Laboratories. The reactor vessels fabricated by Combustion Engineering did not use Linde 80 flux in the fabrication process. In addition, Combustion Engineering (CE) Nuclear Steam Supply System (NSSS) reactor pressure vessels were not fabricated with A302-B plate. One CE NSSS reactor vessel was fabricated with A302-B Modified plate which is very similar to the SA533B Class 1 plate used in the other CE NSSS vessels.

Recently, the NRC staff has stated concern regarding licensee compliance with the required end-of-life upper-shelf energy of 50 ft-lb (Ref. 6). Following preliminary review of Generic Letter 92-01 licensee responses, the NRC staff determined that more information is needed for a large percentage of nuclear power plants to confirm that they meet the minimum upper-shelf energy requirement. During a September 2, 1992 meeting between NRC and industry, Dr. Thomas Murley, Director, Office of Nuclear Reactor Regulation, requested that the industry take a proactive step to address this issue. The approach recommended by Dr. Murley to resolve the issue of upper-shelf energy compliance was to perform generic bounding analyses which demonstrate equivalent margin of safety against fracture using the guidance provided by ASME Code, Section XI, Code Case N-512 (Ref. 7).

Consequently, the industry owner groups, in coordination with NUMARC, agreed to perform generic bounding analyses which would support the NRC staff in dispositioning questions regarding the safety significance of the upper shelf energy issue.

3.0 APPROACH

Appendix G to 10 CFR 50 mandates that equivalent margins of safety against fracture be demonstrated to those of Appendix G of ASME Code for reactor vessel beltline materials which fall below 50 ft-lb Charpy upper-shelf energy. This is to be performed in a manner approved by the Director, Office of NRR. While there is currently no published NRC guidance describing acceptable methods, the ASME Code, Section XI has recently approved Code Case N-512 (Ref. 7) which specifies evaluation methods and acceptance criteria to assess low upper-shelf material. The basis document supporting the Code Case is provided by Reference 8. This Code Case is expected to become a non-mandatory appendix to ASME Code Section XI and modifications to Section XI IWB-3700 have been drafted. Consequently, the methods and criteria of the ASME Code Case N-512 were chosen as an appropriate method supportive of the request of Dr. Murley, Director, Office of NRR. In addition, to facilitate expedient NRC closure of this issue, performance and documentation of a generic bounding analysis was requested by the CEOG by November 2, 1992.

A two phased approach was developed in order to adequately address the technical issue, while meeting the November 2, 1992 objective. The objective of the Phase 1 effort, the subject of this report, was to maximize engineering judgement and minimize engineering man-hours in performing a bounding analysis for a generic CEOG NSSS reactor pressure vessel. The Phase 2 effort, now completed and incorporated within, was to substantiate the validity of the engineering judgements made during the Phase 1 effort.

The Phase 1 effort identified the key analysis input parameters, such as transient loading conditions, reactor vessel geometry and irradiated reactor vessel material properties. To remove redundancy in the evaluation process, bounding transients were selected for Level A, B, C and D transients based on expert judgement using existing transient data to provide the greatest loadings at temperatures corresponding

to the upper-shelf region. A single generic reactor vessel geometry representative of CEOG NSSSs was chosen to be used in the evaluation. A limiting CEOG upper-shelf energy material was identified through direct application of the Regulatory Guide 1.99 (Ref. 9) prediction methods. Material property information (J-R curve data, yield strength, etc.) was developed from publicly available literature and selected to be representative and bounding.

The Phase 2 effort reviewed the selection of the analyzed transients and the limiting CEOG reactor pressure vessel beltline material. A compilation of published data from reactor vessel surveillance capsules specific to CE fabricated vessel materials was performed to provide credibility to the predicted limiting value of upper-shelf energy. The original methodology was improved to reduce conservatisms. Highlights include the use of longitudinal and transverse properties with the applicable flaw orientation, justification of improved J_d properties, and temperature effects for Level C/D analysis. In addition to the re-analysis of the reactor vessel geometry chosen in Phase 1, the smallest and largest CEOG reactor vessels were analyzed.

As noted previously, the evaluation procedure and acceptability criteria employed was based on the ASME Section XI Code Case N-512 (Ref. 7).

4.0 TRANSIENT SELECTION

Bounding pressure and temperature transients were selected for use in the fracture mechanics analysis. These were defined such that they would envelope the pressure and temperature responses of the Anticipated Operational Occurrences (AOOs) and Postulated Accidents (PAs) presented in the Final Safety Analysis Report (FSAR) accident analysis chapter (typically Chapter 14 or 15). As previously noted, existing transient data was utilized and selection was based on expert judgement to provide the greatest loadings at temperatures in the upper-shelf region.

Service Levels A and B

Two service level A/B transients, an RCS heatup and an RCS cooldown transient, were selected for consideration in this evaluation. These transients were defined such that their pressure and temperature responses would bound the pressure and temperature response of the AOOs presented in the FSAR accident analysis chapter. The selection of these transients provide both maximum thermal and pressure stresses in the region of interest.

The heatup transient is assumed to start at the minimum bolt-up temperature (70°F) and the corresponding maximum pressure (600 psia). The plant is assumed to heat up at a rate of 75°F/hr to a temperature of 200°F and a pressure of 2575 psia. The plant is then assumed to heat up at a rate of 100°F/hr to a temperature of 565°F at a constant pressure of 2575 psia. The maximum temperature, 565°F, is the highest cold leg temperature for any C-E plant. The pressure corresponding to 2575 psia was based on a primary safety valve set pressure of 2500 psia and a set pressure tolerance of 3% (which is typical of CE NSSS). Table 4.1 shows the pressures and temperatures associated with the enveloping RCS heatup event.

The cool down transient is assumed to start at a temperature of 565°F and a pressure of 2575 psia. The basis for the pressure of 2575 psia is the same as identified previously for the heatup transient. The plant is assumed to cool down at a rate of 100°F/hr to a temperature of 300°F with pressure held constant at 2575 psia. Table 4.2 shows the pressures and temperatures associated with the enveloping RCS cooldown event.

The Level A and B transients are depicted in Figure 4.1.

Service Levels C and D

Two service level C/D transients, an RCS heatup and pressurization and an RCS cooldown and depressurization transient, were considered for this evaluation. These transients were defined such their pressure and temperature responses would bound the pressure and temperature response of the PAs presented in the FSAR accident analysis chapter.

The most severe Level C/D heatup and pressurization transient is the Feedwater Line Break (FLB) accident. The pressure and temperature response for this transient can vary substantially depending on the analysis inputs and the plant analyzed. For this task, a set of pressures and temperatures were defined which would envelope all C-E reactors and reasonable analysis inputs.

Early C-E designed reactors operate at primary temperatures that are lower than later designs. An initial core inlet temperature 530°F was assumed because this value is typical of the zero power core inlet temperature of early C-E reactors. The coolant entering the reactor vessel is then assumed to heatup to 632°F. This is the maximum coolant temperature that occurs during the FLB simulation initiated from full power for the System 80+ design (which operates at high primary coolant temperatures) described in CESSAR DC. This heatup takes 40 seconds, which is typical for a large

FLB. In a typical FLB simulation, the inlet temperature remains at the peak for only a few seconds and then decreases rapidly. For this analysis, the core inlet temperature is assumed to remain at its peak for 40 seconds before it begins to decrease.

The peak RCS pressure during a typical FLB is no greater than 2750 psia and lasts only about 1 sec. This peak coincides with the primary coolant temperature peak. For this analysis the peak RCS pressure is assumed to peak at 2750 psia at 40 seconds and remain at this level for 1 minute. Table 4.3 shows the enveloping pressure and temperature histories associated with the FLB event.

The Steam Line Break (SLB) is the most severe Class C/D RCS cooldown and depressurization transient. Like the FLB, the pressure and temperature response can vary depending with the plant and the analysis inputs. To envelope these responses, the temperature response from a large zero power SLB (which maximizes the cool down rate and results in a lower coolant temperature) is taken together with the pressure response from a small full power SLB (which results in a relatively slow depressurization of the RCS). This is presented in Table 4.4.

The Level C and D transients are depicted in Figure 4.2.

TABLE 4.1

RCS HEATUP PRESSURE AND TEMPERATURE TRANSIENT DATA

Time (hour)	Pressure (psia)	Temperature (°F)
0	600	70
1.73	2575	200
5.38	2575	565

The pressure and temperature are assumed to vary linearly between values specified at times given above.

TABLE 4.2

RCS COOLDOWN PRESSURE AND TEMPERATURE TRANSIENT DATA

Time (hour)	Pressure (psia)	Temperature (°F)
0	2575	565
2.65	2575	300

The pressure and temperature are assumed to vary linearly between values specified at times given above.

TABLE 4.3

FEEDWATER LINE BREAK PRESSURE AND TEMPERATURE TRANSIENT DATA

Time (sec)	Pressure (psia)	Temperature (°F)
0	2100	530
40	2750	632
75	2750	632
100	2750	612
101	2075	612
600	2075	608

The pressure and temperature are assumed to vary linearly between values specified at times given above.

TABLE 4.4

STEAM LINE BREAK PRESSURE AND TEMPERATURE TRANSIENT DATA

Time (sec)	Pressure (psia)	Temperature (°F)
0	2250	550
10	2100	520
70	2100	465
200	950	400
400	800	325
600	800	325

The pressure and temperature are assumed to vary linearly between values specified at times given above.

Figure 4.1
Level A/B Transients

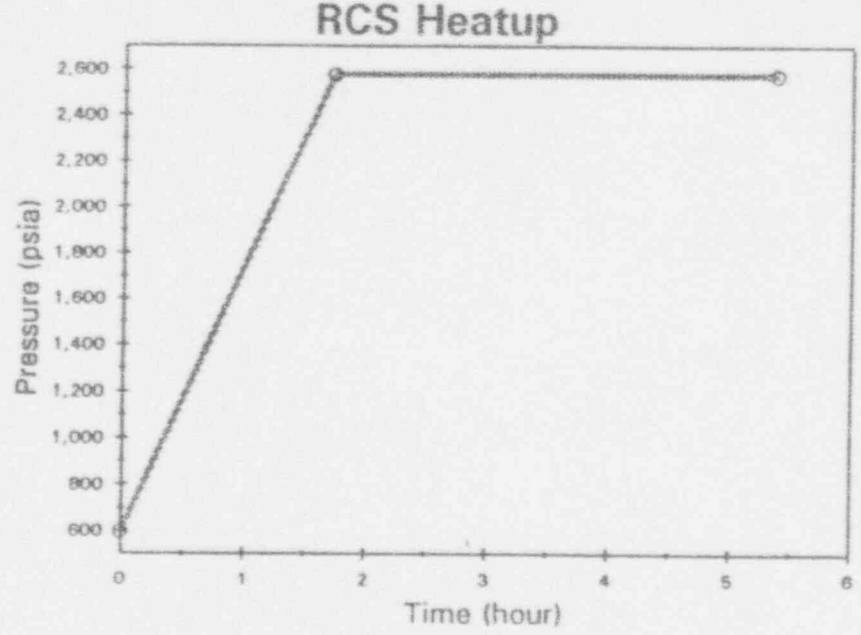

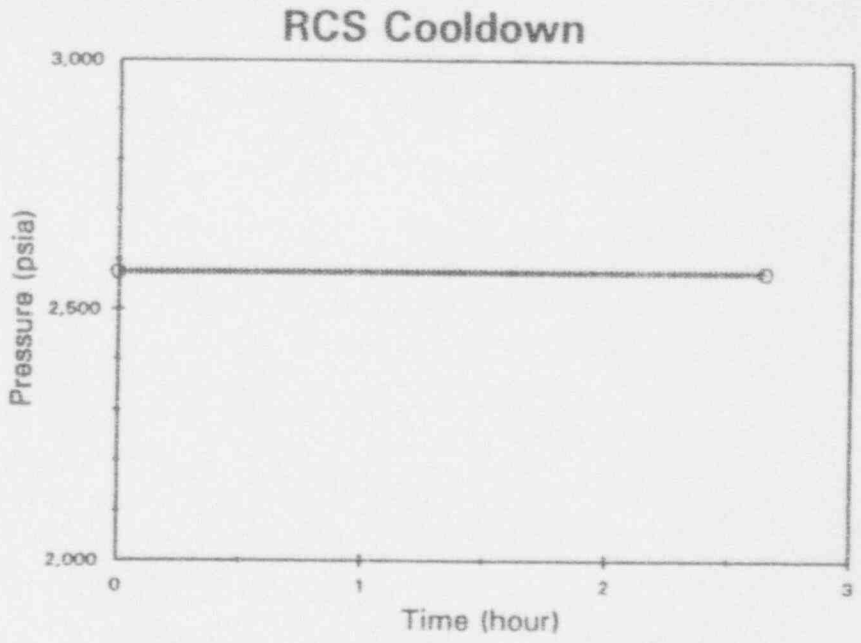

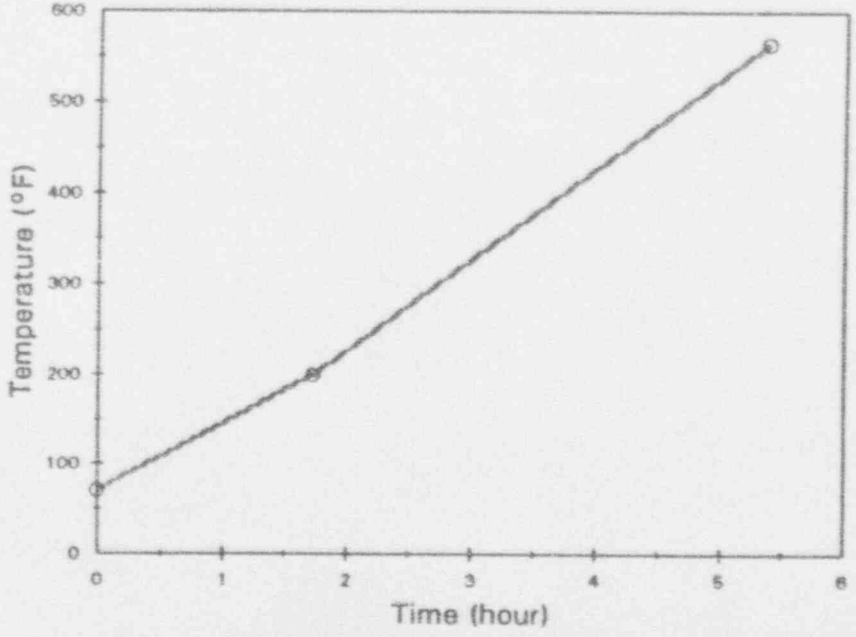

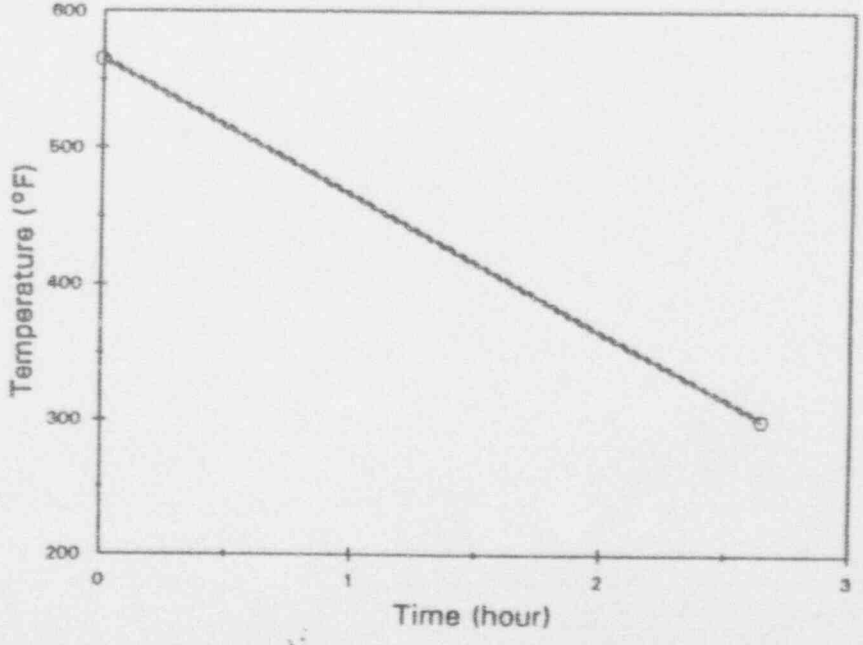

Figure 4.2
Level C/D Transients

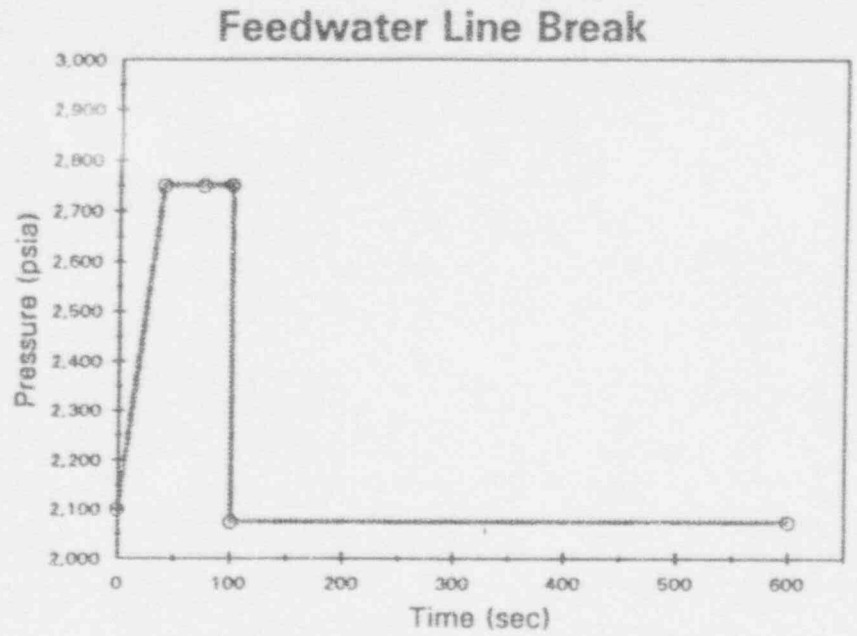

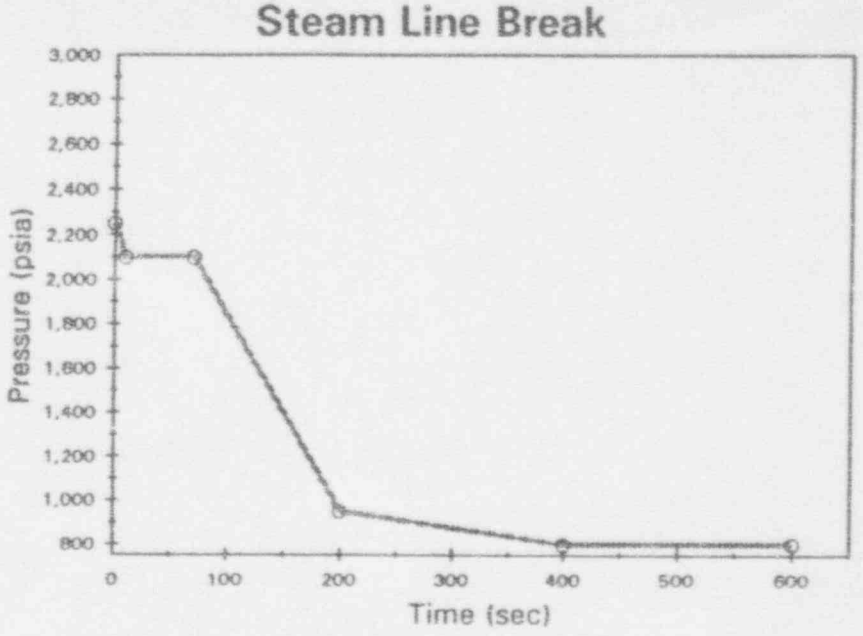

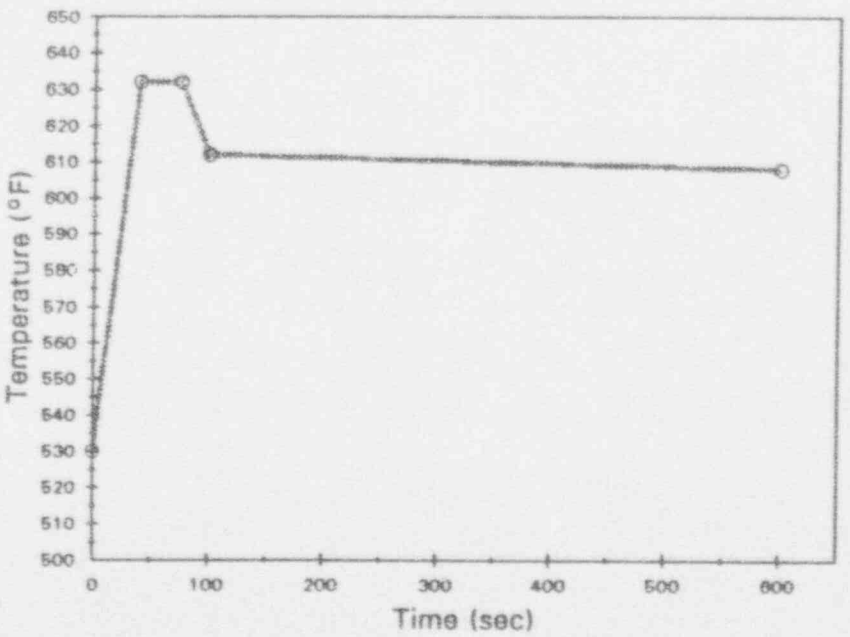

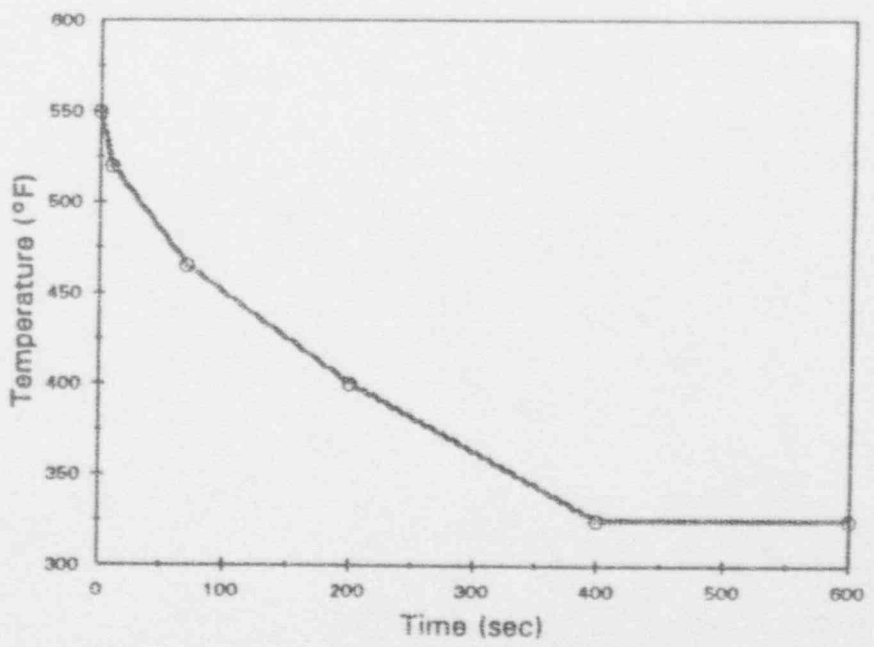

5.0 REACTOR VESSEL MATERIAL PROPERTIES AND GEOMETRY

Material Selection

The analysis performed to evaluate the materials with low Charpy upper shelf energy described in subsequent sections has been performed for the limiting CEOG material and corresponding neutron fluence. The LUSE analysis utilizes specific input data with respect to the limiting material in order to evaluate the J-R properties and assess the acceptability of this material. The purpose of this section is to describe the basis for selecting the material and conditions which are expected to be most limiting with respect to upper shelf energy for CEOG reactor vessels and to describe data which supports the general conclusion that the reactor vessel beltline materials for CEOG vessels are unlikely to fall below the 50 ft-lb screening criterion of 10 CFR 50, Appendix G.

1. Summary of Generic Letter 92-01 Responses - A review was performed of the responses to Generic Letter 92-01 prepared by CEOG member utilities with respect to the Charpy upper shelf energy screening criterion. For the majority of the vessels, values of initial upper shelf energy (USE) for beltline plates (transverse orientation) and welds were available, and projections to end-of-life (EOL) at the one-quarter thickness location yielded USE values well in excess of 50 ft-lb. In other cases where longitudinal orientation plate USE values were converted using Branch Technical Position MTEB 5-2 (Ref. 10), EOL projections using Position 1.2 of Regulatory Guide 1.99 also exceeded 50 ft-lbs.

   In one case involving converted longitudinal plate data and irradiated surveillance plate data, a predicted EOL USE value of 46.8 ft-lb was obtained following Regulatory Position 2.2. (Note: This appears to be an artifact of the Position 2.2 methodology combined with conservatism of the MTEB 5-2

conversion factor. The utility has recently performed tests to measure actual unirradiated transverse orientation USE and will use the data to reassess their EOL USE prediction.) In other cases, some beltline welds were lacking initial USE measurements and relied on the use of generic data; this aspect is further discussed in paragraph 3 of this section.

In general, the CEOG member utility responses concluded that the vessel beltline materials would most likely not fall below the 50 ft-lb screening criterion before EOL. These conclusions were based upon evaluations using the prediction methods of Regulatory Guide 1.99, Revision 2, and post-irradiation test results from individual vessel surveillance programs. In the unlikely event that a CEOG vessel beltline material might fall below the USE criterion, the following review of C-E fabricated vessel welds and plates was performed to determine what material (plate or weld) and their respective values of USE (based on predictions) should constitute the basis for an evaluation.

2. Beltline Plates - CEOG vessel beltline plates were purchased to the requirements of SA 533B Class 1 and A302-Modified specifications. The initial upper shelf energy for CEOG vessel plates in the transverse orientation has been measured for the newer vessels and for plates selected for the RPV surveillance program. The USE of none of those materials is predicted to decrease to a value near the 50 ft-lb screening criteria, and the post-irradiation surveillance measurements consistently exhibited well in excess of the required 50 ft-lb. In cases where transverse orientation Charpy tests were not performed, the USE was estimated based on longitudinal orientation tests using Branch Technical Position MTEB 5-2. Regulatory Guide 1.99 projections based on vessel-specific values of plate copper content, estimated transverse orientation initial upper shelf energy, and EOL neutron fluence yielded values as low as 48.5 ft-lb. Even though it is unlikely based on actual measurements,

it is possible to predict less than 50 ft-lb at EOL based on the methods prescribed by the NRC.

Tables 5.1 and 5.2 provide a list of reactor vessel surveillance program plate USE data extracted from ORNL PR-EDB (Ref. 11) for C-E fabricated vessels (Westinghouse and C-E NSSS designs). Data included both transverse (TL) and longitudinal (LT) Charpy orientation test results for the surveillance plate(s). The measured upper shelf energy decrease after irradiation is provided as well as the predicted decrease based upon Position 1.2 of Regulatory Guide 1.99, Revision 02. The predicted and measured decrease in USE, calculated as the percent change from the initial unirradiated USE, are compared in Figures 5.1 and 5.2 for transverse and longitudinal orientations, respectively. The majority of the measured USE decrease is equal to or less than the predicted value.

Figures 5.3 and 5.4 present the measured values of upper shelf energy for the surveillance plates (transverse and longitudinal orientation, respectively) shown as a function of measured neutron fluence. The data demonstrate that no C-E fabricated reactor vessel surveillance plates have gone below the 50 ft-lb screening criterion for neutron fluences as high as 8.5×10^{19} n/cm^2. The lowest transverse orientation plate irradiated USE values (56 to 59 ft-lb) are for two plates with an initial USE of 67 and 80 ft-lb and a copper content of 0.24% and 0.20%, respectively. The corresponding longitudinal plate data are 82 to 119 ft-lb irradiated and 105 to 134 ft-lb unirradiated USE. The lower bound USE after irradiation for all the longitudinal plates is 72 ft-lb, although the majority of data were 82 ft-lb or greater for neutron fluences as high as 8.4×10^{19} n/cm^2 (i.e., a factor of three higher than for typical CEOG vessel beltline fluence).

The mean initial upper shelf and range for the plates are as follows:

Transverse Orientation $\bar{x}$ = 100.9 ft-lb, Range 67 to 134 ft-lb, for 17 plates

Longitudinal Orientation $\bar{x}$ = 126.8 ft-lb, Range 90 to 159 ft-lb, for 37 plates

The copper content for the plates varied from 0.07% to 0.25%. These surveillance plate data provide a broad cross section of information representative of CEOG vessel plates. Therefore, this gives reasonable assurance that the transverse orientation USE of CEOG reactor vessel beltline plates will be maintained above 50 ft-lb at end-of-life (one-quarter thickness fluence of 2.8×10^{19} n/cm^2 or less) based on the high initial USE for C-E fabricated plates and the surveillance measurements shown in Figure 5.3. The corresponding end-of-life USE for longitudinal orientation plates is 70 ft-lb or higher.

3. Beltline Welds - CEOG vessel beltline welds were fabricated using Linde 1092, 0091, or 124 flux. None of these vessels were fabricated using Linde 80 flux. Table 5.3 provides a list of reactor vessel surveillance program weld USE data extracted from ORNL PR-EDB for C-E fabricated materials (Westinghouse and C-E NSSS designs). Twenty-three of the welds were fabricated using Linde 1092, 0091 and 124 flux or ARCOS flux; the remaining three were manual arc or could not be readily identified for flux type. The mean initial upper shelf energy for the 26 welds is 120 ft-lb with a range of 98 to 160 ft-lb.

Table 5.3 includes the measured upper shelf energy decrease after irradiation as well as the predicted decrease based upon Position 1.2 of Regulatory Guide 1.99, Revision 02. The predicted and measured decrease in USE, calculated as the percent change from the initial unirradiated USE, are compared in

Figure 5.5. Of the forty measurements of drop in USE, twenty-five are equal to or less than the predicted value. Twelve of the fifteen underpredicted measurements are within 5% (measured minus predicted USE decrease) of the predicted values.

Figure 5.6 presents the measured values of upper shelf for the surveillance welds shown as a function of neutron fluence. The data demonstrates that no C-E fabricated vessel surveillance welds have gone below the 50 ft-lb screening criterion for neutron fluences as high as 8.7×10^{19} n/cm^2. Furthermore, the lower bound trend indicates that the bulk of the upper shelf decrease has occurred by approximately 1×10^{19} n/cm^2. The data represent twenty-six different welds ranging in copper content from 0.03% to 0.36% (seventeen with 0.20% Cu or more), and initial upper shelf energies of 98 to 160 ft-lb. Therefore, Figure 5.6 provides a broad cross section of information representative of CEOG vessel welds. By inference, there is reasonable assurance that the USE of CEOG reactor vessel beltline welds will be maintained above 50 ft-lb at end-of-life (one-quarter thickness fluence of 2.8×10^{19} n/cm^2 or less) based on the high initial upper shelf for C-E fabricated vessel welds and the surveillance measurements shown in Figure 5.6.

4. Plate Orientation - The analysis examines postulated flaws in both axial and circumferential orientations. CEOG reactor vessels were fabricated with the circumferential direction parallel to the major rolling direction in the plates. Therefore, extension of an axial flaw would be in the "strong" direction of the plate; i.e., longitudinal Charpy USE properties would be appropriate for analysis of the axial flaws. In contrast, the "weak" direction of the plate would coincide with the extension of circumferential flaws, consequently, transverse Charpy USE properties should be employed. Given that pressure stresses are greater for an axial flaw than for a circumferential flaw, the plates

are oriented in the vessel to yield the greatest toughness in the direction of the maximum stresses. See Appendix A for further details.

5. Assessment of Limiting Material USE - When analyzing axially oriented flaws, Charpy properties associated with the beltline shell course longitudinal seam welds and plates (longitudinal orientation) should be considered. Using the copper contents, initial USE, and end-of-life one-quarter thickness fluence corresponding to each CEOG vessel beltline longitudinal welds as provided by Generic Letter 92-01 responses, USE values were predicted based on Regulatory Guide 1.99, Revision 02, Position 1.2. The minimum predicted USE was 61.7 ft-lb for those welds. Based upon the lower bound trend of Figure 5.6 for a fluence of 2.8×10^{19} n/cm^2 (maximum EOL fluence at one-quarter thickness for CEOG vessels), the surveillance data indicate a minimum USE of approximately 53 ft-lb. Taking the longitudinal surveillance plate data (Figure 5.4) in a similar fashion, the lower bound USE at 2.8×10^{19} n/cm^2 is 73 ft-lb. The most conservative projection is, therefore, 53 ft-lb associated with the analysis of axially oriented flaws.

For analysis of a circumferentially oriented flaw, properties to be considered are beltline shell course circumferential seam welds and plates (transverse orientation). Using the copper contents, initial USE and EOL one-quarter thickness fluence corresponding to each CEOG vessel beltline circumferential welds as provided by Generic Letter 92-01 responses, USE values were predicted based on Regulatory Guide 1.99, Revision 02, Position 1.2. The minimum predicted USE was 58.3 ft-lb for those welds. The lower bound trend from Figure 5.6, as noted above, indicates a minimum USE of approximately 53 ft-lb. For transverse surveillance plate properties, Figure 5.3 yields a lower bound USE at 2.8×10^{19} n/cm^2 of 55 ft-lb. Using the copper contents, initial (transverse) USE, and EOL one-quarter thickness fluence corresponding to each CEOG vessel beltline plate, USE values were predicted

based on Position 1.2. The minimum predicted USE was 48.5 ft-lb. Therefore, the most conservative projection is 48.5 ft-lb associated with the analysis of circumferentially oriented flaws.

In summary, a review of the CEOG beltline materials was performed to predict the EOL upper-shelf-energy values. These predictions provided a minimum USE of 48.5 ft-lb. This value was associated with SA 302B-Modified plate containing 0.19 w% copper with an initial upper shelf energy of 71.8 ft-lb (estimated from longitudinal orientation Charpy test results). The corresponding EOL fluence for this plate was 2.71×10^{19} n/cm^2 (E > 1 MeV, vessel inside surface) resulting in a predicted EOL upper-shelf-energy of 48.5 ft-lb at the one-quarter thickness location.

Material Properties

Material properties needed to perform the RPV assessment for low upper shelf energy include the modulus of elasticity, yield strength and the J-Integral Resistance Curve (J-R Curve) for the material of interest (Refs. 7 and 8). The modulus of elasticity is considered to be independent of exposure to neutron fluence. The yield strength and J-R Curve will be dependent on irradiation exposure and changes in these properties are considered as a function of fluence.

Most of the needed physical and tensile properties for the analysis can be obtained from either the literature or from the ASME Boiler and Pressure Vessel (B&PV) Code (Ref. 12). The modulus of elasticity for the SA302 Grade B modified plate is obtained from Table TM-1 of Section II, Part D to the ASME B&PV Code. The SA302 Grade B modified plate material is classified as a Mn-½Mo-½Ni steel in Material Group A of Table TM-1. The modulus of elasticity as a function of temperature is provided in Table 5.4 for convenience. These values also apply to SA533 Grade B Class 1 plate material.

The yield and tensile strengths for SA302 Grade B modified plate are shown in Table 5.5. These values were obtained from Table Y-1 and Table U of Section II, Part D to the ASME B&PV Code. The yield and tensile strength trend curves for SA533 Grade B Class 1 plate are identical to SA302 Grade B modified plate. The yield strength of RPV steels decreases with increasing temperature. Exposure of RPV steels to neutron irradiation results in an increase in the materials yield strength. The Power Reactor-Embrittlement Database (PR-EDB) (Ref. 11) was used to evaluate the general trend for change in yield strength as a function of neutron fluence.

Figure 5.7 shows the results of PR-EDB evaluation of percent change in yield strength as a function of neutron fluence exposure. Base metal data was sorted from the database and the percent change in yield strength was plotted as a function of the surveillance capsule fluence. Additional sorting or characterization of the base metal data subset was not performed.

A rough fit of the general trend of the base metal data shown in Figure 5.7 was performed by linear regression analysis for a power law fit. The mean trend curve for this data is shown in Figure 5.7.

Tensile properties were obtained from surveillance capsule test results for the material under consideration. These results can also be used to evaluate the material properties to be used in the analysis. The initial elevated-temperature yield strength for the equivalent surveillance plate material was 57.8 ksi at 550°F. The yield strength at 550°F was 73.9 ksi and 81.0 ksi, respectively, for the capsule fluences of 2.71×10^{19} and 4.3×10^{19} (n/cm^2, $E > 1$ MeV). The percent change from the initial yield strength at these fluence levels for these data have been included as the solid points in Figure 5.7.

The two surveillance data points indicate that the behavior of the material is significantly above the mean trend curve shown for change in yield strength as a

function of fluence. Based on this assessment of the change in materials yield strength as a function of fluence, the mean trend curve shown in Figure 5.7 was used in the current analysis to arrive at yield strength values for the neutron exposure being considered.

Requirements for determining the J-R Curve for the material of interest are defined in Code Case N-512 (Ref. 7). The J-Integral resistance versus crack extension curve should be a conservative representation of the vessel material under evaluation. The J-R curve should represent the toughness of the controlling material at upper-shelf temperatures. The following options are provided for determining the J-R curve:

1. J-R Curve generated for the actual material under consideration. Tests should address proper crack orientation, temperature and fluence.
2. J-R Curve generated from a database for the same class of material, with the same orientation and correlations for the effects of fluence, temperature and chemical composition.
3. When (1) or (2) are not possible, indirect methods of estimating the J-R curve may be used, provided the methods are justified for the material under consideration.

One method for estimating the J-R curve for a material is to utilize Charpy data or a justifiable estimate, if no data are available, for the upper-shelf energy of the material (Refs. 8, 13, 14). The upper-shelf energy of the material under consideration is then used as an index to estimate the J-R curve behavior for the initial condition of the material and after irradiation, taking into account the measured or predicted drop in upper-shelf energy. This method has been applied to Linde 80 welds by performing regression analysis on an extensive database of J-R curve data. Charpy upper-shelf energy was used as a regression variable to permit J-R Curves to be generated as a function of the upper-shelf energy of the material (Refs. 13 and 14).

Similar multivariable modeling of J-R curve behavior has also been performed for RPV base materials (Refs. 15 and 16). A model of Deformation-J was fitted to available data on reactor pressure vessel steels (Ref. 16). The model consisted of the form:

$$J_d = C1(\Delta a)^{C2} \exp[C3(\Delta a)^{C4}]$$

where the fitting constants for RPV base metals were functions of USE, temperature, thickness, and fluence.

Charpy model for the RPV base material Deformation J-R Curve model was selected to develop the representative material toughness properties for this analysis. This model was selected over the pre-irradiated Charpy USE or CVN_p model, which uses the vessel fluence as a variable. In order to use the pre-irradiated Charpy model in this analysis, it would have been necessary to determine the initial USE, determine the fluence level of interest, estimate the change in USE due to irradiation using Regulatory Guide 1.99, Rev. 2, and then calculate the J-R curves predicted by the correlation of Reference 16. It was concluded that the Charpy Model provided a more direct approach by assuming the irradiated USE of interest for the material. This approach avoids possible errors of basing estimated J-R curve behavior on estimated values of decreased USE due to irradiation.

To evaluate J_d, the coefficients were evaluated utilizing the Charpy model correlation for use in the analysis. The coefficients were obtained from Reference 16, and are as follows:

$$\ln C1 = a_1 + a_2 \ln CVN + a_3 T + a_4 \ln B_n$$

$$C2 = d_1 + d_2 \ln C1 + d_3 \ln B_n$$

$$C3 = d_4 + d_5 \ln C1 + d_6 \ln B_n$$

$$C4 = -0.409$$

The constants necessary for determining the required coefficients were provided by Table 11 of Reference 16. Again, those applicable constants are those associated with the Charpy model. A value of B_n = 1.0 in. was utilized because the data used to develop the correlations were predominately obtained from small specimens with thicknesses of approximately 1.0 inch.

In addition, it is important to note this correlation provides mean J-R properties. To estimate J-R curves for a lower bound curve (mean-2σ), a factor of 0.749 is applied to the mean J_d value.

Corresponding J-R curves for the longitudinal Charpy orientation of the base material were developed using the same USE values divided by 65%, which is the conversion factor recommended by the NRC Branch Technical Position for estimating transverse properties from longitudinal data. The J-R curves for the longitudinal Charpy orientation of the plate were used for the evaluation of axially oriented flaws.

A review of the correlation basis was performed to identify the applicability to all USE values. It was determined that values below 30 foot-pounds are outside the data base range. The lowest USE data used to develop the correlation for base materials was 58 foot-pounds and for weld metals 33 foot-pounds. Comparison of the predicted base metal and weld metal curves showed that they were within approximately 10% of one another at 30 foot-pounds but this was at the extreme of the range of data used to develop the correlations. Consequently, lower USE values should be treated with extreme care or supported with additional testing.

Lastly, J_{Ic} values for each upper-shelf energy level were determined for each of the J-R Curves derived from the correlation at a conservative temperature of 550°F. These are provided in Table 5.6. Values of J_{Ic} were determined in accordance with ASTM E 813-87 from simple power law regression analysis curve fits.

Reactor Vessel Geometry

A review of the CEOG NSSS reactor vessel geometries was performed to enable selection of a generic geometry. The results of the review are shown in Table 5.7A.

The Phase 1 analysis was based on a nominal reactor vessel inside diameter of 172 inches and corresponding vessel beltline wall thickness of 8.625 inches. The basis for this selection was that this geometry was consistent with the vessel which contained the identified limiting plate material and represents approximately sixty-seven (67) percent of the CEOG vessel geometries.

To ensure the bounding geometry was analyzed, the Phase 2 effort included the analysis of the bounding CEOG vessel geometries. Consequently, the reactor vessels with the minimum and maximum inside diameters along with their corresponding vessel beltline wall thickness, were chosen for analysis. As shown in Table 5.7A, these vessels correspond to a nominal inside diameter of 140 inches, and 182 inches along with a beltline thickness of 7.125 inches and 9.06 inches, respectively. In addition, all of the CEOG reactor vessels have a radius to thickness ratio of approximately 10. Consequently, equivalent pressure stress intensities would be expected between each size vessel for flaw depths postulated as a percentage of wall thickness (i.e, $a/t = 0.10$).

The analysis was based on three selected reactor vessels' as-built dimensions. The pertinent information used in the analysis, inside diameter, clad thickness, and beltline thickness, are provided in Table 5.7B.

TABLE 5.1

Low Upper Shelf Energy (Measured & Predicted)
Plate Orientation = TL

Plant ID	Capsule	Fluence	Unirradiated USE	Measured Irradiated USE	Copper Content	Predicted Decrease in USE (%)	Predicted Irradiated USE	Measured Decrease in USE (%)
AN2	W97	.3330E+19	134	120	0.08	14.5	114.6	10.4
BV1	U	.6540E+19	80	78	0.20	26.0	59.2	2.5
BV1	W	.9490E+19	80	59	0.20	29.0	56.8	26.3
BV1	V	.2550E+19	80	75	0.20	21.0	63.2	6.3
CK1	T	.1800E+19	94	84	0.14	15.3	79.6	10.6
CK1	Y	.1060E+20			0.14	23.4	0.0	0.0
CL1	U	.3270E+19	104	93	0.07	14.5	88.9	10.6
DC2	U	.3510E+19	95	94	0.15	19.0	77.0	1.1
FA1	X	.2800E+20	90	80	0.14	29.2	63.7	11.1
FA1	Y	.5830E+19	90	90	0.14	20.1	71.9	0.0
FA1	U	.1650E+20	90	82	0.14	25.9	66.7	8.9
FA2	W	.1540E+20	95	76	0.20	32.0	64.6	20.0
FA2	U	.5610E+19	95	69	0.20	25.5	70.8	27.4
FC1	W265	.9000E+19	120	93	0.10	18.5	97.8	22.5
IP3	T	.2920E+19	67	58	0.24	25.2	50.1	13.4
IP3	Z	.1070E+20	67	56	0.24	33.5	44.6	16.4
IP3	Y	.8050E+19	67	57	0.24	31.1	46.2	14.9
MC1	U	.4140E+19	101	100	0.09	15.5	85.3	1.0
ML2	W97	.3670E+19	108	79	0.14	18.2	88.3	26.9
MY	A35	.8520E+20	115	71	0.15	40.0	69.0	38.3
MY	W263	.6600E+19	115	96	0.15	22.0	89.0	16.5
PAL	A240	.4400E+20	102	68	0.25	48.0	53.0	33.3
PAL	W290	.1130E+20	102	84	0.25	35.0	66.3	17.6
SA2	T	.2560E+19	97	89	0.10	13.5	83.9	8.2
SA2	U	.5700E+19	97	84	0.10	16.5	81.0	13.4
SL1	W97	.5400E+19	103	78	0.15	21.0	81.4	24.3
SL2	W83	.1630E+19	117	111	0.11	13.1	101.7	5.1
WC1	U	.3390E+19	93	95	0.07	14.8	79.3	-2.2

TABLE 5.2

Low Upper Shelf Energy (Measured & Predicted)
Plate Orientation = LT

Plant ID	Capsule	Fluence	Unirradiated USE	Measured Irradiated USE	Copper Content	Predicted Decrease in USE (%)	Predicted Irradiated USE	Measured Decrease in USE (%)
AN2	W97	.3410E+19	159	140	0.080	14.8	114.6	11.9
BV1	W	.9490E+19	134	114	0.200	29.0	95.1	14.9
BV1	V	.2550E+19	134	114	0.200	21.0	105.9	14.9
BV1	U	.6540E+19	134	99	0.200	26.0	99.2	26.1
CC1	W263	.6000E+19	138	115	0.120	18.8	112.1	16.7
CC2	W263	.8060E+19	146	115	0.140	22.0	113.9	21.2
CK1	T	.1800E+19	130	108	0.140	15.3	110.1	16.9
CK1	Y	.1340E+20			0.140	24.4	0.0	0.0
CL1	U	.3270E+19	126	124	0.070	14.5	107.7	1.6
CTY	F	.4040E+19			0.120	16.8	0.0	0.0
CTY	A	.2070E+19			0.100	13.0	0.0	0.0
CTY	H	.1790E+19	135	130	0.100	12.5	118.1	3.7
CTY	H	.1790E+19	120	117	0.120	13.9	103.3	2.5
CTY	F	.4040E+19			0.100	15.5	0.0	0.0
CTY	D	.2220E+20	126	110	0.120	25.4	94.0	12.7
CTY	F	.4040E+19			0.120	16.8	0.0	0.0
CTY	H	.1790E+19	126	122	0.120	13.9	108.5	3.2
DC1	S	.2980E+19	122	126	0.077	14.0	104.9	-3.2
DC2	U	.3510E+19	144	124	0.150	19.0	116.6	13.9
FA1	U	.1650E+20	140	110	0.140	25.9	103.7	21.4
FA1	X	.2800E+20	140	114	0.140	29.2	99.1	18.6
FA1	Y	.5830E+19	140	128	0.140	20.1	111.9	8.6
FA2	W	.1540E+20	130	102	0.200	32.0	88.4	21.5
FA2	U	.5610E+19	130	94	0.200	25.5	96.9	27.7
FC1	W225	.4500E+19	141	122	0.100	15.7	118.9	13.5
FC1	W265	.9000E+19	141	109	0.100	18.5	114.9	22.7
HB2	V	.4510E+19	100	100	0.100	15.8	84.2	0.0
HB2	S	.3690E+19	113	109	0.090	15.0	95.2	3.5
HB2	T	.4110E+20	114	105	0.090	26.5	83.8	7.9
HB2	S	.3690E+19	90	88	0.100	15.0	76.5	2.2
HB2	S	.3690E+19	91	85	0.120	16.6	75.9	6.6
IP2	V	.4570E+19	117	111	0.140	19.2	94.5	5.1
IP2	Z	.1200E+20			0.140	24.0	0.0	0.0
IP2	T	.2550E+19			0.140	17.6	0.0	0.0
IP2	Y	.4720E+19			0.140	19.2	0.0	0.0
IP2	Z	.9620E+19			0.140	23.0	0.0	0.0
IP2	T	.2020E+19	113	88	0.140	15.8	95.1	22.1
IP2	T	.2020E+19	116	103	0.140	15.8	97.7	11.2
IP2	T	.2930E+19			0.140	17.2	0.0	0.0
IP2	T	.2930E+19			0.250	26.0	0.0	0.0
IP2	T	.2020E+19	118	100	0.250	23.5	90.3	15.3
IP2	Z	.1200E+20			0.250	35.5	0.0	0.0
IP3	T	.2920E+19	105	96	0.240	25.2	78.5	8.6
IP3	T	.2920E+19	132	119	0.180	20.4	105.1	9.8
IP3	Z	.1070E+20	130	108	0.190	28.5	93.0	16.9
IP3	Z	.1070E+20	105	82	0.240	33.5	69.8	21.9
MC1	U	.4140E+19	140	133	0.087	15.5	118.3	5.0

TABLE 5.2

Low Upper Shelf Energy (Measured & Predicted)
Plate Orientation = LT

Plant ID	Capsule	Fluence	Unirradiated USE	Measured Irradiated USE	Copper Content	Predicted Decrease in USE (%)	Predicted Irradiated USE	Measured Decrease in USE (%)
ML2	W97	.3750E+19	131	94	0.140	18.2	107.2	28.2
MY	W263	.6600E+19	140	113	0.150	22.0	109.2	19.3
MY	A25	.1300E+20	140	96	0.150	25.5	104.3	31.4
MY	A35	.8390E+20	140	85	0.150	40.0	84.0	39.3
PAL	A240	.4500E+20	155	92	0.250	28.0	111.6	40.6
PAL	W290	.1100E+20	155	112	0.250	35.0	101.0	27.7
SA1	T	.2560E+19	108	89	0.220	22.6	83.6	17.6
SA1	Z	.1330E+20	108	90	0.220	33.0	72.4	16.7
SA1	Z	.1330E+20	116	102	0.230	34.0	76.6	12.1
SA1	Z	.1330E+20	130	108	0.220	33.0	87.1	16.9
SA1	T	.2560E+19	116	103	0.230	23.4	88.9	11.2
SA1	T	.2560E+19	130	130	0.220	22.6	100.6	0.0
SA1	Y	.8910E+19	130	113	0.220	30.0	91.0	13.1
SA2	T	.2560E+19	122	115	0.100	13.5	105.5	5.7
SA2	U	.5700E+19	122	112	0.100	16.5	101.9	0.0
SL1	W97	.5400E+19	139	107	0.150	21.0	109.8	23.0
SL2	W83	.1620E+19	133	118	0.110	13.1	115.6	11.3
SO1	F	.5140E+20	97	71	0.180	39.2	59.0	26.8
WC1	U	.3390E+19	148	145	0.070	14.8	126.2	2.0

TABLE 5.3

Low Upper Shelf Energy (Measured & Predicted)
for Welds

Plant ID	Capsule	Fluence	Unirradiated USE	Measured Irradiated USE	Copper Content	Predicted Decrease in USE (%)	Predicted Irradiated USE	Measured Decrease in USE (%)
AN2	W97	.3340E+19	154	147	0.040	14.5	131.7	4.5
BV1	V	.2550E+19	112	88	0.260	29.6	78.8	21.4
BV1	U	.6540E+19	112	83	0.260	36.4	71.2	25.9
BV1	W	.9490E+19	112	78	0.260	39.2	68.1	30.4
CC1	W263	.6100E+19	160	119	0.240	34.1	105.4	25.6
CC2	W263	.7970E+19	137	105	0.200	32.5	92.5	23.4
CK1	Y	.1060E+20			0.270	41.2	0.0	0.0
CK1	T	.1800E+19	110	80	0.270	27.9	79.3	27.3
CL1	U	.3270E+19	112	101	0.060	15.3	94.9	9.8
CTY	A	.2070E+19			0.220	25.2	0.0	0.0
CTY	D	.2220E+20	105	83	0.220	43.4	59.4	21.0
DC1	S	.2980E+19	98	87	0.210	26.8	71.7	11.2
DC2	U	.3510E+19	121	85	0.220	28.6	86.4	29.8
FA1	Y	.5830E+19	149	130	0.140	24.6	112.3	12.8
FA1	U	.1650E+20	149	108	0.140	31.4	102.2	27.5
FA1	X	.2800E+20	149	115	0.140	35.7	95.8	22.8
FA2	W	.1540E+20	144	144	0.030	21.0	113.8	0.0
FA2	U	.5610E+19	144	132	0.030	16.5	120.2	8.3
FC1	W265	.9000E+19	104	59	0.350	42.0	60.3	42.9
FC1	W225	.4200E+19	104	65	0.350	37.5	65.0	37.5
HB2	V	.4510E+19	112	70	0.340	37.8	69.7	37.5
HB2	T	.4110E+20	112		0.340	52.0	53.8	0.0
IP2	Y	.5890E+19			0.230	33.0	0.0	0.0
IP2	V	.5590E+19	118	75	0.230	32.4	79.8	36.4
IP3	Y	.8050E+19	120	68	0.150	27.5	87.0	43.3
IP3	T	.2920E+19	120	91	0.150	22.0	93.6	24.2
IP3	Z	.1070E+20	120	76	0.150	29.5	84.6	36.7
KWE	R	.2070E+20	126	78	0.200	40.0	75.6	38.1
KWE	P	.2890E+20	126	76	0.200	44.0	70.6	39.7
KWE	V	.5590E+19	126	82	0.200	30.0	88.2	34.9
MC1	U	.4140E+19	112	75	0.210	28.8	79.7	33.0
ML2	W97	.3770E+19	132	98	0.300	35.0	85.8	25.8
MY	A25	.1300E+20	105	57	0.360	44.0	58.8	45.7
MY	A35	.8690E+20	105	50	0.360	60.0	42.0	52.4
MY	W263	.6800E+19	105	59	0.360	40.0	63.0	43.8
PAL	W290	.1030E+20	118	64	0.220	37.0	74.3	45.8
PAL	A240	.4600E+20	118	52	0.220	51.0	57.8	55.9
SA1	Y	.8910E+19	104	75	0.160	29.0	73.8	27.9
SA2	U	.5700E+19	111	74	0.230	32.7	74.7	33.0
SA2	T	.2560E+19	111	79	0.230	27.1	80.9	28.8
SL1	W97	.5300E+19	144	100	0.230	32.4	97.3	30.6
SL2	W83	.1620E+19	115	99	0.050	12.0	101.2	13.9
SO1	F	.5140E+20	99	80	0.190	48.4	51.1	19.2
WC1	U	.3390E+19	100	92	0.040	14.8	85.3	8.0

TABLE 5.4

MODULUS OF ELASTICITY FOR SA302 GRADE B MODIFIED PLATE
(FROM TABLE TM-1, SECTION II, PART D)

Temperature (°F)	Modulus of Elasticity, E ($x10^6$ psi)
-325	31.1
-200	30.5
-100	29.9
70	29.2
200	28.5
300	28.0
400	27.4
500	27.0
600	26.4
700	25.3
800	23.9
900	22.2

TABLE 5.5

YIELD AND TENSILE STRENGTHS FOR SA302 GRADE B MODIFIED PLATE
(FROM TABLES Y-1 & U, SECTION II, PART D)

Temperature (°F)	Yield Strength (ksi)	Tensile Strength (ksi)
-20 to 100	50.0	80.0
200	47.5	80.0
300	46.1	80.0
400	45.1	80.0
500	44.5	80.0
600	43.8	80.0
650	43.5	80.0
700	43.1	80.0

TABLE 5.6

J_{Ic} VALUES DETERMINED FROM ESTIMATED J-R CURVES

(Bn = 1.0, T = 550°F)

USE Transverse/Longitudinal (ft-lb)	J_{Ic}, Fracture Toughness (in-lb/in^2)			
	Transverse Orientation		Longitudinal Orientation	
	Mean-2σ	Mean	Mean-2σ	Mean
30/46	296.5	402.2	365.1	500.0
35/54	319.3	433.7	395.3	541.6
40/62	340.4	464.9	422.6	582.5
45/69	360.9	494.0	448.8	621.2
50/77	380.8	521.5	47.50	658.8
55/85	399.3	548.0	499.4	695.5
60/92	417.0	574.7	523.3	730.3
65/100	434.4	599.9	546.4	765.8
70/108	451.1	624.5	570.4	799.6
75/115	467.6	648.5	591.9	832.9

TABLE 5.7A

SUMMARY OF

CEOG NSSS NOMINAL REACTOR VESSEL GEOMETRIES

No. of Vessels	Nominal I.D. (in.)	Vessel Beltline Wall Thickness (in.)
1	140	7.125
1	157	7.875
10	172	8.625
3	182	9.06

TABLE 5.7B

SUMMARY OF

AS-BUILT DIMENSIONS UTILIZED FOR ANALYSIS

As-Built Vessel I.D. (in.)	Clad Thickness (in.)	Vessel Beltline Wall Thickness (in.)
141.28	0.2188	7.125
173.92	0.3125	8.625
183.90	0.160	9.060

FIGURE 5.1
DECREASE IN UPPER SHELF ENERGY MEASURED VERSUS PREDICTED PLATE ORIENTATION = TL

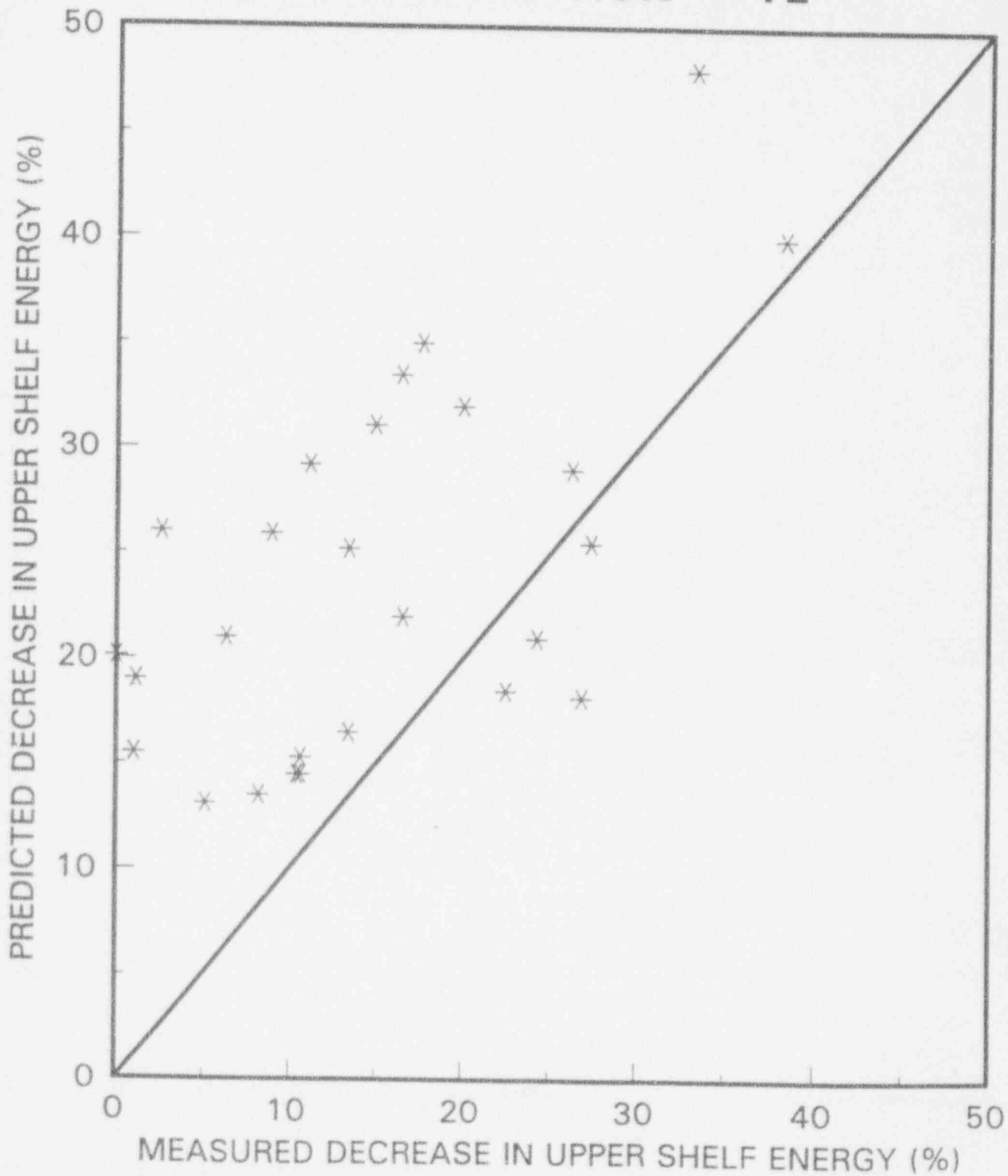

FIGURE 5.2
DECREASE IN UPPER SHELF ENERGY
MEASURED VERSUS PREDICTED
PLATE ORIENTATION = LT

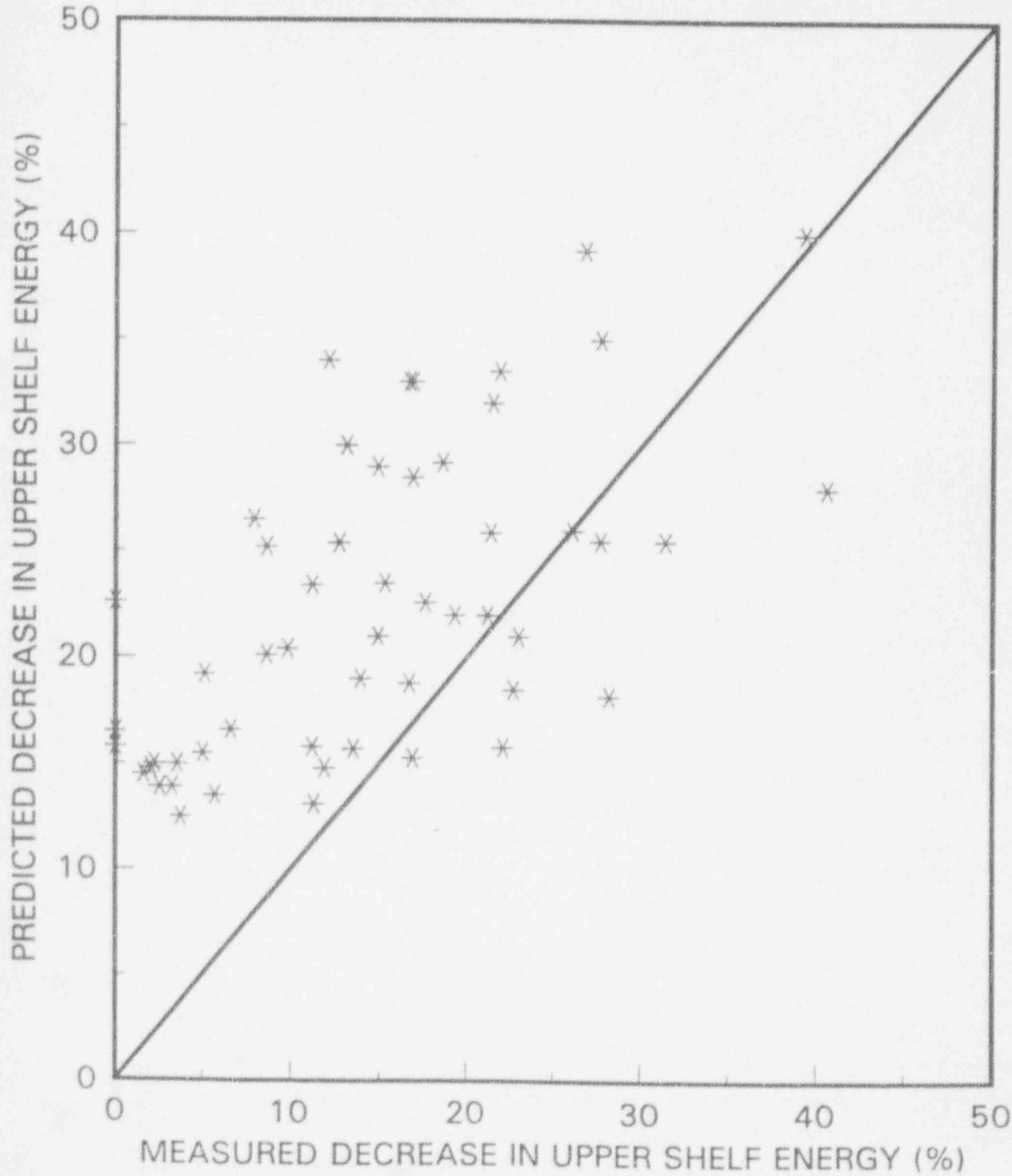

FIGURE 5.3
MEASURED USE VERSUS NEUTRON FLUENCE
PLATE ORIENTATION = TL

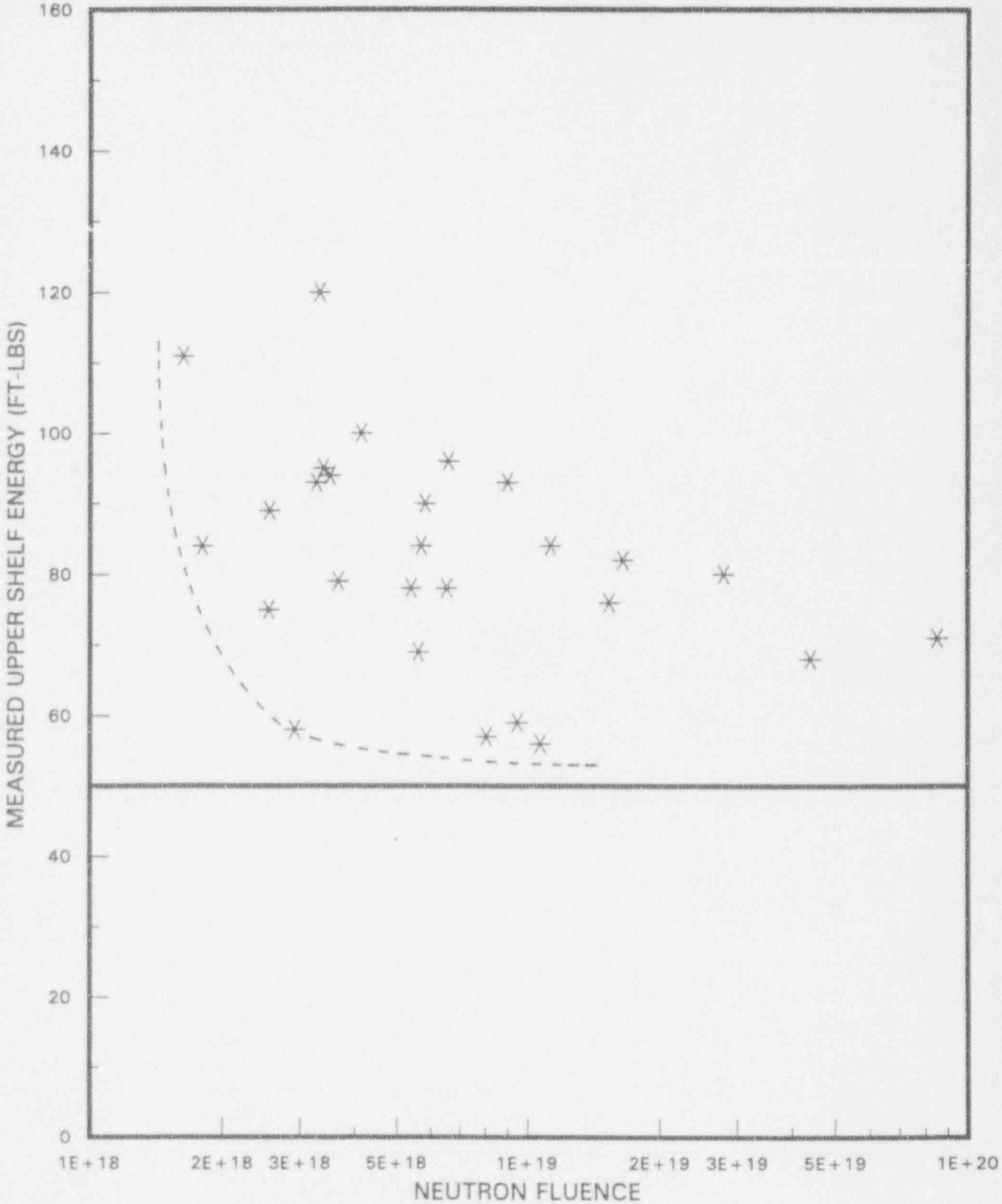

FIGURE 5.4
MEASURED USE VERSUS NEUTRON FLUENCE
PLATE ORIENTATION = LT

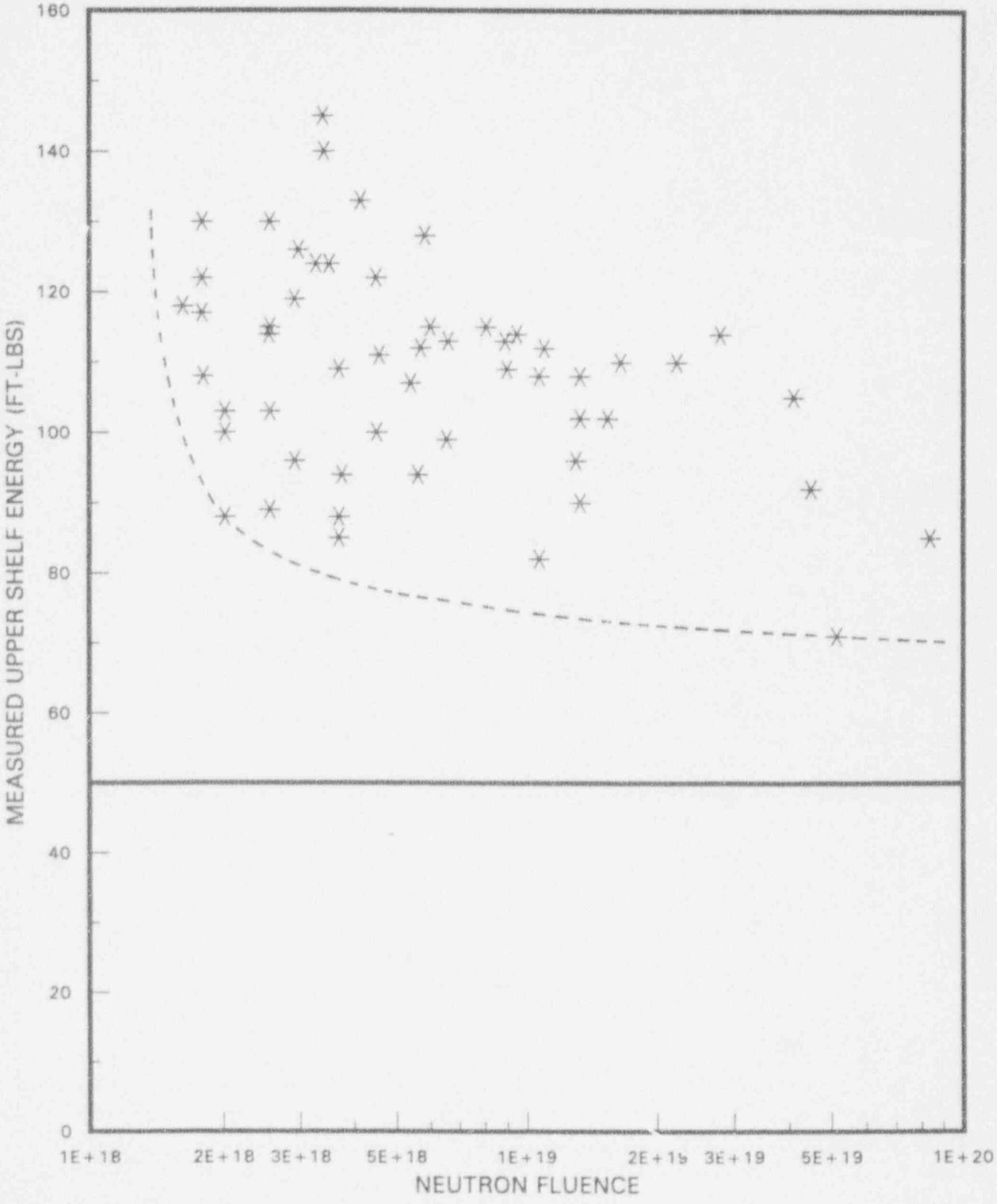

FIGURE 5.5
DECREASE IN UPPER SHELF ENERGY MEASURED VERSUS PREDICTED FOR WELDS

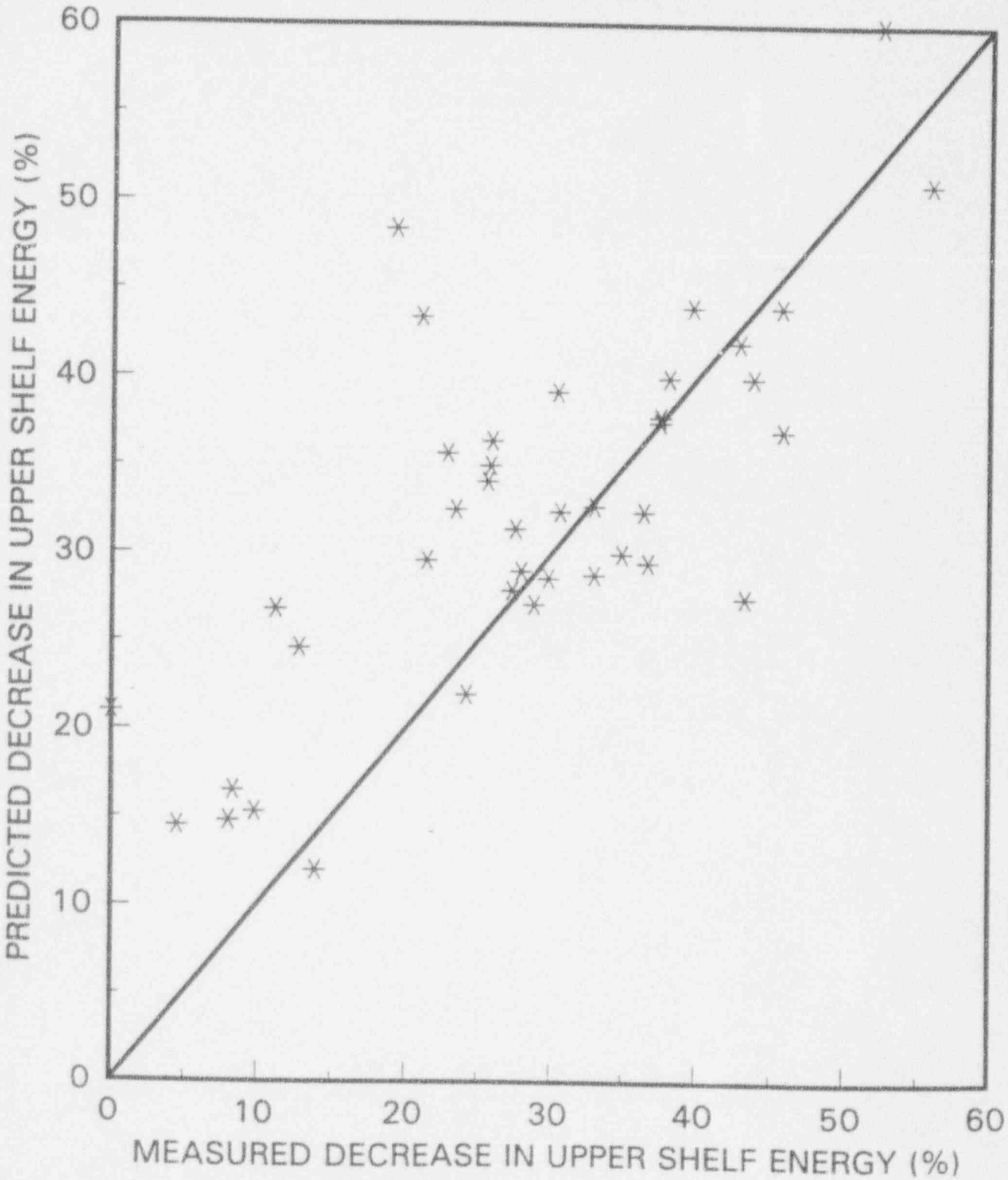

FIGURE 5.6
MEASURED USE VERSUS NEUTRON FLUENCE FOR WELDS

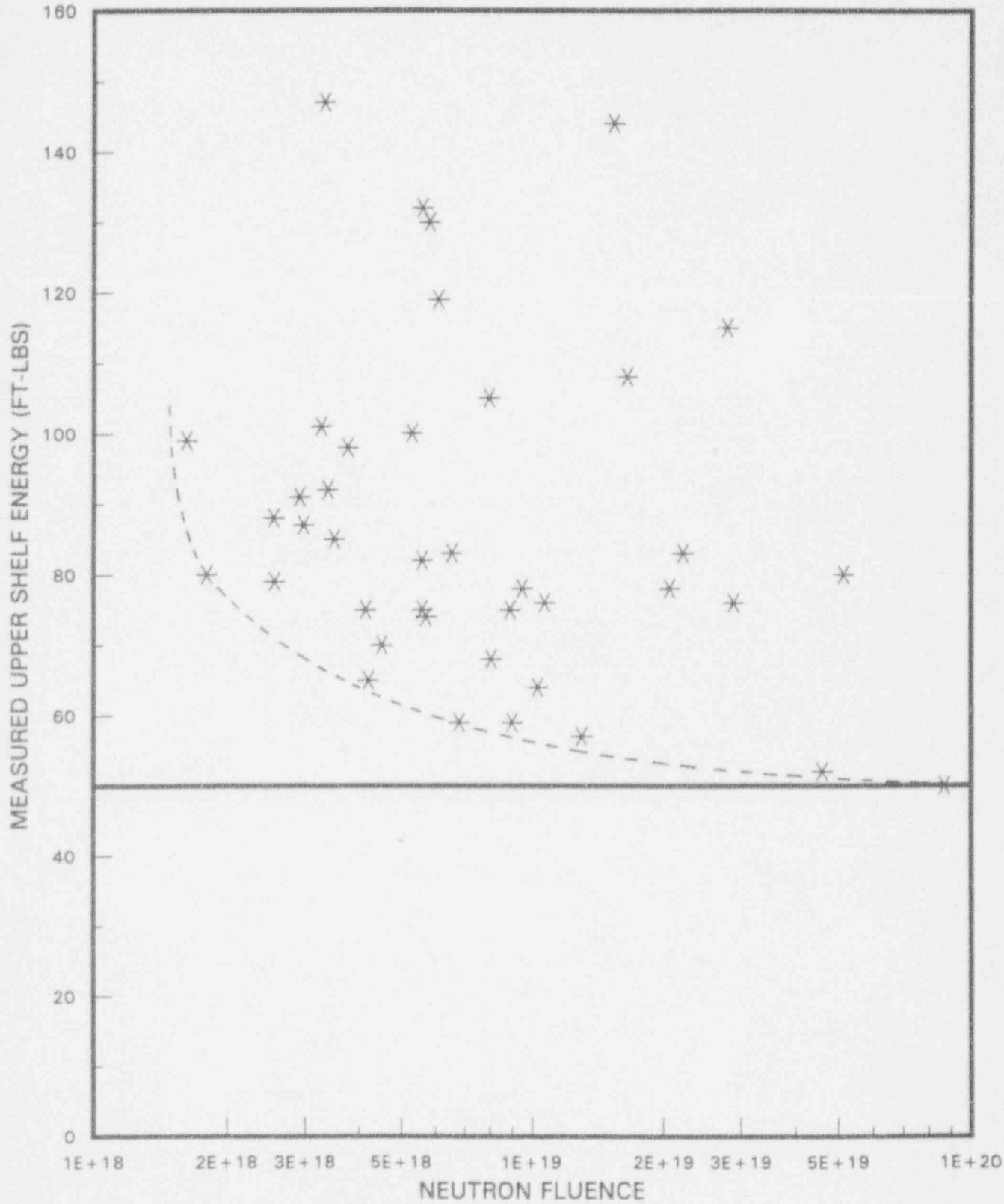

FIGURE 5.7

PERCENT CHANGE IN YIELD STRENGTH VERSUS

FLUENCE FOR RPV BASE METALS IN PR-EDB

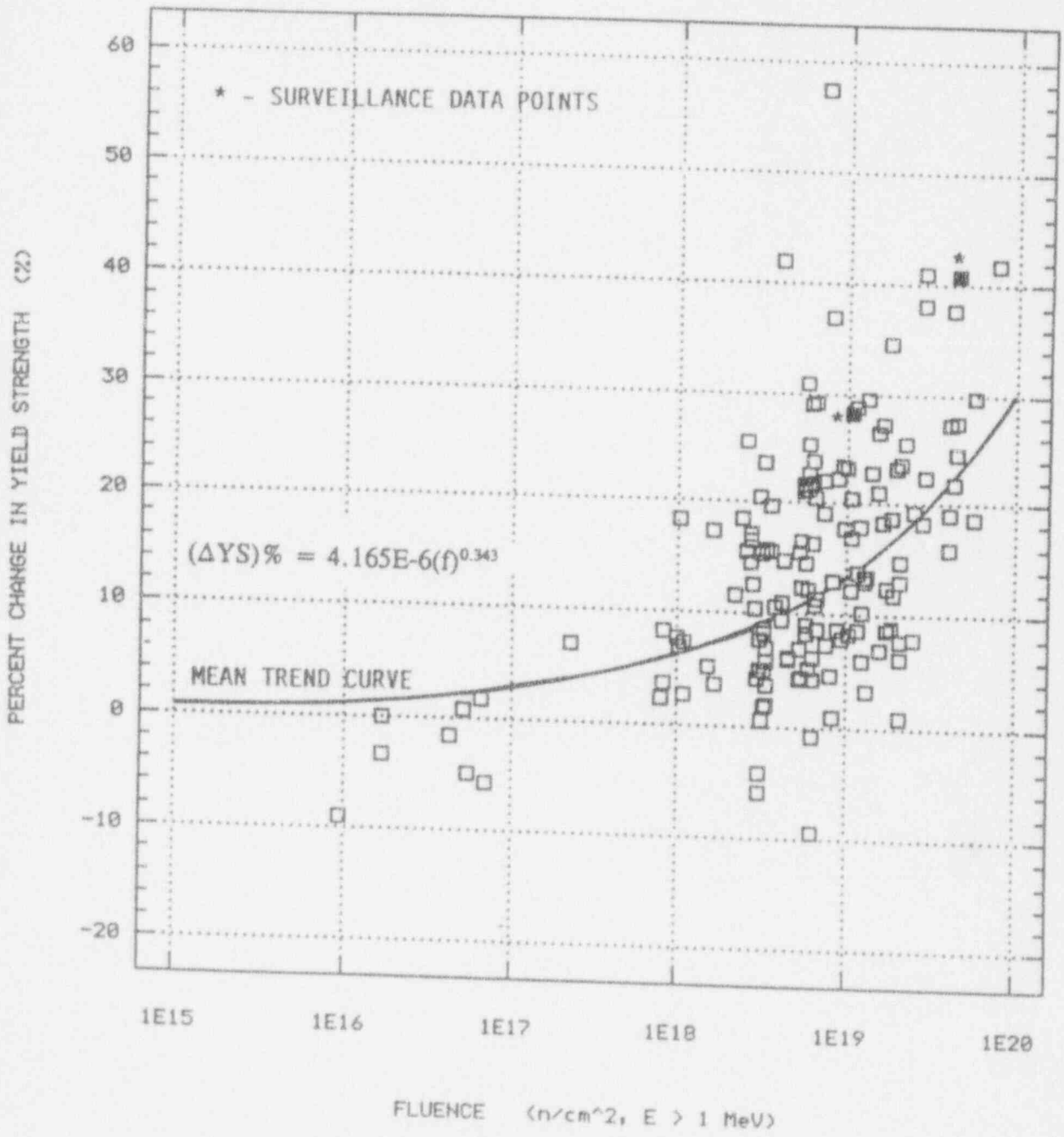

6.0 LEVEL A/B SERVICE LOADINGS EVALUATION METHODOLOGY

The purpose of this evaluation is to assess the margins to ductile flaw growth for low Charpy upper-shelf energy materials at operating temperatures where upper-shelf (ductile) behavior is controlling. ASME Code, Section XI, Code Case N-512 (Ref. 7) provides an explicit evaluation procedure and acceptance criteria for reactor vessels with low upper shelf energy subject to Level A and B (Normal and upset respectively) design-basis transients.

The postulated flaw required by the ASME Section XI Code Case N-512 is an interior semi-elliptical surface flaw with a depth equal to one-quarter the wall thickness and length six times the depth. The flaw orientation is dependent upon whether weld or base metal adequacy is being evaluated. As described in Section 5.0, the controlling material for CEOG NSSS reactor vessels was assessed to be base metal. Consequently, both axial and circumferential flaw orientations are required to be evaluated.

The Code Case provides an explicit two-step evaluation procedure for the calculation of the applied J-Integral which accounts for small scale yielding for both axial and circumferential flaws. This procedure, as provided in Reference 7 and reiterated below for completeness, was employed directly.

Applied J-Integral Calculation

To determine the applied J-Integral, the applied stress intensity factor is first determined for the applied Level A and B pressure and thermal loads.

The stress intensity factor due to internal pressure, including crack face pressure, is calculated by the following equations for either an axial or circumferential flaw.

- Axial Flaw

  $K_{Ip} = (SF)P\,[1 + (R_i/t)]\,(\pi a)^{0.5}\,F_1$ (ksi $\sqrt{in}$)

  where: $F_1 = 0.982 + 1.006\,(a/t)^2$

- Circumferential Flaw

  $K_{Ip} = (SF)P\,[1 + (R_i/(2t))]\,(\pi a)^{0.5}\,F_2$ (ksi $\sqrt{in}$)

  where: $F_2 = 0.885 + 0.233\,(a/t) + 0.345\,(a/t)^2$

The stress intensity factor due to radial thermal gradients for either an axial or circumferential flaw is determined using the following equation.

- Axial and Circumferential Flaw

  $K_{It} = ((CR)/1000)\,t^{2.5}\,F_3$ (ksi $\sqrt{in}$)

  where: $F_3 = 0.584 + 2.647\,(a/t) - 6.294\,(a/t)^2 + 2.990\,(a/t)^3$

The preceding equations are valid for the flaw size range given by the expression, $0.20 \leq a/t \leq 0.50$ and for cooldown rates (CR) satisfying the criteria given as $0 \leq (CR) \leq 100°F/hr$.

Utilizing the following equation, an effective flaw depth can be determined which approximates small-scale yielding:

$$a_e = a + (1/(6\pi))[K_{Ip} + K_{It}/\sigma_y]^2$$

Utilizing the effective flaw depth, the stress intensity factors (K'_{Ip} and K'_{It}) due to small scale yielding can be determined from the previous equations by replacing the flaw depth, (a), by the effective flaw depth, (a_e). These equations are valid for an effective flaw size range meeting the criteria expressed by $0.20 \leq a_e/t \leq 0.50$. Utilizing the applied loads due to small scale yielding, the J-Integral for small scale yielding can be computed by:

$$J = 1000(K_{IP}^{I} + K_{It}^{I})^2/E \qquad (in\text{-}lb/in^2)$$

The applied J-Integral was evaluated for a range of flaw sizes to $0.20 \leq a_c/t \leq 0.50$.

Two criteria are required to be satisfied for both axial and circumferential flaws. The first criteria is that the applied J-integral shall be shown to be less than the J-integral characteristic of the material resistance to ductile tearing flaw growth of 0.10 in. This was evaluated as required utilizing a SF equal to 1.15 on the pressure loading and a SF equal to 1.0 on thermal loading. The second criteria is that the flaw be stable, with the possibility of ductile flaw growth. This was evaluated, as required, with a SF equal to 1.25 on the pressure loading and a SF equal to 1.0 on the thermal loading. The applied pressure and thermal loads were the same as previously stated.

One method recommended by the Code Case, the J-R Curve-Crack Driving Force Diagram, was used to assess flaw stability. This criteria can be expressed mathematically by:

$$\frac{\partial J}{\partial a} < \frac{dJ_R}{da}$$

where $\partial J/\partial a$ is the partial derivative of the applied J-Integral with respect to the flaw depth (a) while the applied load is held constant and dJ_R/da is the slope of the J-R curve. The J-R Curve-Crack Driving Force Diagram approach provides a graphical approach to validate criteria compliance.

The transients applicable to service Level A/B transients were defined in Section 4.0 as a normal heatup and cooldown. The analysis performed explicitly considered the cooldown transient since the Code Case provided no requirements for considering

heatup transients. Qualitatively, the heatup transients should produce a lower applied J-Integral than the cooldown transient due to the pressure and thermal stresses acting in opposition (the pressure load creates a tensile stress and the thermal stress creates a compressive stress at the I.D. thereby reducing the total stress). The cooldown analysis treated the applied pressure (accumulation pressure) as the maximum allowed by ASME Code Section III, NB-7300 and equal to 1.10 times the design pressure although the defined transient (see Table 4.2) provided a lower value. The thermal load was the maximum permitted by design criteria and Technical Specifications being 100°F/hr.

To evaluate the applied J-Integral the required material properties are noted in Section 5.0. In summary, the analysis utilized the following:

$E = 29.0 \times 10^6$ psi

$\nu = 0.3$

$\sigma_y = 50.0$ ksi

The yield stress utilized in the analysis corresponds to a temperature of 550°F. The yield strength was adjusted accounting for attenuation to the one-quarter thickness location of the thickest vessel and subsequently modified using the correlation presented by Figure 5.7. The value was rounded down to 50 ksi.

To ensure that the limiting vessel geometry was considered, the three vessel geometries provided by Table 5-4B were analyzed.

The material properties for J_d were developed for both the longitudinal and transverse orientations, as described in Section 5.0. These J_d values were representative of a lower bound curve (mean minus 2σ), as recommended by ASME Code Case N-512. Due to the method of treatment of Level A/B transients by the Code Case, the thermal stress is based solely on the magnitude of the cooldown rate resulting in the

peak thermal stress at any time point during the transient. In addition, since the values of J_d are dependent upon material temperature (J_d is inversely related to temperature; i.e., the higher the temperature, the lower J_d), the material temperature was conservatively treated as a constant 550°F. This results in the maximum applied J-Integral and the minimum J_d. The applied J-Integral for the axial and circumferential flaws were compared to the longitudinal and transverse J_d properties, respectively.

7.0 LEVEL C/D SERVICE LOADING EVALUATION METHODOLOGY

Code Case N-512 provided by ASME Code, Section XI (Reference 7) specifies that Level C/D events be considered to properly assess reactor vessels with low upper shelf Charpy energy levels. The Code Case provides explicit acceptance criteria and procedures with which to demonstrate margins of safety equivalent to those provided by Appendix G to Section III of ASME Code and is applicable when operation provides vessel metal temperatures in the upper shelf range. The Code Case methodology is based on the principles of elastic-plastic fracture mechanics and requires the prediction of the applied J-Integral for various flaw sizes which is then compared with the J-Integral fracture resistance of the material to determine acceptability.

Although the Code Case provides a very explicit method of calculating J-Applied for Level A/B events, it does not do so for Level C/D events. This is primarily due to the fact that these events typically involve secondary stresses such as thermal transient stresses, stresses due to faulted conditions, etc, which can result in high stress gradients through the wall of the reactor vessel. While these stresses are relatively low in magnitude, the concern is that when these stresses are combined with uniform pressure stresses, local yielding can occur at the postulated crack tip. The methods presented in the Code Case to calculate J-Applied for Level A/B events may be inadequate to analyze Level C/D situations correctly. Consequently, it is left up to the analyst to account for these effects in calculating J-Applied for Level C/D events.

To precisely account for the secondary stresses present during these events it would be necessary to perform complex elastic-plastic finite element analyses using the actual sequence of loadings and the actual stress-strain curve of the irradiated material. This approach would be most beneficial in cases of large plastic deformation, but in cases where there are only small amounts of plastic deformation an elastically based solution which provides correction for small scale yielding is

judged to be adequate. This analysis will verify that there is only small scale yielding and that an elastically based solution adequately predicts J-Applied for the events considered.

The evaluation was performed consistent with the principles discussed in the Code Case, NUREG-0744 and the ASME Code. The specific method employs Linear Elastic Fracture Mechanics (LEFM) to calculate stress intensities due to all loadings which include internal and crack face pressure, radial thermal gradients and differential thermal expansion stresses between the cladding and base metal. These stress intensities are used as a basis from which a conservative correction is applied to adjust for local yielding. The adjustment is based on guidance suggested in NUREG-0744, Reference 17, where the basis of the J-Applied equations are discussed in detail. In these discussions, it is noted that J-Applied is closely related to applied strain. Consequently, when secondary stresses are solved for by an elastic analysis, the stress values are higher (above yield) than the actual stresses in the metal, but the calculated strains are nearly correct. Therefore, by averaging the calculated applied strains over the crack area of a surface flaw and transforming them back to equivalent stresses by using a Ramberg-Osgood relation, they can be used in a surface flaw analysis and give reasonable results. The results of such a procedure were judged to be a conservative method of handling secondary stresses.

Input to the analysis included both the event temperature and pressure profile of the chosen Level C/D transients. The development of these profiles is discussed in Section 3.0. The steam line break transient depicted in Figure 4.2 was evaluated against both Level C and D requirements for completeness, although Level C requirements are more stringent. The feedwater line break, depicted in Figure 4.2, was evaluated against Level D requirements. The three reactor vessel geometries defined in Table 5.7B were evaluated to assure the limiting geometry was analyzed.

The additional material inputs are provided below and selected from the information provided in Section 5.0.

E	=	27.0×10^6 psi
σ_y	=	45 ksi (unirradiated)
υ	=	0.3

The following sections discuss the methodologies used in the calculation of J-Applied for Level C/D events. They describe the LEFM methods used to calculate the combined stress intensity, K_I, accounting for secondary stresses due to thermal and differential expansion stresses and also the conversion of K_I to J-Applied. A more detailed description of the LEFM methodology used is presented in CEN-381-P and CEN-381-P Attachment 1-P (References 18 and 19, respectively).

7.1 Fracture Mechanics Methodology

7.1.1 Loading Conditions

Level C/D evaluation procedures utilize realistic flaw sizes and minimal margins of safety. Consequently, all loadings applied to the vessel are considered in the analysis. This includes stresses due to internal pressure, crack face pressure, radial thermal gradients, and cladding induced stresses.

Internal pressure is considered to be acting uniformly on the vessel inside surface. When considering hypothetical flaws, the vessel internal pressure is assumed to act perpendicularly to the crack face from the vessel inside surface to the crack tip contributing to the applied load at the crack tip.

Stresses induced due to the presence of the clad have also been incorporated in the methodology. Specifically, these stresses are due to the difference in thermal expansion coefficients of the stainless steel cladding and the carbon steel base metal vessel wall. During operation of the plant, large coolant temperature changes are possible ranging from the 550°F full power operation to shutdown where temperatures are approximately 100°F, resulting in varying stresses due to the difference in thermal expansion coefficients. The stresses resulting from the difference in cladding and base metal expansion coefficients is conservatively assumed to be negligible at 550°F (stress free).

7.1.2 Flaw Sizes and Shape

To address the criteria provided by the Code Case, explicit consideration was given to the following flaws sizes:

Postulated Inside Surface Flaws

- Clad/base metal interface (t_c)
- Clad thickness into base metal ($2t_c$)
- 5% into base metal (t_c+5%)
- 10% into base metal (t_c+10%)

The postulated flaw shape is semi-elliptical with an aspect ratio (length/depth) of 6/1. All flaws are conservatively postulated to be surface flaws.

7.1.3 Fracture Mechanics Influence Coefficients

Fracture mechanics influence coefficients applicable to the vessel beltline region were utilized to determine the Stress Intensity Factor (SIF) for the specified load. These influence coefficients are developed from 2-D finite element analyses which employed quarter point crack tip elements to calculate the SIF. These influence coefficients are then corrected for 2-D to 3-D effects (infinite length to finite length). These influence coefficients are based on unit loads which eliminates the need to determine stresses saving one step in the calculational process.

7.1.4 Heat Transfer Analysis

To determine the through wall temperature profile a one-dimensional, three noded, isoparametric finite element is used to solve the radial heat transfer equation,

$$\frac{1}{r}\frac{\partial}{\partial r}(kr\frac{\partial T}{\partial r}) = \rho C_p \frac{\partial T}{\partial t_i}$$

Subjected to the boundary conditions on the inner surface of,

$$q = h(T_C - T_s)$$

The inside surface has a convective film coefficient of 1000 Btu/hr ft^2-F°. The outside surface is assumed to be insulated.

Using shape functions N(r) for temperatures in the isoparametric formulation for the finite element,

$$T(r,t_i) = [N(r)]\{T_n(t_i)\} \text{ with}$$

$T_n(t)$ as the nodal temperatures and T(r,t) as the temperature field, the equation can be reduced to

$$[K]\ \{T_n\} + [C]\ \{\frac{\partial T_n}{\partial t}\} = \{Q(t_i)\}$$

where [K] and [C] represent thermal conductivity and capacitance matrices and {Q} represents external heat flux.

7.1.5 Calculation of J-Applied

As stated earlier, the calculation of J-Applied for level C/D events is based on equations and concepts discussed in NUREG-0744, Reference 17. This document provides the NRC position with respect to the safety analysis required when the upper shelf energy of the reactor pressure vessel steel is reduced to 50 ft-lbs or less after exposure to the neutron irradiation. It also provides an elastic-plastic fracture mechanics methodology to calculate J-applied in the beltline region of a pressurized water reactor vessel.

In essence, NUREG-0744 begins with established LEFM principles and extends them to account for small scale yielding around the crack tip. The methodology estimates the non-linear plastic effects through correction factors, which are based on extensive research performed by industry and other research institutions. These correction factors are well documented and were developed for use in this type of evaluation. The major points of the method are as follows:

Starting with the K_I equation from ASME Section XI, the stress intensity is given as:

$$K_I = \sigma M_m \sqrt{\pi a/Q} \tag{1}$$

and the elastic conversion of K_I to J is given as

$$J = K_I^2/E' \tag{2}$$

where $E' = E/(1-\upsilon^2)$ for plane strain. Substituting (1) into (2) and introducing σ_y^2, the above equations transform to

$$J = \frac{\sigma_y^2 a}{E'} \pi \frac{\sigma^2}{\sigma_y^2} \frac{M_m^2}{Q} \tag{3}$$

Then assuming,

$$G(a/t,a/l) = M_m^2/Q \tag{4}$$

and

$$F(\sigma/\sigma_o) = \pi(\sigma/\sigma_y)^2 \tag{5}$$

where G(a/t,a/l) is a geometric constant determined from the curves in ASME Section XI, Appendix A which is assumed not to change for the problem. The stress bracket $F(\sigma/\sigma_o)$ is the elastic-plastic correction factor for the method and accounts for these effects through a Ramberg-Osgood stress-strain relation. This stress bracket was developed through extensive research and is defined in tabular form in Reference 17, Appendix B, page B-35. Substituting, we then have the final working form of J-Applied as:

$$J = \frac{\sigma_y^2 a}{E'} F(\frac{\sigma}{\sigma_y}) G(a/t,a/l) \tag{6}$$

This format is very advantageous, in that the geometry and stress concentration factors are completely separate and independent factors on J-applied. This allows the calculation of each of these factors independently and without the influence of the other.

The next step is to determine the J-Applied of a flaw, a, accounting for secondary stresses. As stated earlier, LEFM Methods are used to calculate stress intensities due to both primary and secondary loadings. The concern is that, in some situations, this combination of loads increases the stress in the component well above the yield strength of the material where the methods described above do not adequately account for plastic effects and consequently an inappropriate J-applied. A conservative, approximate approach to account for these plastic effects is defined in NUREG-0744. The approach is based on the premise that in cases of elastically calculated stresses higher than yield, the stress value is not an accurate representation of the loading condition but the strain is nearly correct for small scale yielding and conservative for high values of elastically calculated stress. This strain is used to adjust elastically calculated stresses to more reasonable equivalent stresses using a Ramberg-Osgood stress-strain relation. This equivalent stress is then used to determine the stress bracket correction factor, $F(\sigma/\sigma_y)$.

To convert from LEFM calculated stress intensities to stresses in the component the following approach was used. Since the equations developed in NUREG-0744 are based on the premise of using the average stress field of the uncracked structure, the elastically calculated stress can be calculated by rearranging equation (1) of Article A-3000 of Appendix A, Section XI to solve for stress, σ. This would then represent the average stress needed to generate the stress intensity, K_I, due to primary and secondary stresses.

From this average stress, the average strain is, therefore, calculated using Hookes Law, $\sigma = E\epsilon$. This elastic strain is used to calculate an equivalent Ramberg-Osgood adjusted stress as described above. The following equation summarizes these steps.

$$\bar{\epsilon} = \frac{K_{I_{Total}}}{E'} \sqrt{\pi \; a \; \overline{M_m^2 / Q}} \qquad (7)$$

The following steps describe the process used to calculate J-Applied for the range of flaws considered:

(1) Calculate geometry effects using equation (4). This is a direct application of ASME Section XI, Appendix A.

(2) Calculate the equivalent strain using equation (7) and then use the fluence adjusted yield strength to calculate the equivalent stress using the Ramberg-Osgood stress-strain relation. The fluence is attenuated based on Regulatory Guide 1.99 Rev. 2 (Ref. 9) procedures and the change in yield strength is computed with the correlation provided by Figure 5.7.

(3) Calculate the stress-bracket correction factor using the equivalent stress calculated above.

(4) Calculate J-Applied for a given flaw depth, a, using equation (6).

Since the limiting material was assessed to be base metal, the Code Case requires the consideration of both axial and circumferential flaws. For axially oriented flaws, K_I calculated through LEFM methods can be used directly to calculate J-Applied as described above. For circumferentially oriented flaws, K_I is calculated using modified axial flaw results from the stress intensities calculated. They are stress intensity due to pressure, K_{Ip} and stress intensity due to temperature effects, K_{It}. Considering the required flaw depths for the Level C/D evaluation (≤ 1.0" depth), there is little, if any difference in the calculation of K_{It} in either the axial or circumferential direction. Further, the value of K_{It} is orientation independent and can be used directly. However, the K_{Ip} must be reduced by one-half, since the governing stress field in a

pressurized cylinder for circumferentially oriented flaws is known to be half that of the axially oriented flaw. With this adjustment, these K_I's are then summed into a $K_{I_{Total}}$ and used in the calculation of J-Applied for circumferential flaws.

The above approach was used to calculate the J-Applied for a range of crack depths, a, and as a function of transient time.

The material J-R curves were established using the Charpy model described in Section 5.0. Level C analysis utilized a lower bound curve (mean-2σ) while Level D analysis utilized mean properties, as recommended by ASME Code Case N-512 (Ref. 7). The J_d was evaluated over a range of USE values for the limiting flaw depth and utilized the computed crack tip temperature for each analysis time point. J_d was evaluated for both longitudinal and transverse Charpy orientations for assessment against axial and circumferential flaws, respectively.

The evaluation was performed to first identify the limiting time throughout the duration of the transient. The applied J-Integral was compared to J_d at each time point analyzed. Upon selection of the limiting time point, the Code Case N-512 criteria were evaluated to assess whether adequate margins were maintained.

The results of these analyses are discussed further in Section 8.0.

8.0 RESULTS AND CONCLUSIONS

Level A/B Service Loads

To assess the concern regarding the low upper-shelf energy material, the cooldown transient was analyzed using the methodologies recommended by ASME Code as described previously. The applied J-integral was predicted for a range of flaw sizes and compared to the J-deformation characteristics of the material to determine if the recommended criteria were satisfied.

The first criterion requires that the applied J-Integral be less than the J-Integral resistance of the material (J_d) given 0.1 inch of flaw growth. Figures 8.1 through 8.3 (A and B) depict the results obtained for reach of the analyzed vessel geometries. These figures provide the applied J-Integral for each flaw orientation along with the appropriate J-Integral resistance for the material. The applied J-Integral values, given 0.1 flaw extension, are summarized in Table 8.1 for convenience. The J-Integral resistance for the material (J_d) given 0.1 inch flaw extension are summarized as a function of USE in Table 8.2 for convenience.

The results show that the largest (limiting) applied J-Integral values of 564.9 in-lb/in^2 and 184.8 in-lb/in^2 corresponds to the 91.95 inch inside radius vessel for the axial and circumferential flaw orientations, respectively. Given an axially oriented flaw and comparing the J_d for the Charpy longitudinal orientation provided by Table 8.2, a value of 35.4 ft-lb longitudinal USE would provide the lower bound. This value substantially bounds the limiting material USE of 73 ft-lb for plates and 53 ft-lb for welds described in Section 5.0. An assessment of the circumferentially oriented flaw utilizing the J_d for the transverse orientation provides a bounding USE below 13 ft-lb transverse USE, again providing substantial margin for the limiting material USE of 48.5 ft-lb for plates and 53 ft-lb for welds described in Section 5.0.

The second criterion requires that the flaw be stable under Level A/B loadings. Figures 8.4A through 8.4C depict the applied J-Integral for an axial flaw, utilizing the requisite factor of safety, along with the J_d values corresponding to the longitudinal orientation. The criteria requires that the slope of the applied J-Integral be less than the slope of J_d at the point of intersection. Review of the limiting vessel geometry (Figure 8.4C) shows the bounding longitudinal USE to be approximately 38 ft-lb. Utilizing Figures 8.4D through 8.4F, flaw stability can be verified for the circumferential flaw providing a bounding transverse USE of approximately 13 ft-lb.

In summary, the Level A/B evaluation identified an axially oriented flaw with a corresponding longitudinal USE of approximately 38 ft-lbs as the bounding value. A circumferential flaw was shown to be acceptable for transverse USE as low as 13 ft-lb. Consequently, materials exhibiting greater than 38 ft-lbs from longitudinal Charpy impact tests and greater than 13 ft-lbs from transverse Charpy impact tests would meet Code Case N-512 requirements showing equivalent margins to ASME Code, Section III, Appendix G.

Level C Service Loadings

The results of the Level C transient evaluation are provided in Figures 8.5 to 8.7 (A and B). These figures depict the applied J-Integral at 0.1 inch flaw extension throughout the duration of the steam line break transient for both axial and circumferential flaws for each of the vessel geometries analyzed. In addition, the J-Integral resistance of the material (J_d) are also shown as a function of transient time for various Charpy USE values.

The first criterion given by Code Case N-512 is that the applied J-Integral be less than the J_d at a ductile flaw extension of 0.1 inch for the requisite loading. Review of Figures 8.5 to 8.7 (A and B) shows that the applied J-Integral for both the axial and circumferential flaw orientations are substantially below the values of J_d calculated for

the identified Charpy USE values. Therefore, the first criterion has adequately been met.

The second criterion is that flaw extension be stable and ductile. To assess flaw growth stability, potential initiation and postulated flaw extension have been reviewed. The maximum applied J-Integral for the steam line break transient is reported in Table 8.3 for each reactor vessel geometry analyzed for both axial and circumferential flaw orientations. The peak applied J-Integral are 137.5 and 113.5 in-lb/in^2 for an axial and circumferential flaw, respectively, corresponding to a vessel with a 86.96 inch inside radius. The J_{Ic} for this material was estimated in Section 5.0 and provided in Table 5.6. Utilizing the values estimated for the lower bound (mean-2σ) material, it was verified that initiation has not occurred (J_{Ic} values of 365.1 and 296.5 in-lb/in^2 for the longitudinal and transverse Charpy orientations) for the lowest USE values provided. Flaw stability was also verified at the time point with the smallest margin between the applied J-Integral and J_d for both axial and circumferential flaws using the previously applied graphical method. This is depicted graphically in Figures 8.8 to 8.10 (A and B). As for Level A/B, review shows that the slope of the applied J-Integral is less than the slope of the J_d at the point of intersection, hence, flaw stability has been verified for Level C transients.

In summary, the Level C evaluation has shown the Code Case N-512 criteria have been met. Materials with longitudinal and transverse Charpy USE values as low as 20 ft-lb and 13 ft-lb, respectively, are adequate to provide equivalent margins to ASME Code, Section III, Appendix G. Additional margin exists which could be used to justify lower Charpy values or increased loadings.

Level D Service Loadings

The steam line break transient and the feedwater line break transients were analyzed and assessed against Level D criteria.

The applied J-Integral and J_d for the steam line break are depicted as a function of transient time in Figures 8.11 to 8.13 (A and B). These figures provide results obtained for both axially and circumferentially oriented flaws. The resultant applied J-Integral is the same as the Level C analysis, however, the J_d is significantly higher due to the use of mean deformation properties. The initial time point during the transient coincides with the smallest margins.

The applied J-Integral for the axial and circumferential flaws and corresponding J_d values due to the feedwater line break transient are depicted in Figures 8.14 to 8.16 (A and B). The results are provided as a function of transient time.

The criteria for Level D analysis are (1) the flaw be stable given the possibility of ductile growth and (2) the flaw depth not exceed seventy-five percent of the vessel thickness, with the remaining ligament being safe from tensile instability.

To address flaw stability, the potential for flaw initiation and postulated flaw extension of 0.1 inch have been reviewed. The maximum loadings have been identified previously for the steam line break transient. The maximum applied J-Integral for the feedwater line break transient is provided in Table 8.4. These values are provided for each analyzed reactor vessel geometry and both axial and circumferential oriented flaws. The peak applied J-Integral are 69.1 and 17.2 in-lb/in^2 for an axial and circumferential flaw, respectively, and correspond to a vessel with an inside radius of 86.96 inches. Using the J_{Ic} values for mean properties provided by Table 5.6 (600.0 and 402.2 in-lb/in^2 for longitudinal and transverse Charpy orientations, respectively), it was verified that initiation does not occur. The applied J-Integral at 0.1 inch flaw extension under constant loading (factor of safety equal to 1.0) has been plotted against the mean J_d values over the range of flaw sizes at the time point with the smallest margin and are depicted in Figures 8.17 to 8.22 (A and B). Review of the slopes of the applied J- Integral and J_d at the point of intersection show no concern of unstable flaw growth. The criterion for the

remaining ligament to be safe from tensile instability is moot since initiation never occurs.

In summary, the Level D evaluation has demonstrated that the Code Case criteria have been met for materials with 20 ft-lb and 13 ft-lb Charpy USE for longitudinal and transverse orientation, respectively. Consequently, equivalent margins to ASME Code, Section III, Appendix G have been shown.

In conclusion, based on recommendations of ASME Code Case N-512, equivalent margins to ASME Code, Section III, Appendix G have been shown for CEOG reactor vessel materials. In addition, a lower bound corresponding to 38 ft-lb longitudinal Charpy USE has been identified.

TABLE 8.1

Cooldown Level A/B Transient

Peak Applied J-Integral @ 0.1 Inch Flaw Extension

Vessel I.R (in)	Crack Depth @ 0.1 in Extension (in)	Applied J-Integral (in-lb/in^2)	
		Axial Flaw	Circumferential Flaw
70.64	1.781	349.6	105.2
86.96	2.156	489.7	158.5
91.95	2.365	564.9	184.8

TABLE 8.2

Cooldown Level A/B Transient

J_d @ 0.1 Inch Flaw Extension

Longitudinal USE (ft-lb)	J_d Longitudinal Orientation (in-lb/in^2)	Corresponding Transverse USE (ft-lb)	J_d Transverse Orientation (in-lb/in$_2$)
20	357.8	13	253.3
25	427.9	16.25	302.9
30	495.2	19.5	350.6
35	560.3	22.75	396.7
40	623.6	26.0	441.5
45	685.4	29.25	485.2
50	745.8	32.5	528.0
55	805.0	35.75	569.9
60	863.2	39.0	611.1

TABLE 8.3

SLB Level C/D Transient

Peak Applied J-Integral @ 0.1 Inch Flaw Extension

Vessel I.R (in.)	Applied J-Integral (in-lb/in^2)	
	Axial Flaw	Circumferential Flaw
70.64	123.3	99.1
86.96	137.5	113.5
91.95	129.5	107.9

TABLE 8.4

FLB Level D Transient

Peak Applied J-Integral @ 0.1 Inch Flaw Extension

Vessel I.R (in.)	Applied J-Integral (in-lb/in^2)	
	Axial Flaw	Circumferential Flaw
70.64	67.7	16.9
86.96	69.1	17.2
91.95	54.9	13.7

FIGURE 8.1A

J-INTEGRAL VS. CRACK DEPTH
100 F/HR CD, PRESSURE = 2750 psia
AXIAL FLAW ORIENTATION, LEVEL A, PLATE MATERIAL

VESSEL SIZE: NOMINAL ID = 140 in, BELTLINE THICKNESS = 7.125 in
FLAW GROWTH

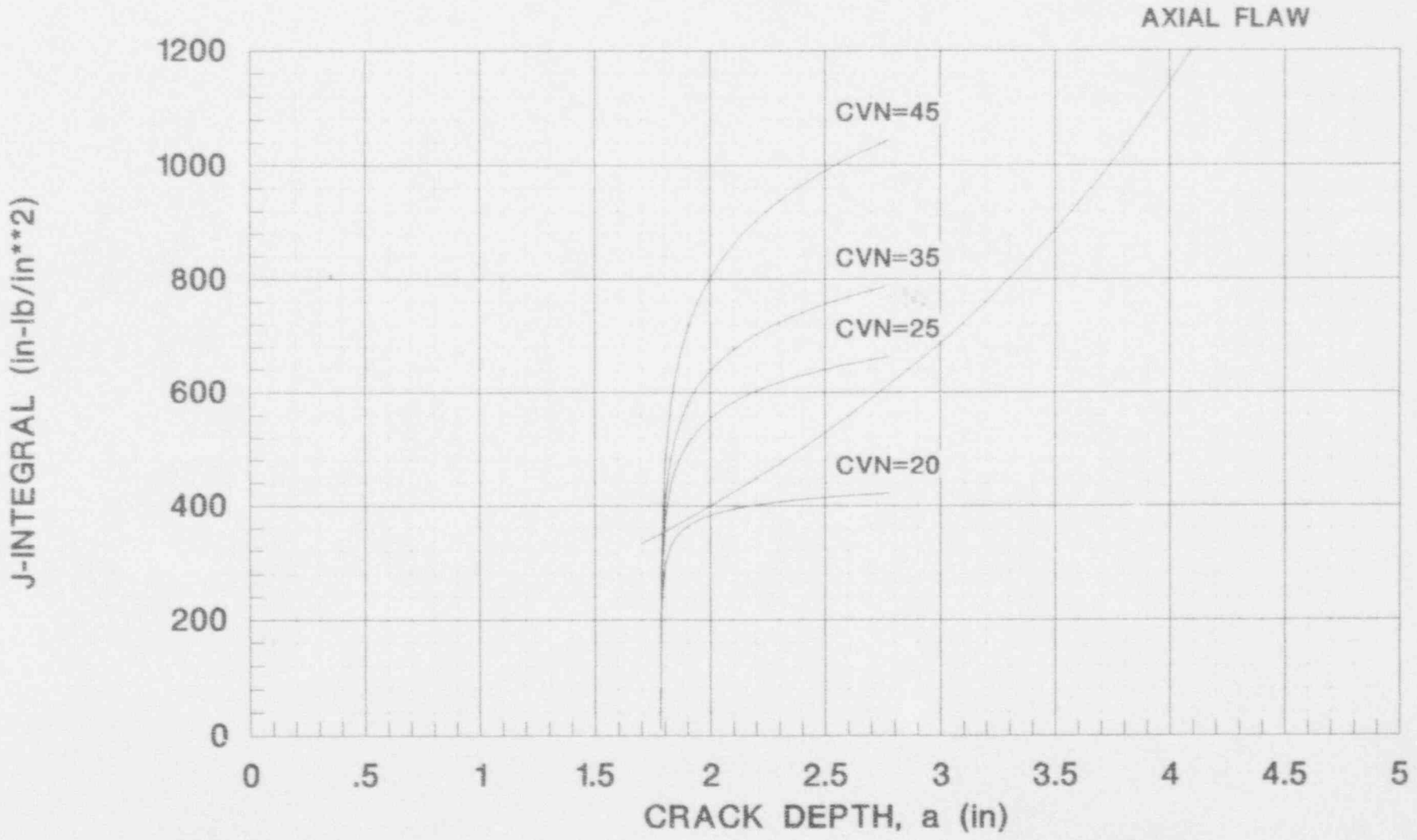

FIGURE 8.1B

J-INTEGRAL VS. CRACK DEPTH
100 F/HR CD, PRESSURE = 2750 psia
CIRC FLAW ORIENTATION, LEVEL A, PLATE MATERIAL

VESSEL SIZE: NOMINAL ID = 140 In, BELTLINE THICKNESS = 7.125 In
FLAW GROWTH

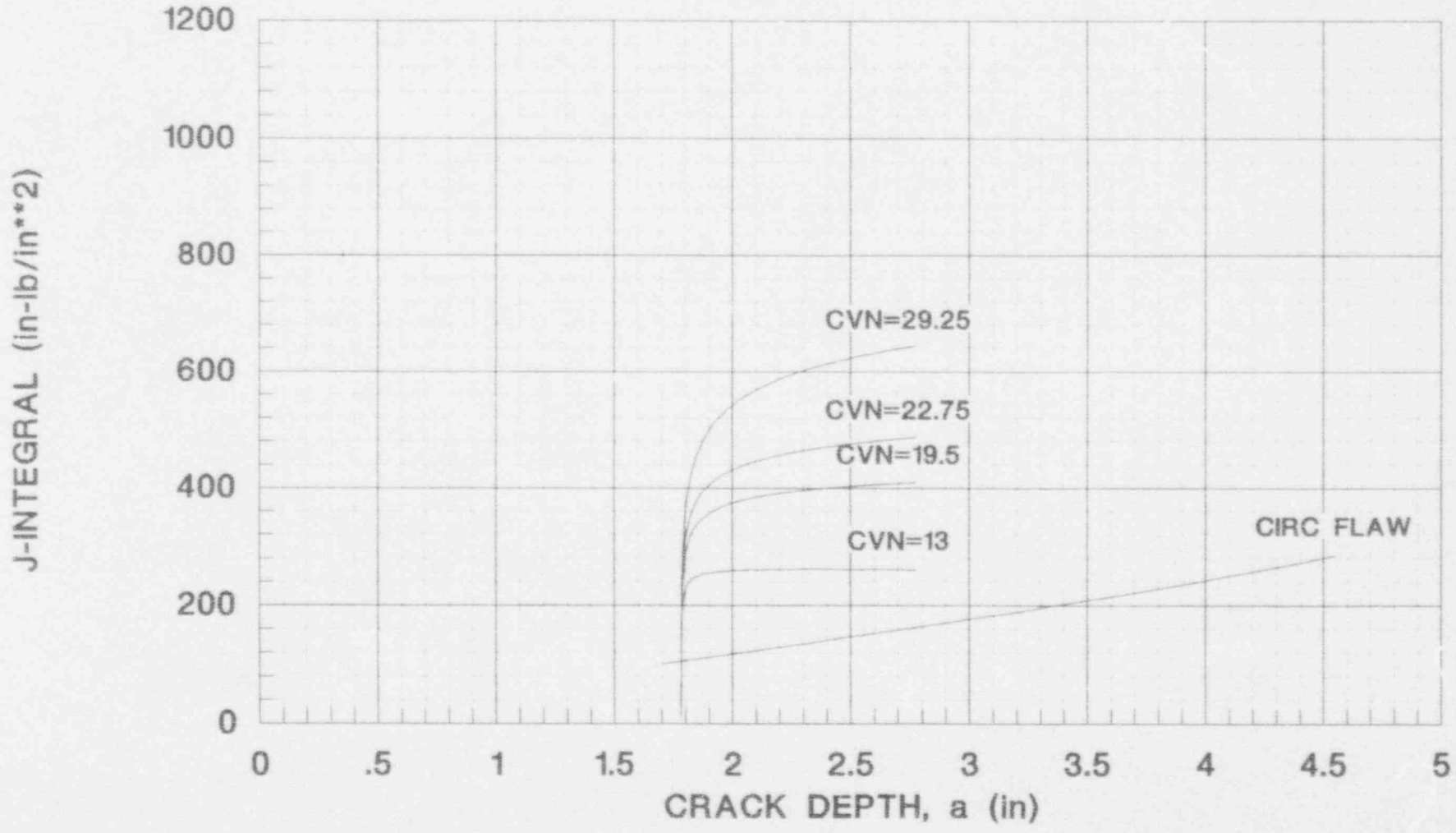

FIGURE 8.2A

J-INTEGRAL VS. CRACK DEPTH
100 F/HR CD, PRESSURE = 2750 psia
AXIAL FLAW ORIENTATION, LEVEL A, PLATE MATERIAL

VESSEL SIZE: NOMINAL ID = 172 In, BELTLINE THICKNESS = 8.625 In
FLAW GROWTH

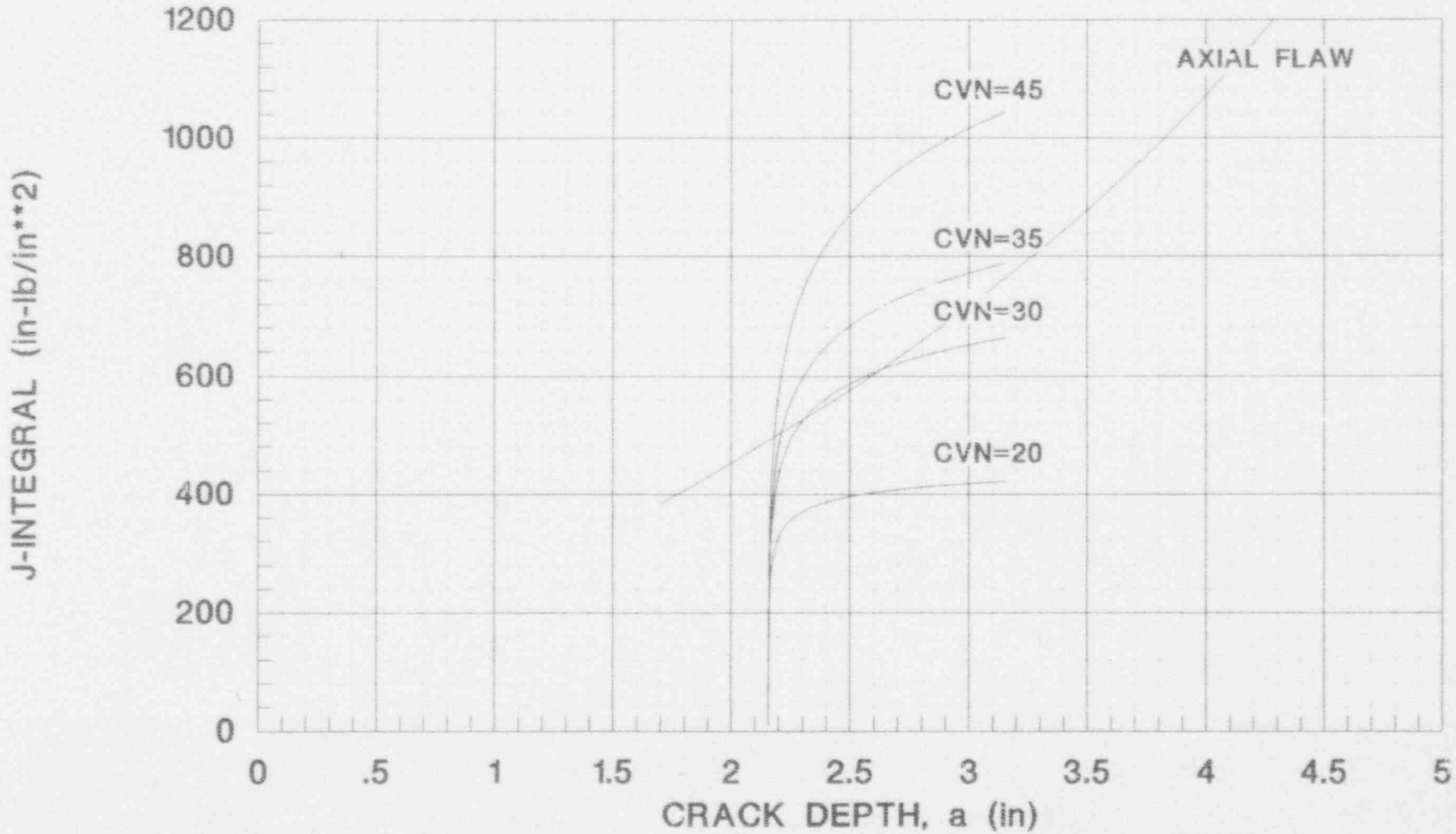

FIGURE 8.2B

J-INTEGRAL VS. CRACK DEPTH
100 F/HR CD, PRESSURE = 2750 psia
CIRC FLAW ORIENTATION, LEVEL A, PLATE MATERIAL

VESSEL SIZE: NOMINAL ID = 172 In, BELTLINE THICKNESS = 8.625 In
FLAW GROWTH

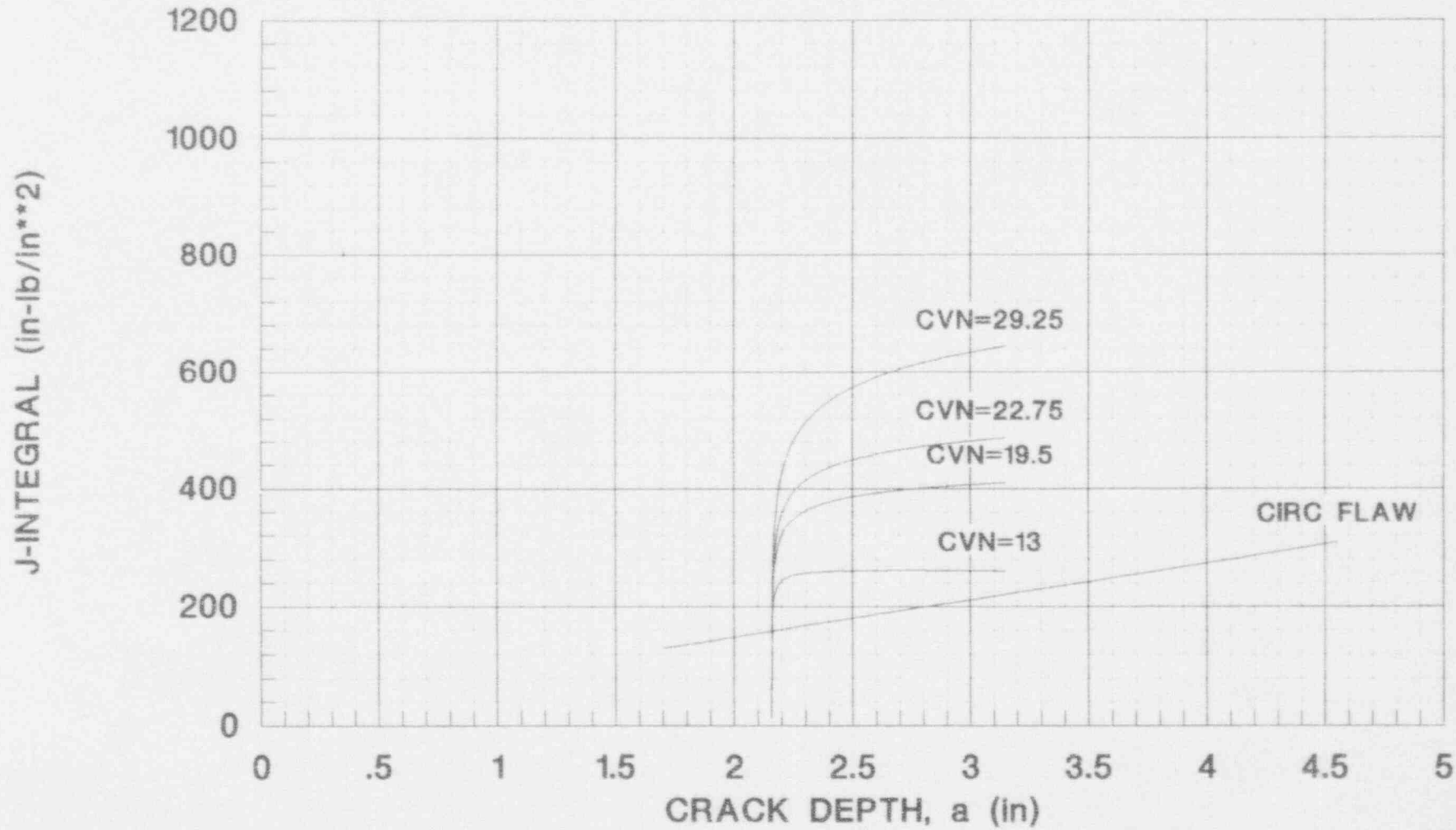

FIGURE 8.3A
J-INTEGRAL VS. CRACK DEPTH
100 F/HR CD, PRESSURE = 2750 psia
AXIAL FLAW ORIENTATION, LEVEL A, PLATE MATERIAL

VESSEL SIZE: NOMINAL ID = 182 In, BELTLINE THICKNESS = 9.06 In
FLAW GROWTH

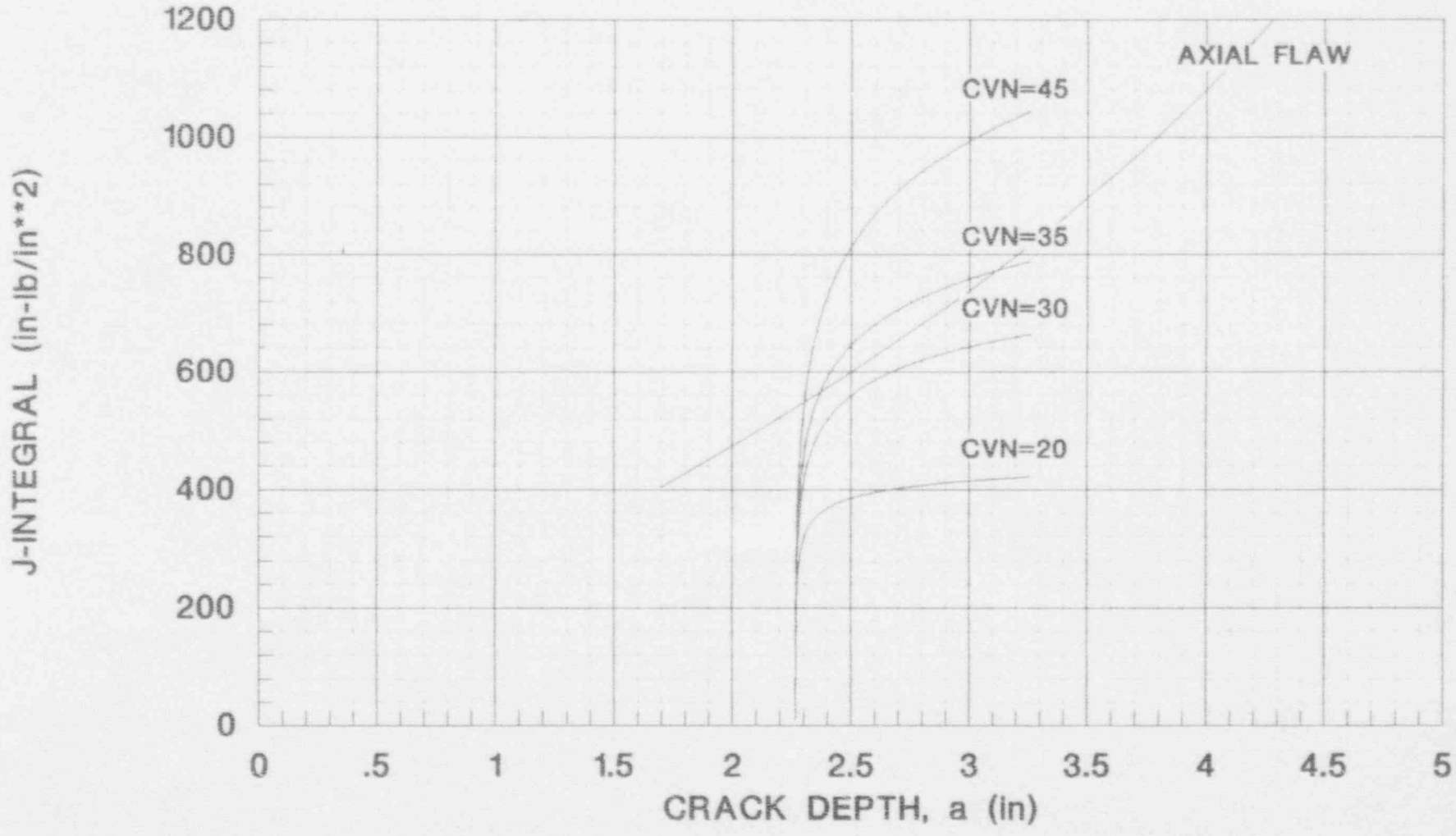

FIGURE 8.3B
J-INTEGRAL VS. CRACK DEPTH
100 F/HR CD, PRESSURE = 2750 psia
CIRC FLAW ORIENTATION, LEVEL A, PLATE MATERIAL

VESSEL SIZE: NOMINAL ID = 182 In, BELTLINE THICKNESS = 9.06 In
FLAW GROWTH

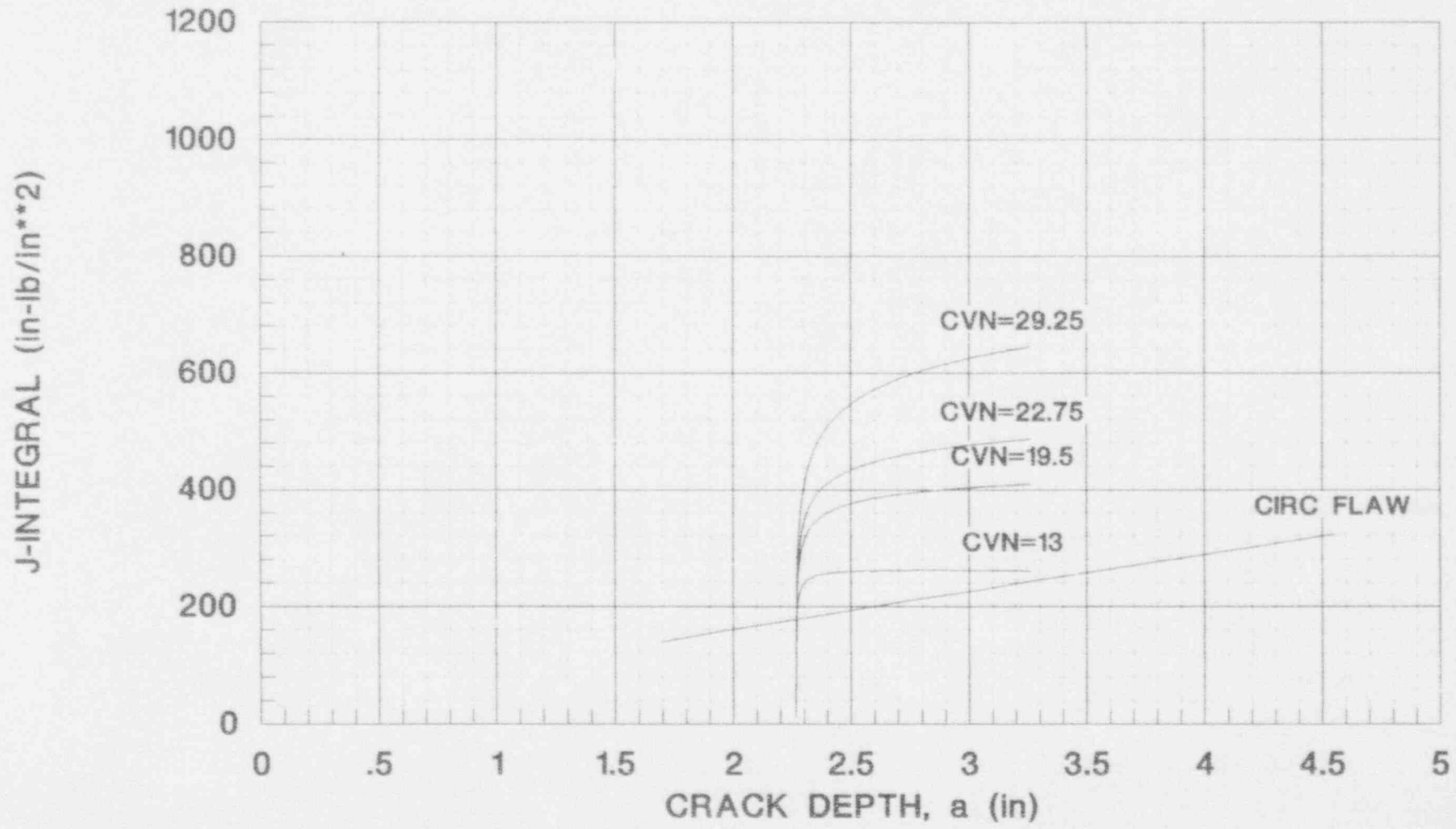

FIGURE 8.4A

J-INTEGRAL VS. CRACK DEPTH
100 F/HR CD, PRESSURE = 2750 psia
AXIAL FLAW ORIENTATION, LEVEL A, PLATE MATERIAL

VESSEL SIZE: NOMINAL ID = 140 In, BELTLINE THICKNESS = 7.125 In
FLAW STABILITY

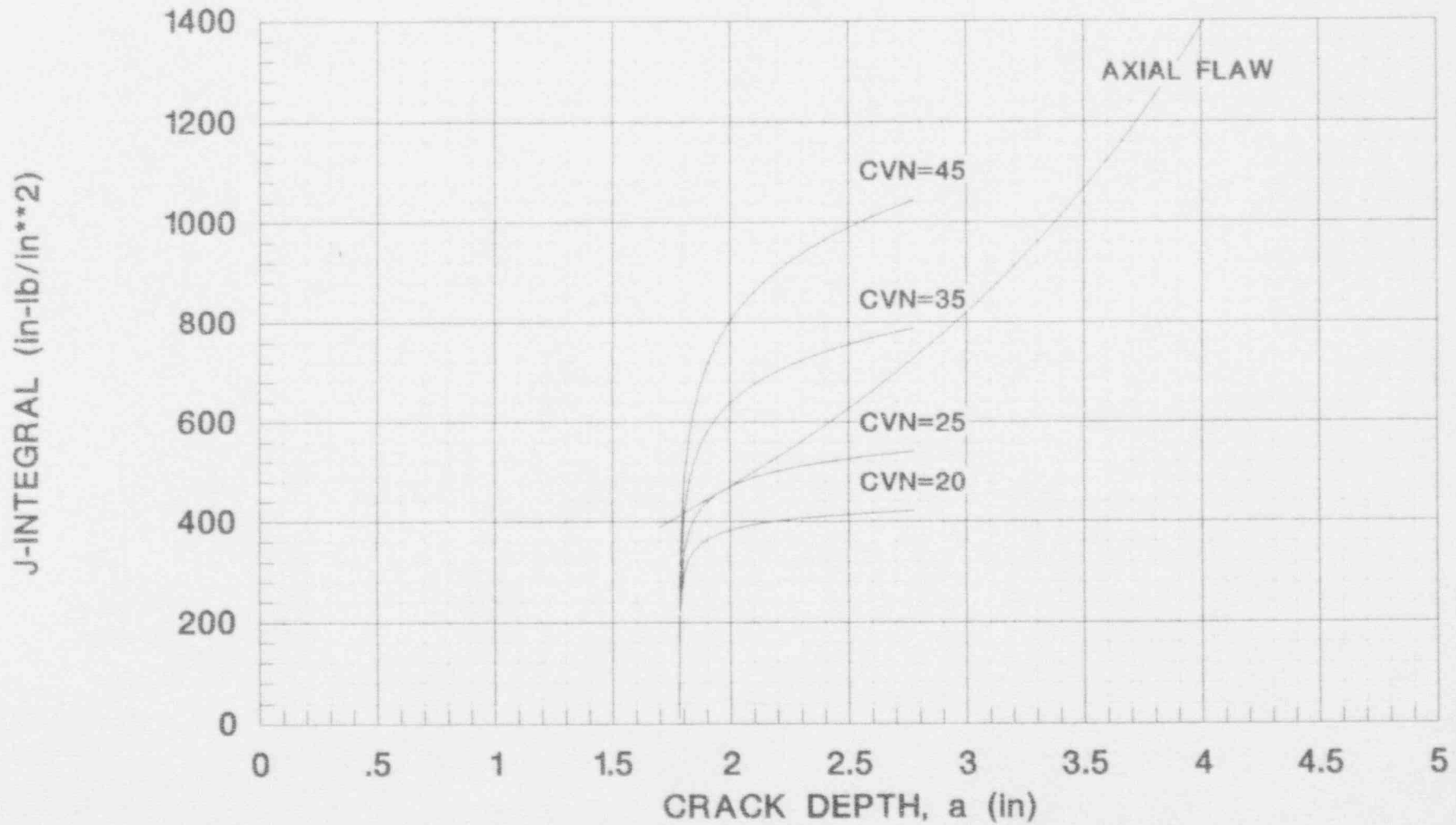

FIGURE 8.4B

J-INTEGRAL VS. CRACK DEPTH
100 F/HR CD, PRESSURE = 2750 psia
AXIAL FLAW ORIENTATION, LEVEL A, PLATE MATERIAL

VESSEL SIZE: NOMINAL ID = 172 in, BELTLINE THICKNESS = 8.625 in
FLAW STABILITY

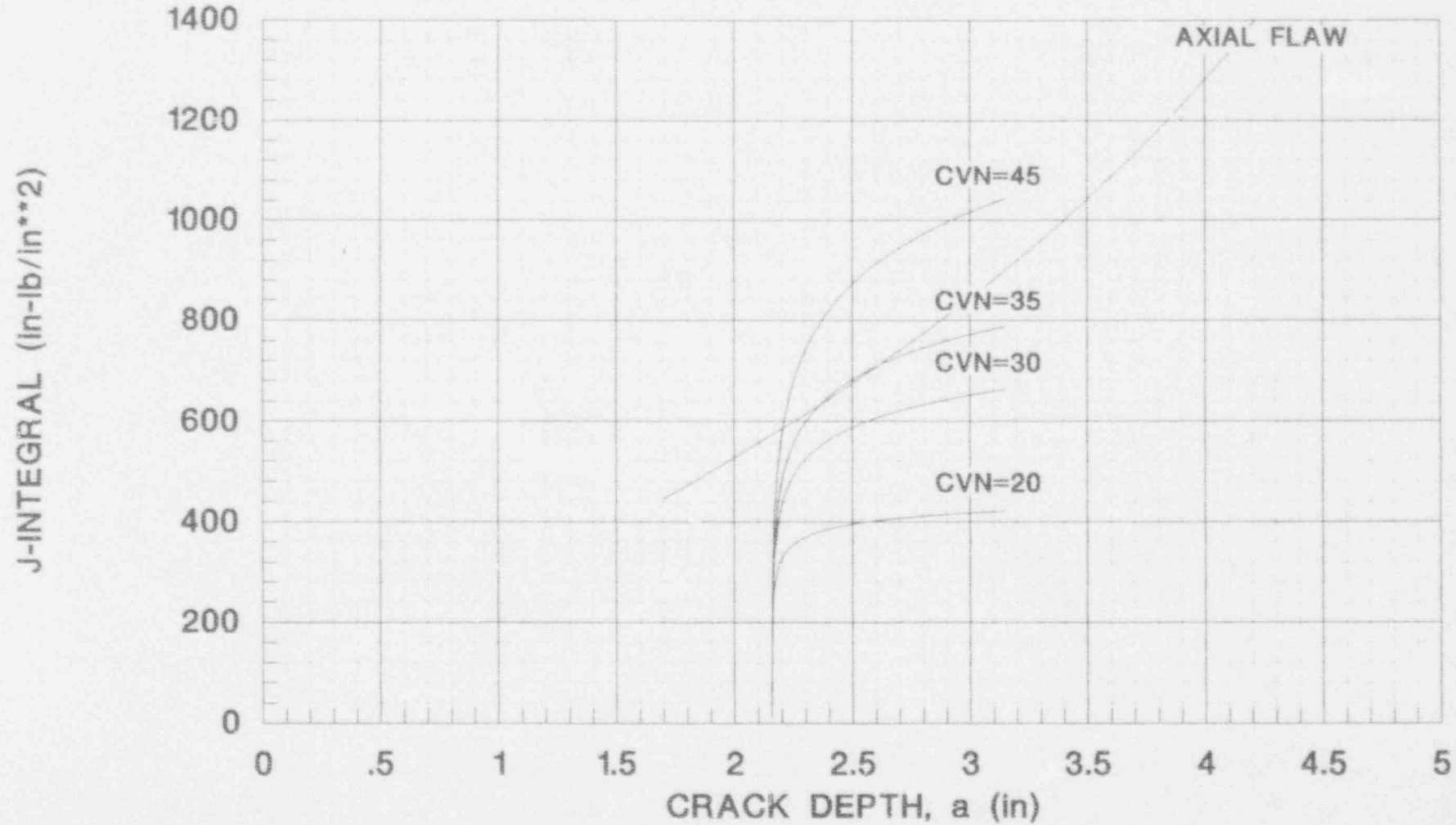

FIGURE 8.4C
J-INTEGRAL VS. CRACK DEPTH
100 F/HR CD, PRESSURE = 2750 psia
AXIAL FLAW ORIENTATION, LEVEL A, PLATE MATERIAL

VESSEL SIZE: NOMINAL ID = 182 In, BELTLINE THICKNESS = 9.06 In
FLAW STABILITY

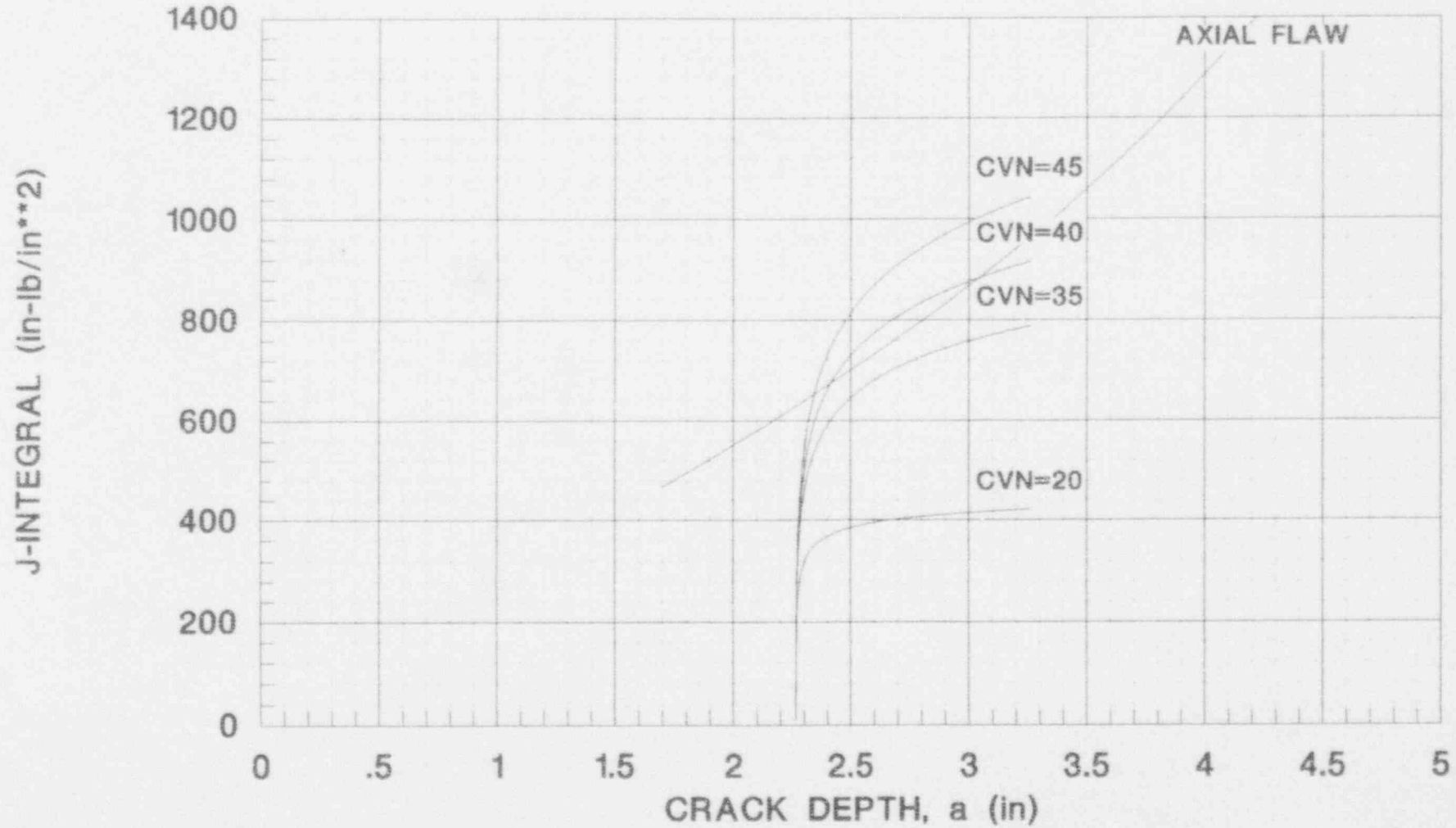

FIGURE 8.4D
J-INTEGRAL VS. CRACK DEPTH
100 F/HR CD, PRESSURE = 2750 psia
CIRC. FLAW ORIENTATION, LEVEL A, PLATE MATERIAL

VESSEL SIZE: NOMINAL ID = 140 In, BELTLINE THICKNESS = 7.125 In
FLAW STABILITY

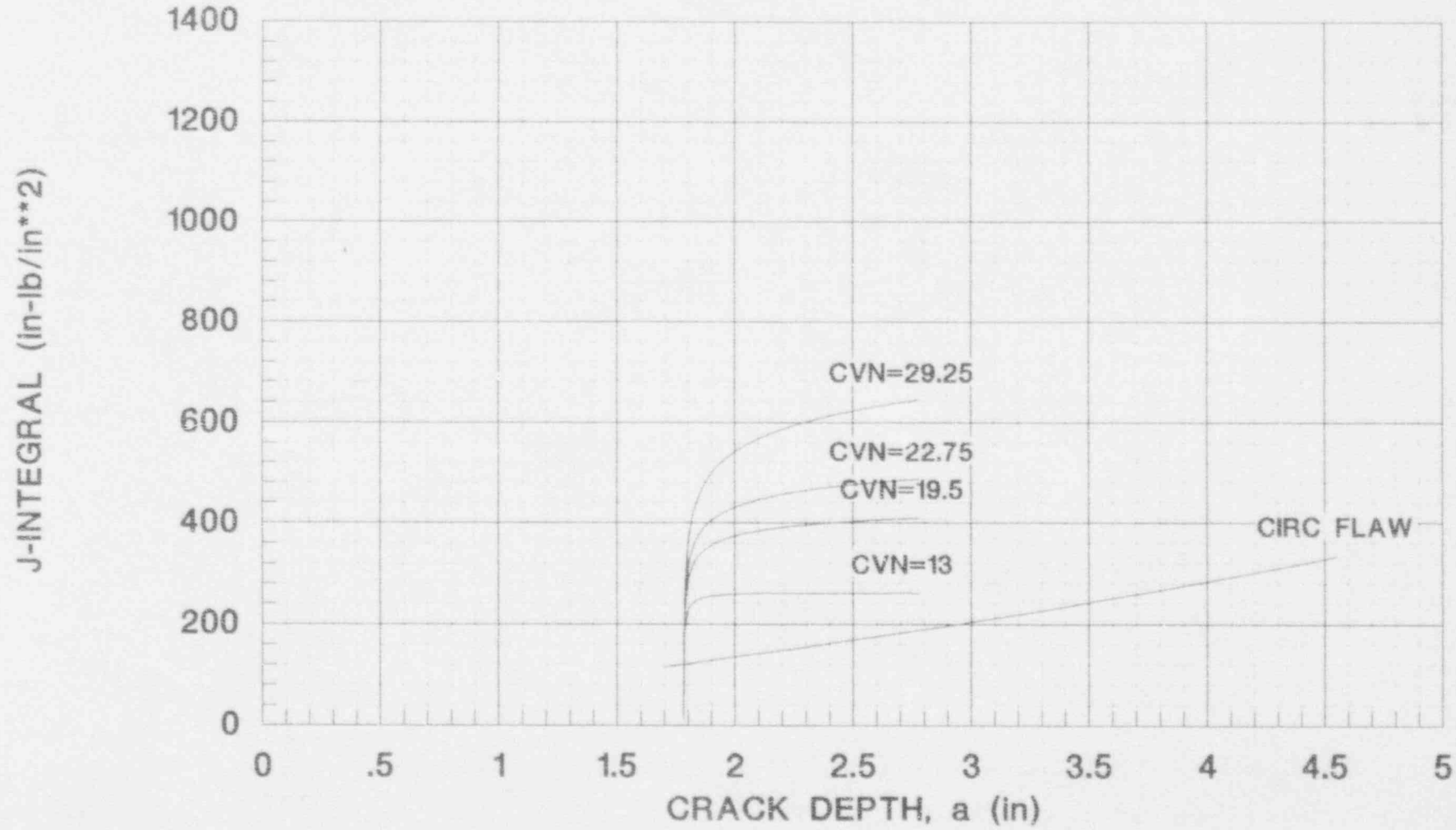

FIGURE 8.4E
J-INTEGRAL VS. CRACK DEPTH
100 F/HR CD, PRESSURE = 2750 psia
CIRC. FLAW ORIENTATION, LEVEL A, PLATE MATERIAL

VESSEL SIZE: NOMINAL ID = 172 In, BELTLINE THICKNESS = 8.625 In
FLAW STABILITY

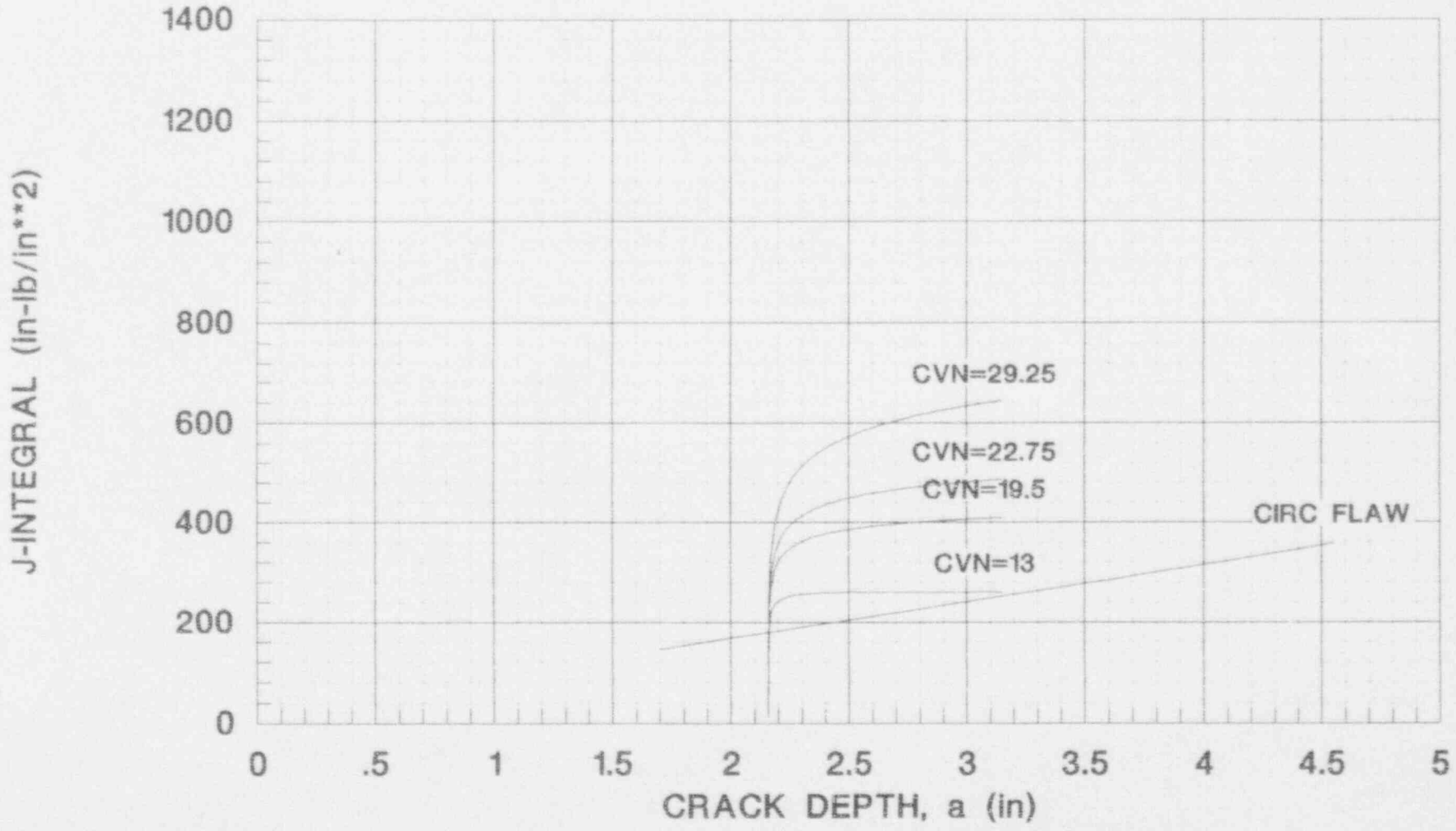

FIGURE 8.4F
J-INTEGRAL VS. CRACK DEPTH
100 F/HR CD, PRESSURE = 2750 psia
CIRC. FLAW ORIENTATION, LEVEL A, PLATE MATERIAL

VESSEL SIZE: NOMINAL ID = 182 In, BELTLINE THICKNESS = 9.06 In
FLAW STABILITY

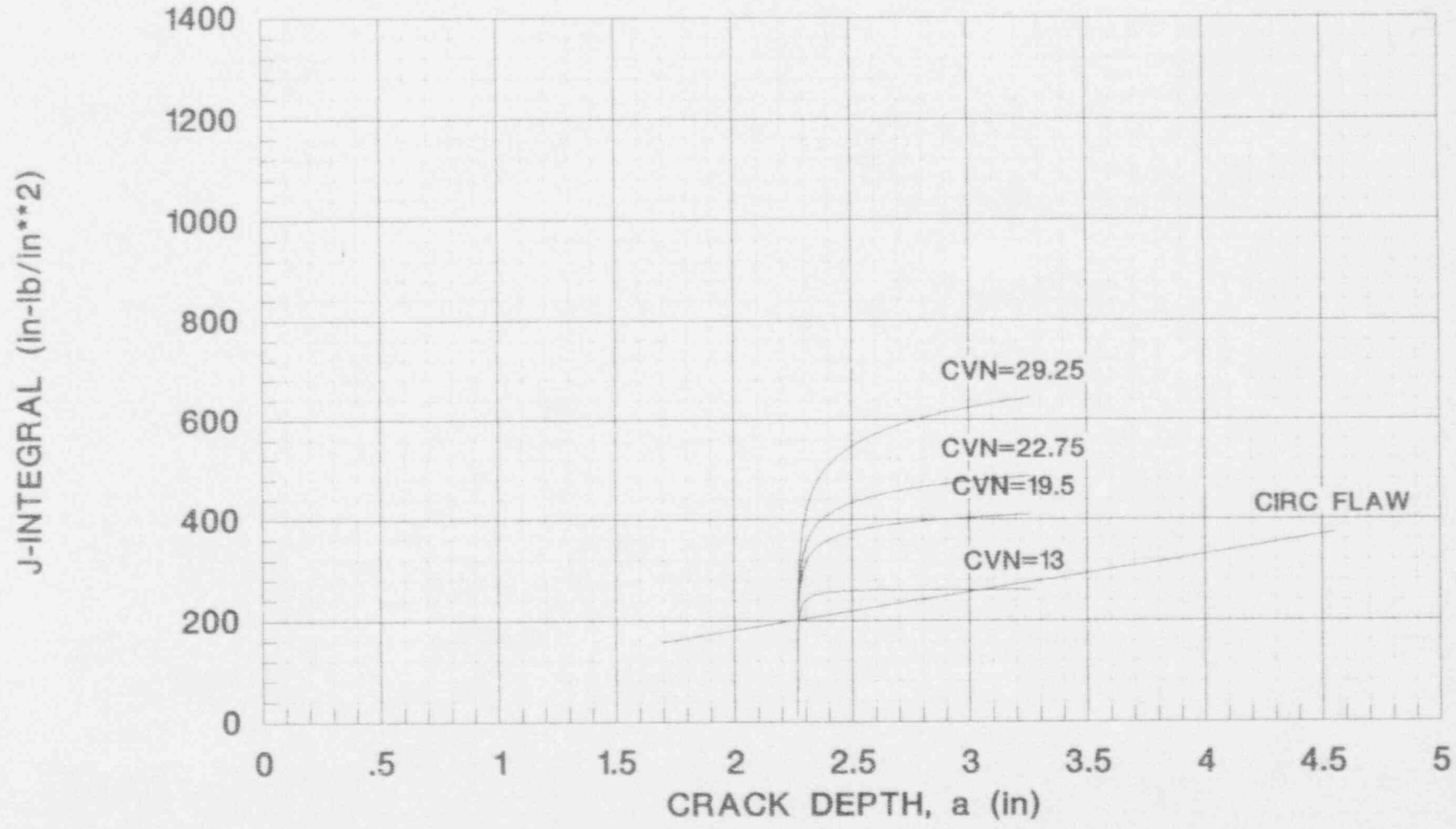

FIGURE 8.5A
J-INTEGRAL VS. TIME
STEAM LINE BREAK
AXIAL FLAW ORIENTATION, LEVEL C, PLATE MATERIAL

VESSEL SIZE: NOMINAL ID = 140 In, CLAD THICKNESS = 0.2188 In
BELTLINE THICKNESS = 7.125 In

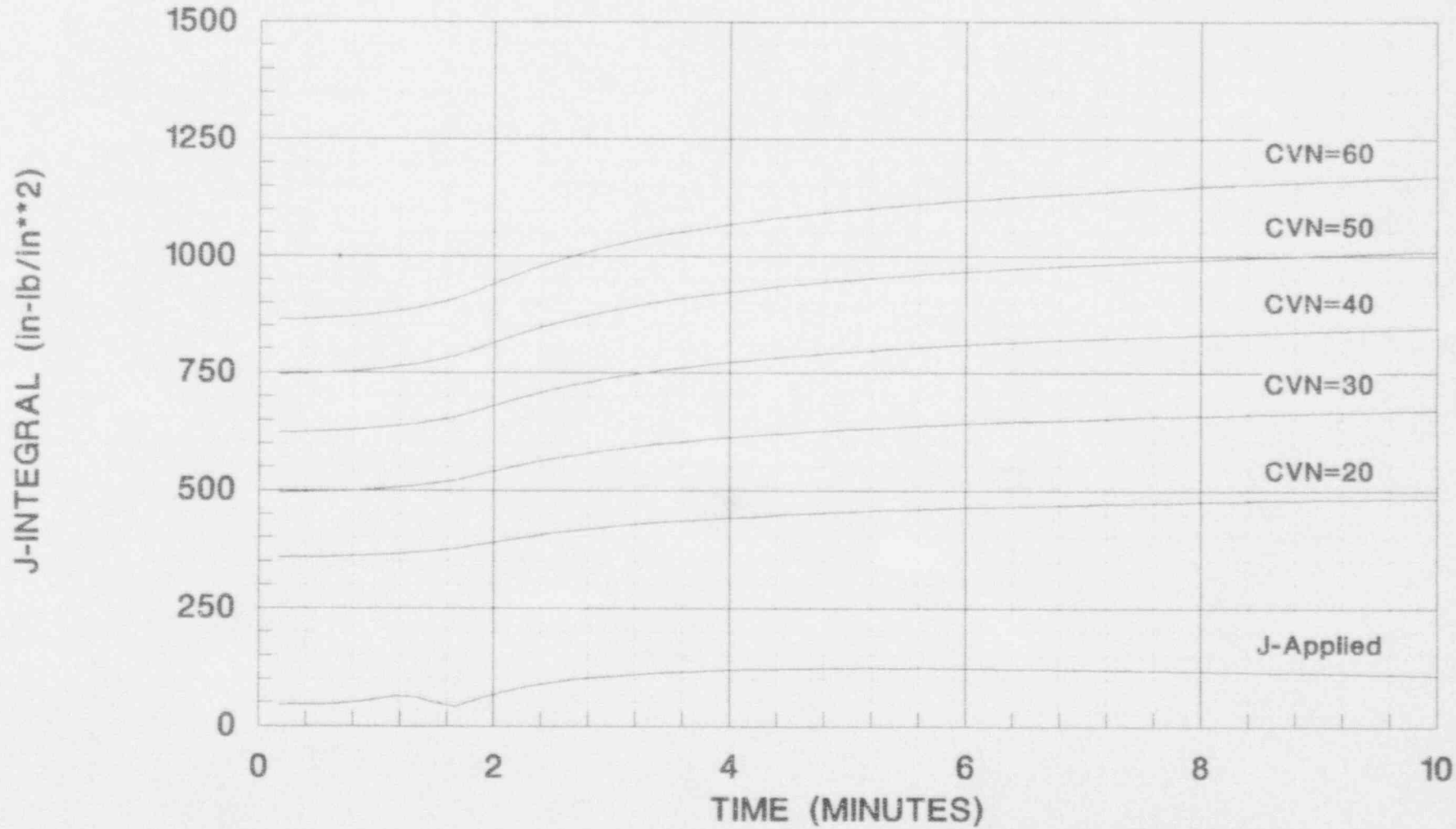

FIGURE 8.5B
J-INTEGRAL VS. TIME
STEAM LINE BREAK
CIRC. FLAW ORIENTATION, LEVEL C, PLATE MATERIAL

VESSEL SIZE: NOMINAL ID = 140 in, CLAD THICKNESS = 0.2188 in
BELTLINE THICKNESS = 7.125 in

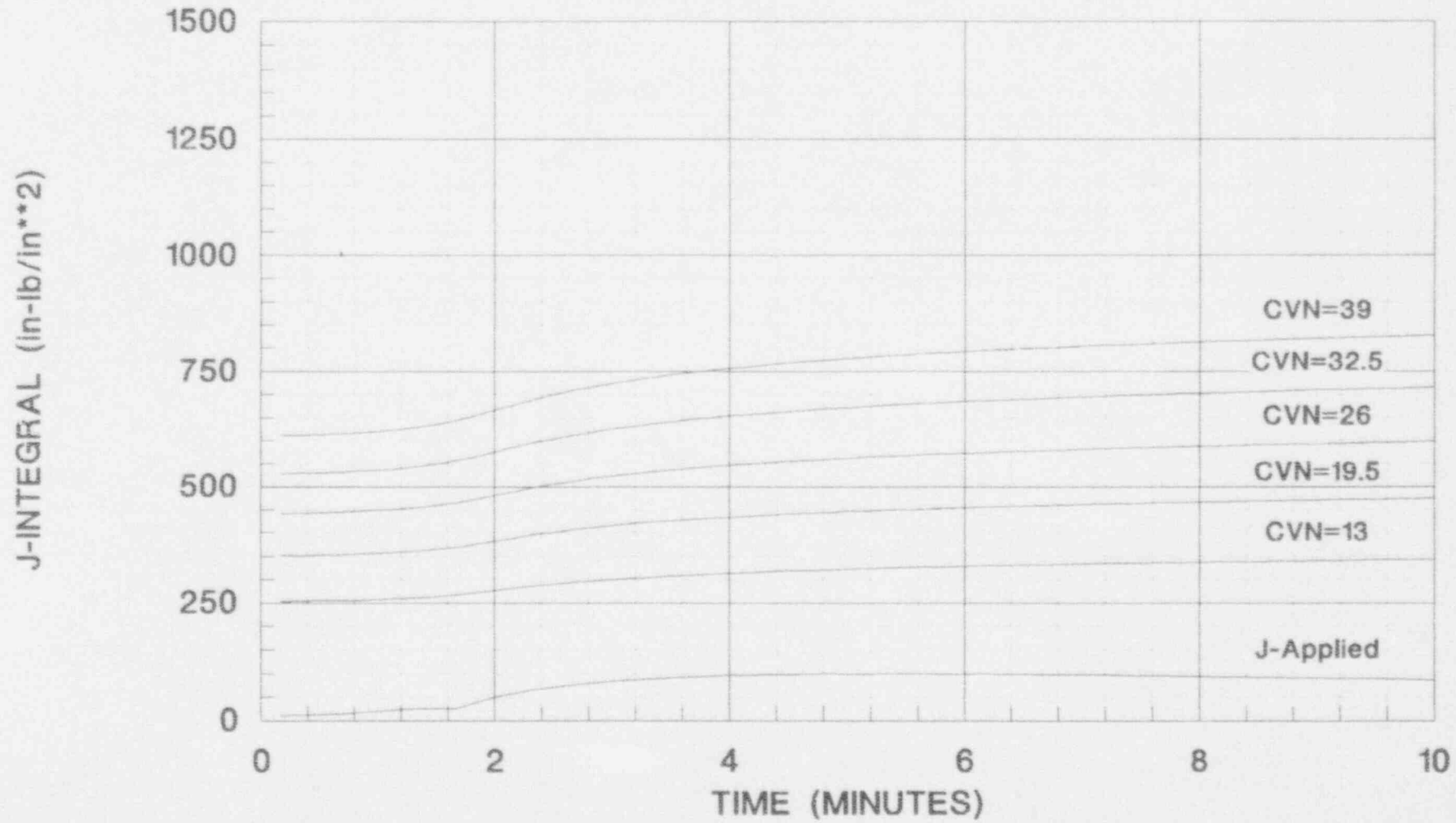

FIGURE 8.6A
J-INTEGRAL VS. TIME
STEAM LINE BREAK
AXIAL FLAW ORIENTATION, LEVEL C, PLATE MATERIAL

VESSEL SIZE: NOMINAL ID = 172 In, CLAD THICKNESS = 0.3125 In
BELTLINE THICKNESS = 8.625 In

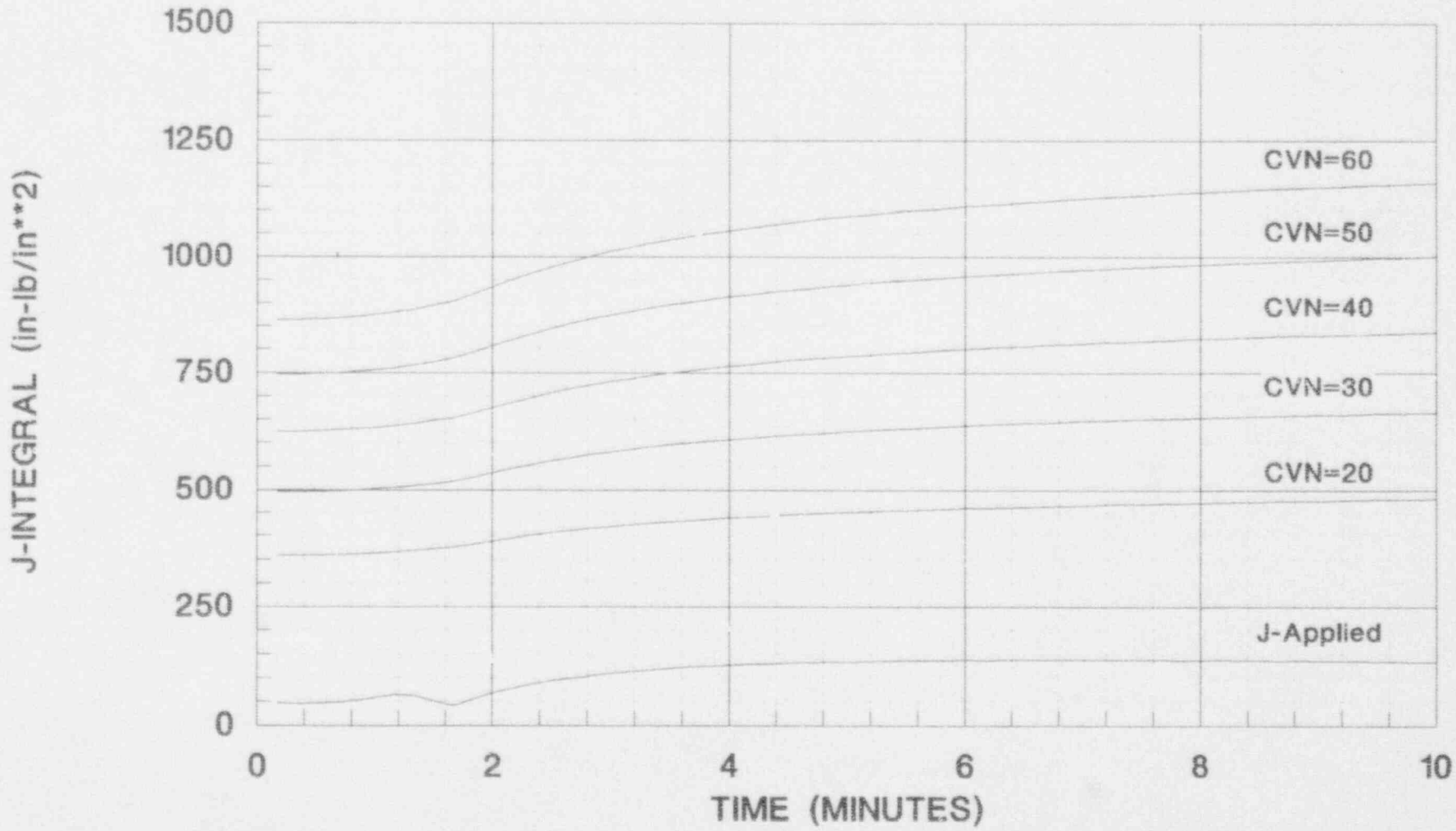

FIGURE 8.6B
J-INTEGRAL VS. TIME
STEAM LINE BREAK
CIRC. FLAW ORIENTATION, LEVEL C, PLATE MATERIAL

VESSEL SIZE: NOMINAL ID = 172 In, CLAD THICKNESS = 0.3125 In
BELTLINE THICKNESS = 8.625 In

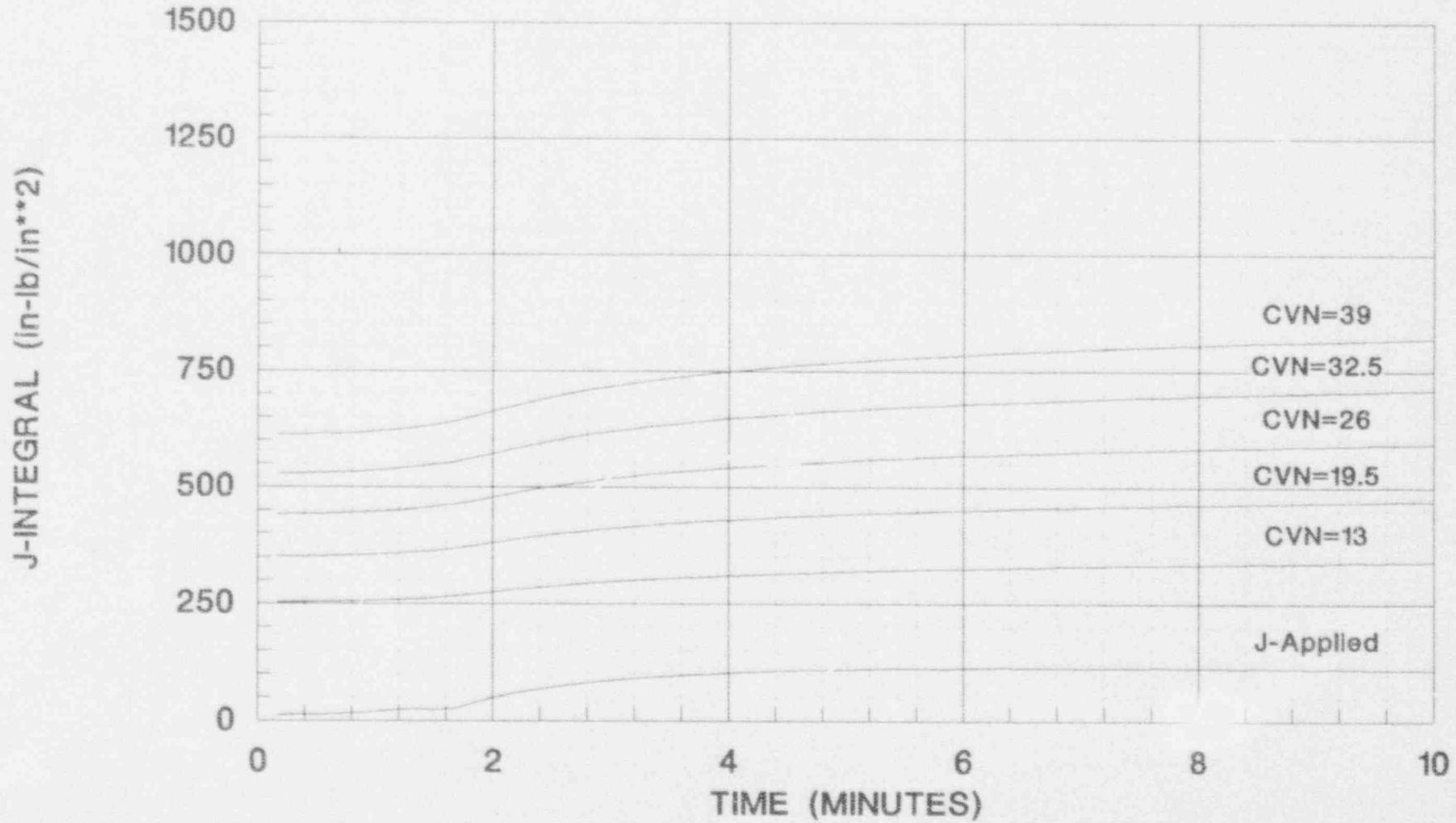

FIGURE 8.7A
J-INTEGRAL VS. TIME
STEAM LINE BREAK
AXIAL FLAW ORIENTATION, LEVEL C, PLATE MATERIAL

VESSEL SIZE: NOMINAL ID = 182 in, CLAD THICKNESS = 0.16 in
BELTLINE THICKNESS = 9.06 in

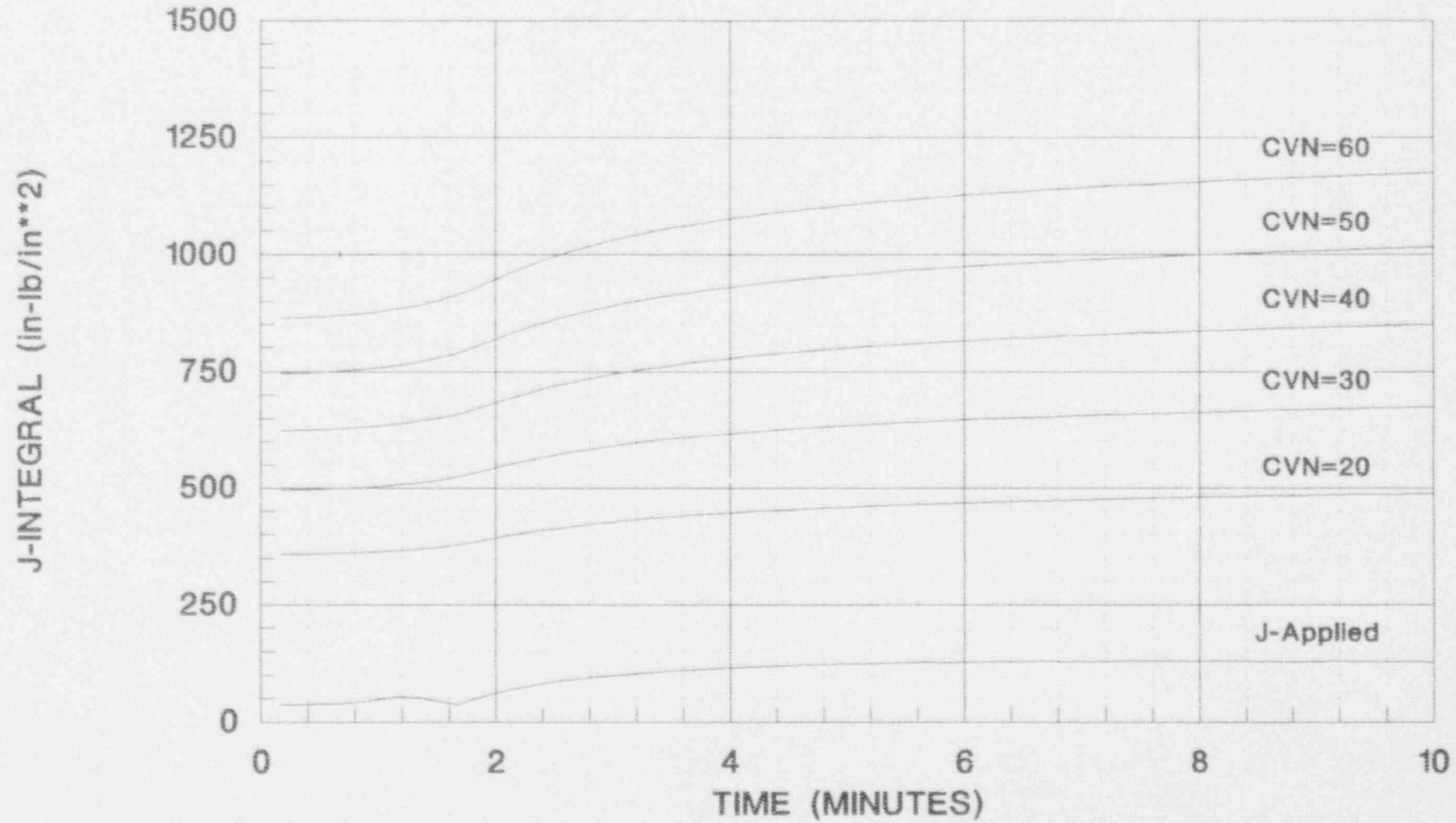

FIGURE 8.7B
J-INTEGRAL VS. TIME
STEAM LINE BREAK
CIRC. FLAW ORIENTATION, LEVEL C, PLATE MATERIAL

VESSEL SIZE: NOMINAL ID = 182 in, CLAD THICKNESS = 0.16 in
BELTLINE THICKNESS = 9.06 in

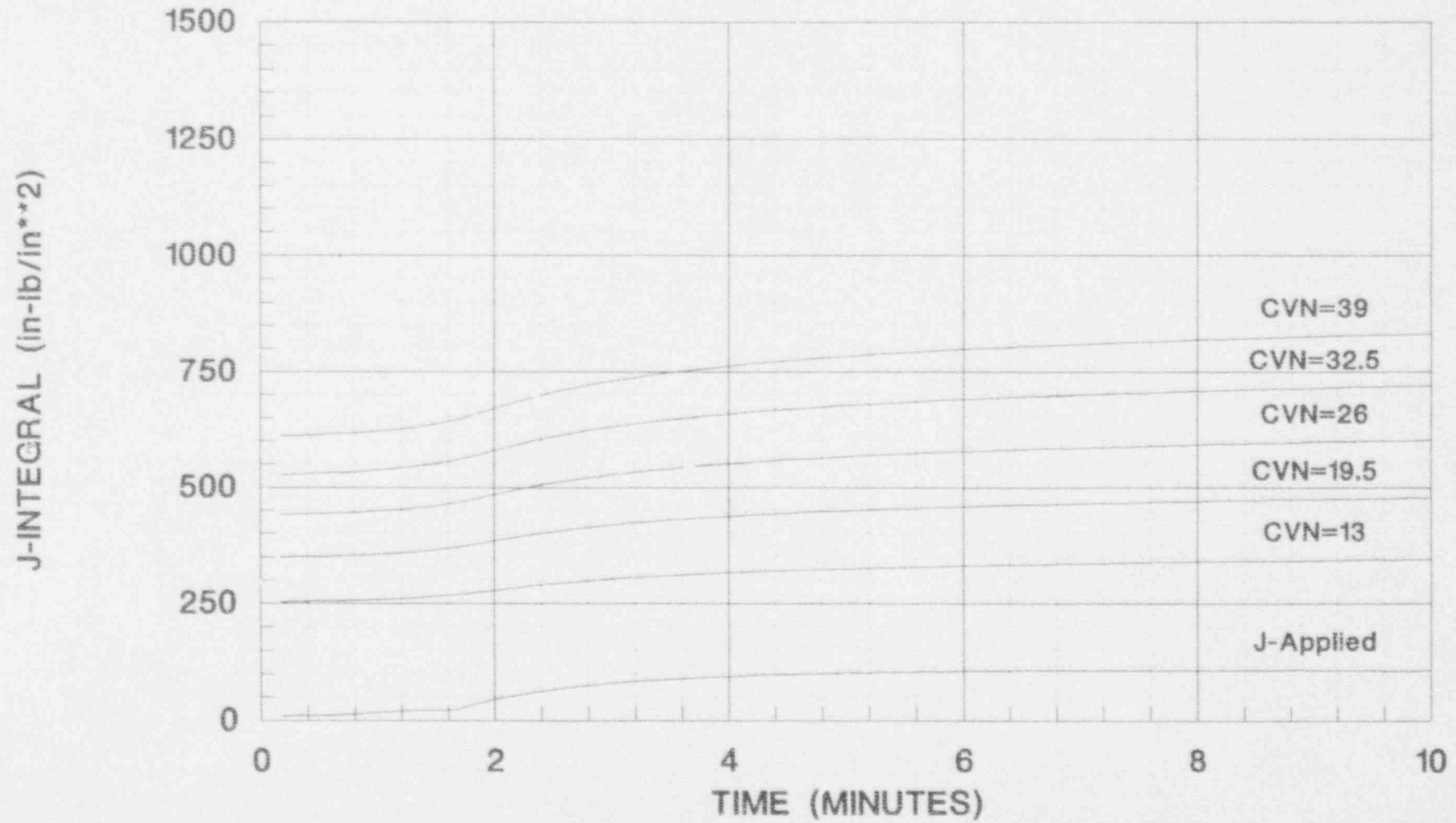

FIGURE 8.8A
J-INTEGRAL VS. CRACK DEPTH
STEAM LINE BREAK
AXIAL FLAW ORIENTATION, LEVEL C, PLATE MATERIAL

VESSEL SIZE: NOMINAL ID = 140 in, BELTLINE THICKNESS = 7.125 in
FLAW GROWTH

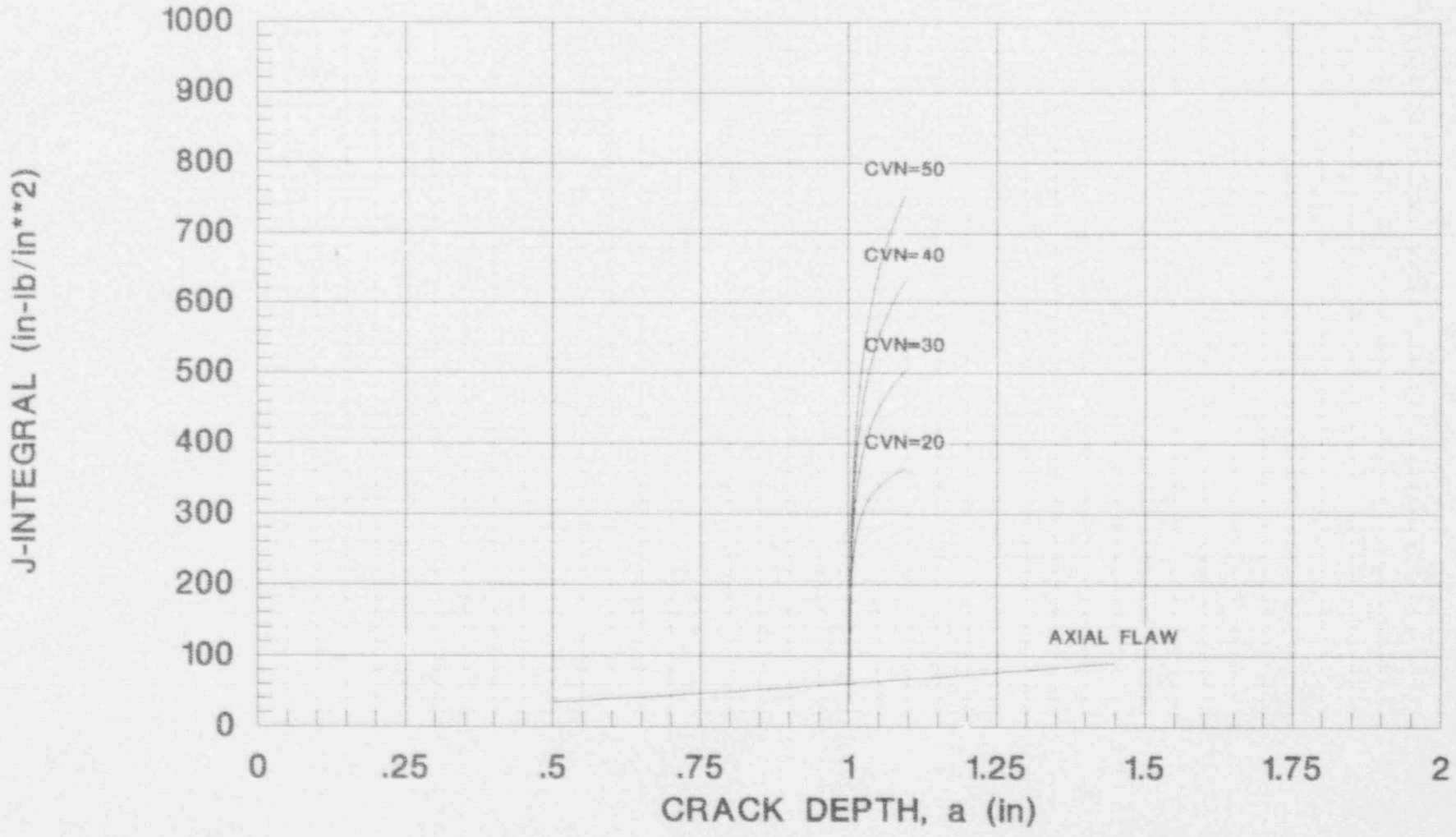

FIGURE 8.8B
J-INTEGRAL VS. CRACK DEPTH
STEAM LINE BREAK
CIRC FLAW ORIENTATION, LEVEL C, PLATE MATERIAL

VESSEL SIZE: NOMINAL ID = 140 in, BELTLINE THICKNESS = 7.125 in
FLAW GROWTH

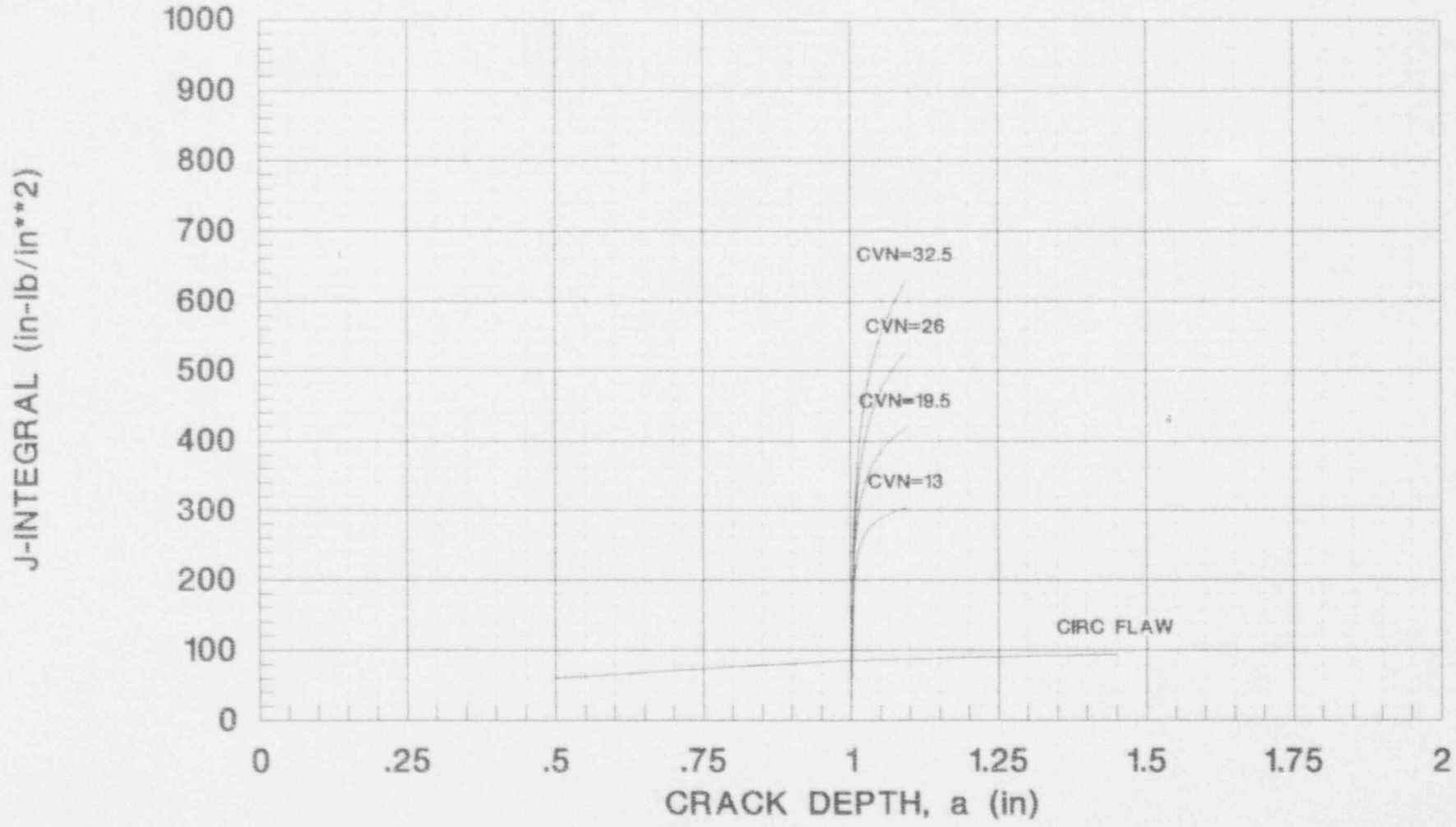

FIGURE 8.9A
J-INTEGRAL VS. CRACK DEPTH
STEAM LINE BREAK
AXIAL FLAW ORIENTATION, LEVEL C, PLATE MATERIAL

VESSEL SIZE: NOMINAL ID = 172 in, BELTLINE THICKNESS = 8.625 in
FLAW GROWTH

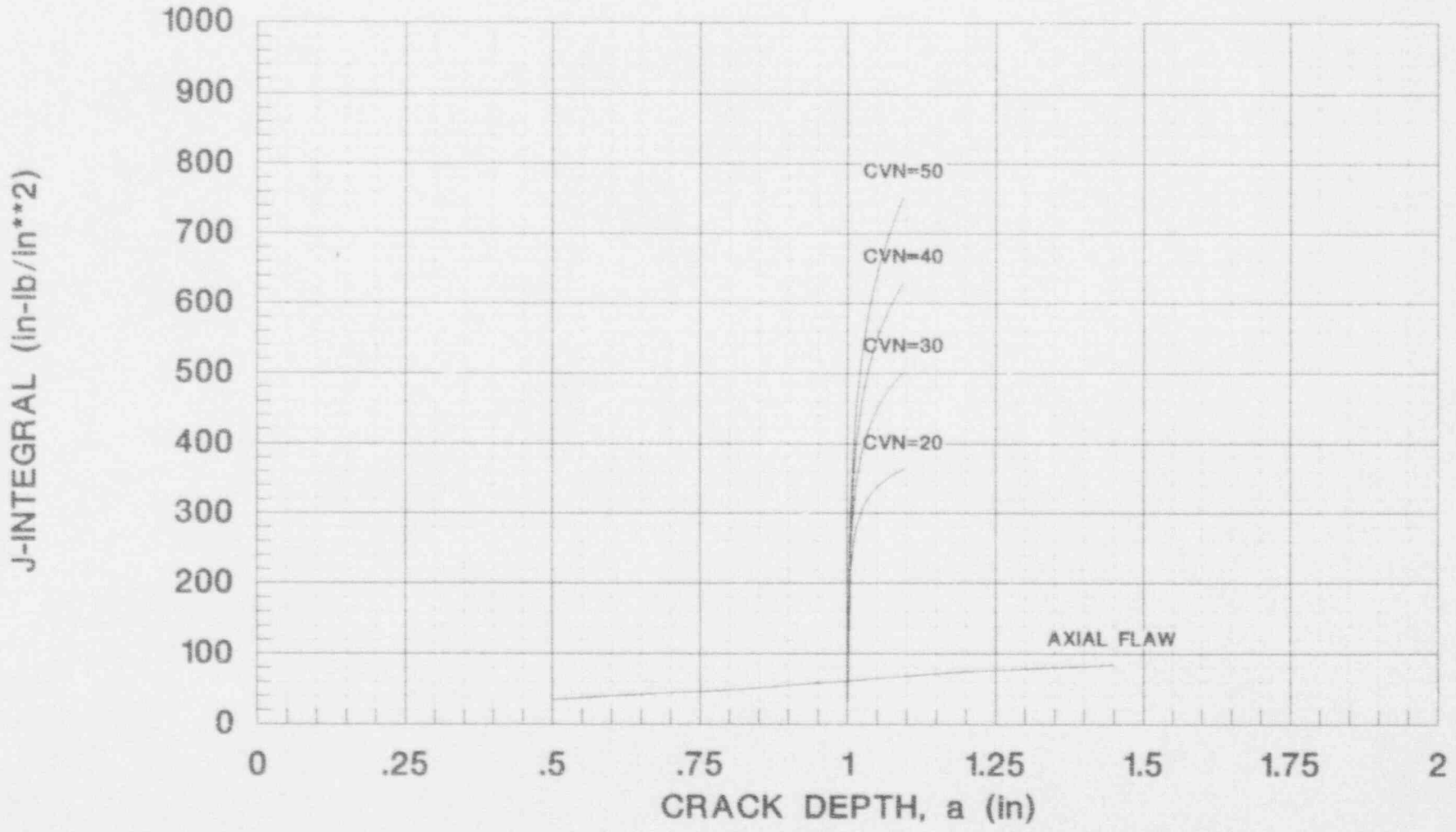

FIGURE 8.9B
J-INTEGRAL VS. CRACK DEPTH
STEAM LINE BREAK
CIRC FLAW ORIENTATION, LEVEL C, PLATE MATERIAL

VESSEL SIZE: NOMINAL ID = 172 In, BELTLINE THICKNESS = 8.625 In
FLAW GROWTH

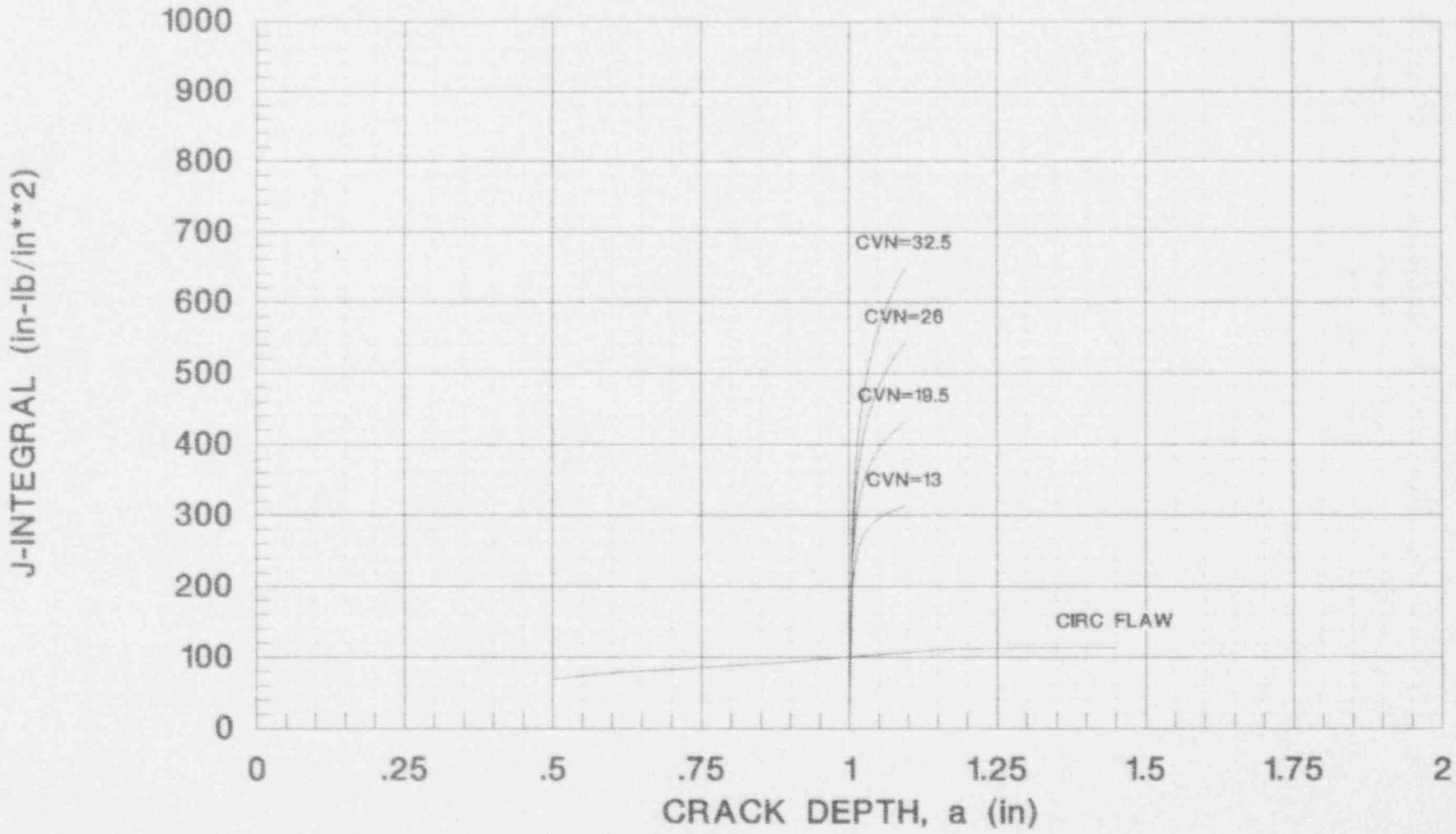

FIGURE 8.10A
J-INTEGRAL VS. CRACK DEPTH
STEAM LINE BREAK
AXIAL FLAW ORIENTATION, LEVEL C, PLATE MATERIAL

VESSEL SIZE: NOMINAL ID = 182 In, BELTLINE THICKNESS = 9.06 In
FLAW GROWTH

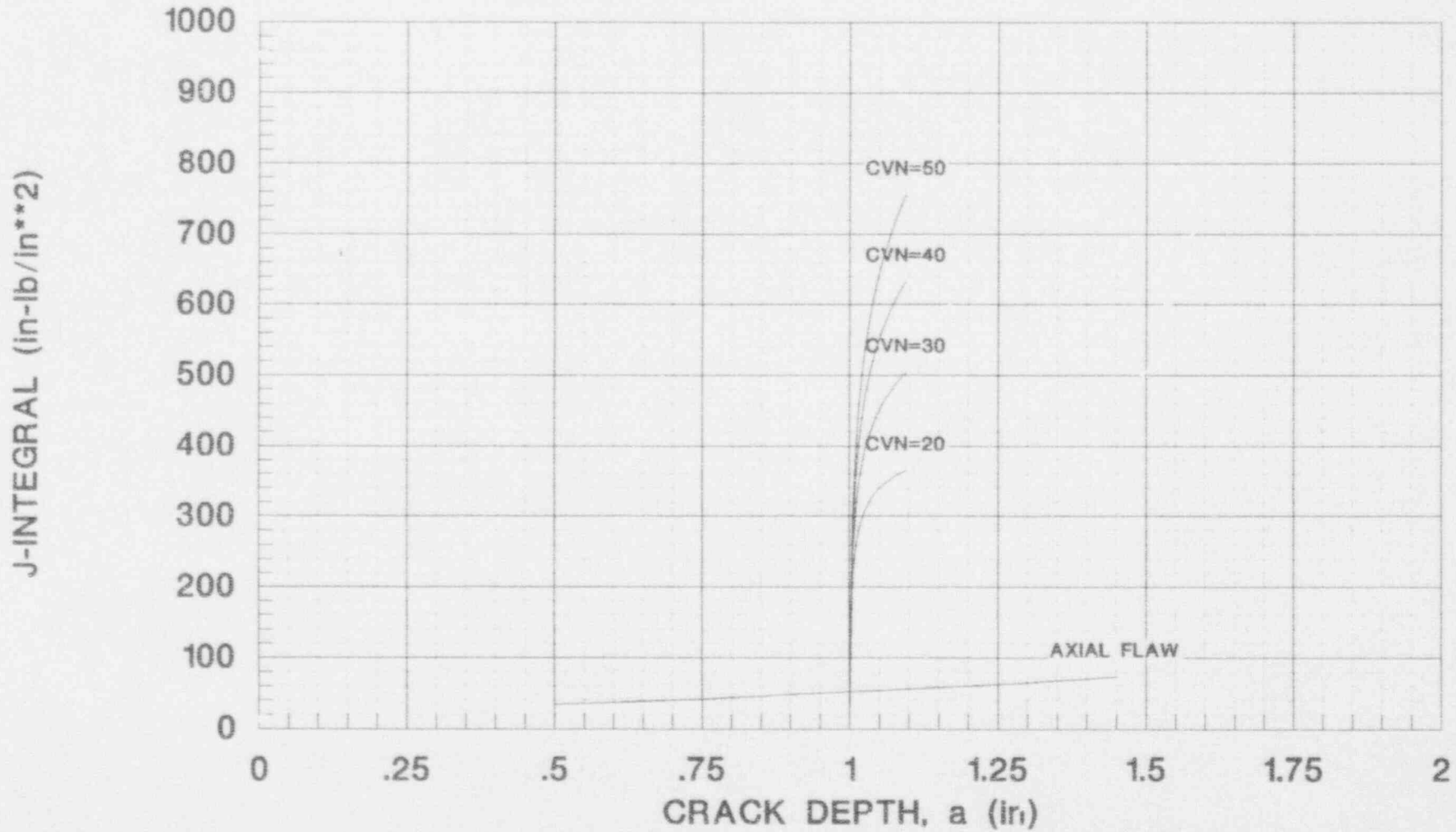

FIGURE 8.10B
J-INTEGRAL VS. CRACK DEPTH
STEAM LINE BREAK
CIRC FLAW ORIENTATION, LEVEL C, PLATE MATERIAL

VESSEL SIZE: NOMINAL ID = 182 In, BELTLINE THICKNESS = 9.06 In
FLAW GROWTH

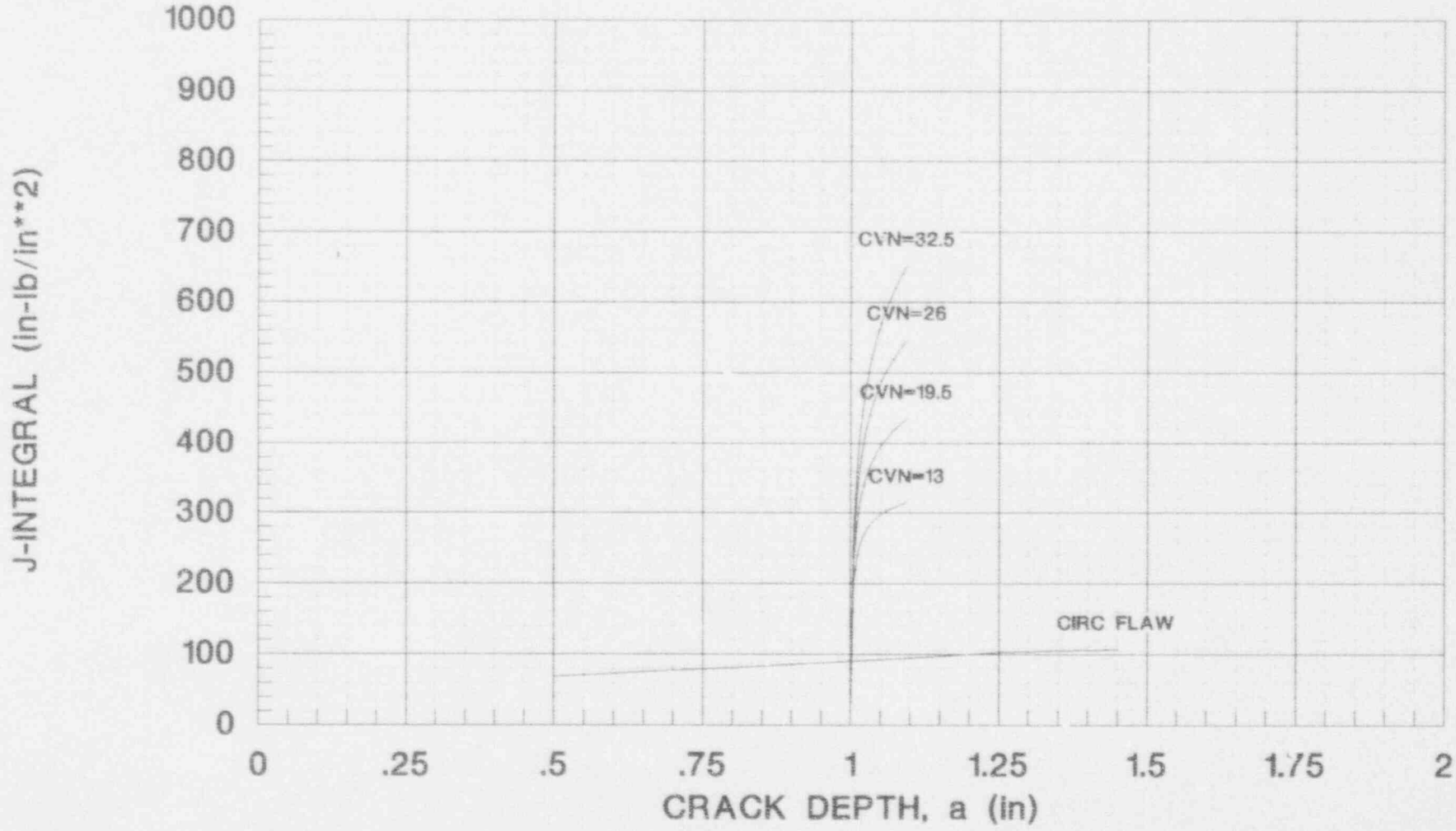

FIGURE 8.11A
J-INTEGRAL VS. TIME
STEAM LINE BREAK
AXIAL FLAW ORIENTATION, LEVEL D, PLATE MATERIAL

VESSEL SIZE: NOMINAL ID = 140 In, CLAD THICKNESS = 0.2188 In
BELTLINE THICKNESS = 7.125 In

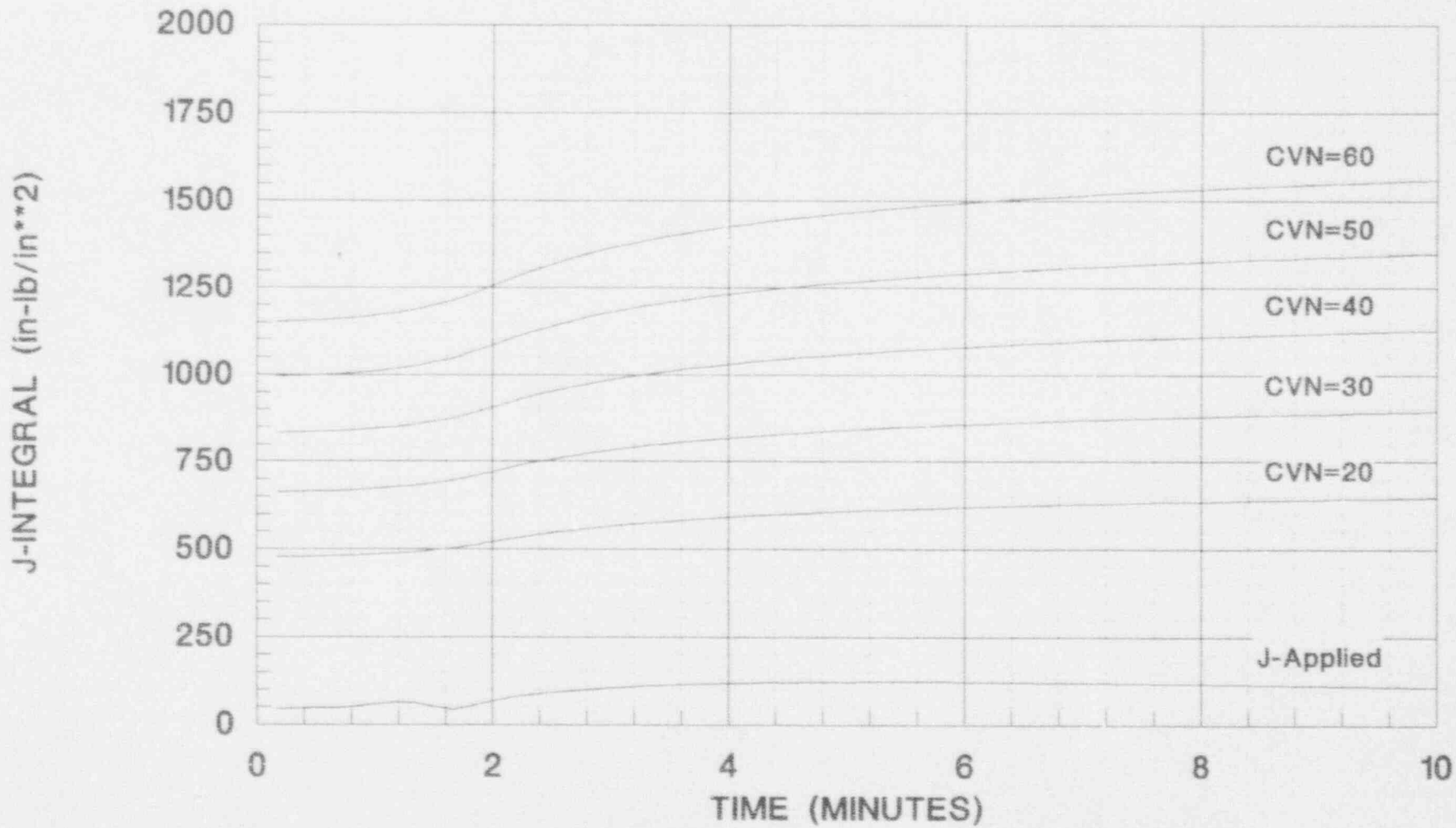

FIGURE 8.11B
J-INTEGRAL VS. TIME
STEAM LINE BREAK
CIRC. FLAW ORIENTATION, LEVEL D, PLATE MATERIAL

VESSEL SIZE: NOMINAL ID = 140 In, CLAD THICKNESS = 0.2188 In
BELTLINE THICKNESS = 7.125 In

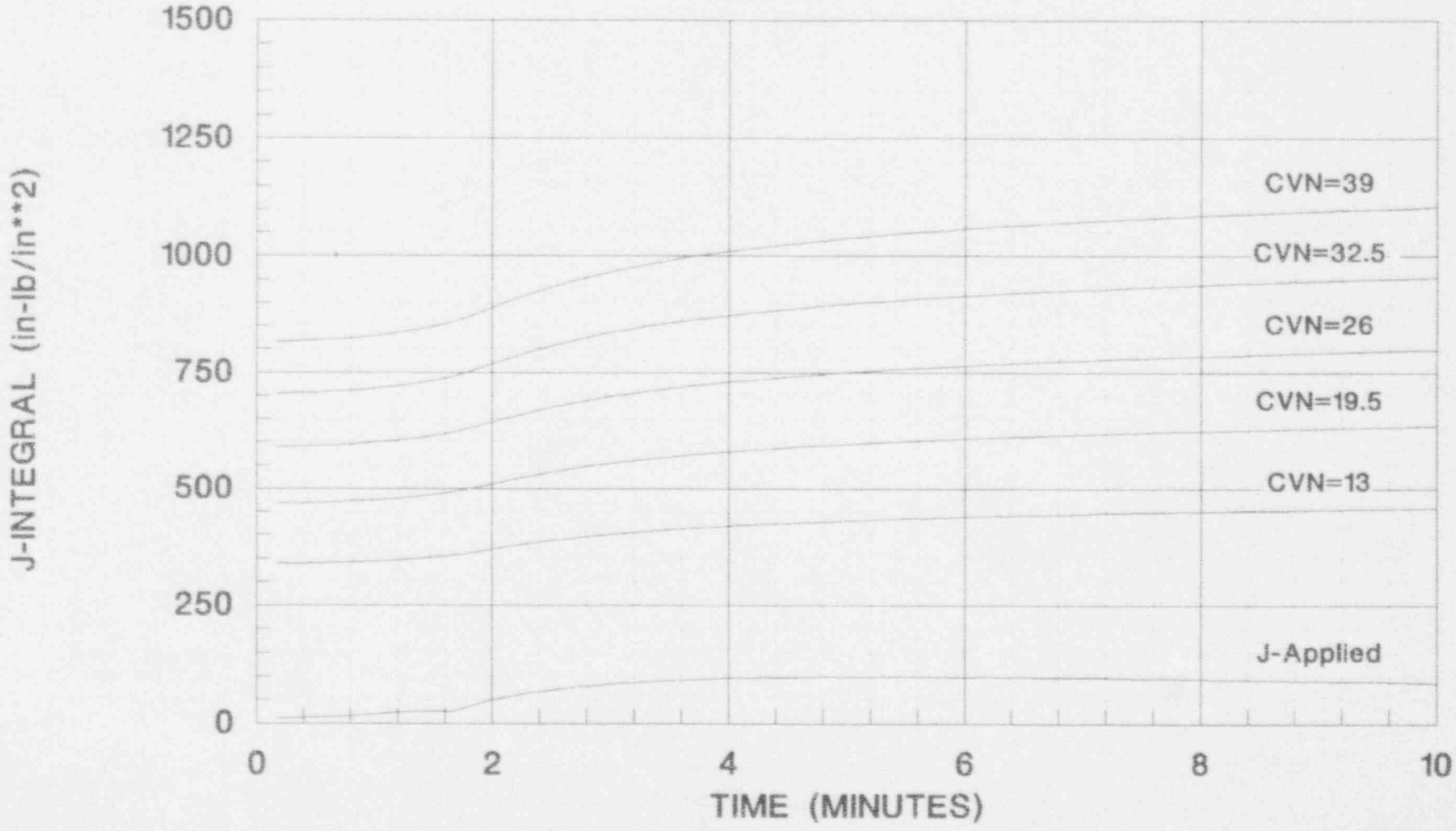

FIGURE 8.12A
J-INTEGRAL VS. TIME
STEAM LINE BREAK
AXIAL FLAW ORIENTATION, LEVEL D, PLATE MATERIAL

VESSEL SIZE: NOMINAL ID = 172 In, CLAD THICKNESS = 0.3125 In
BELTLINE THICKNESS = 8.625 In

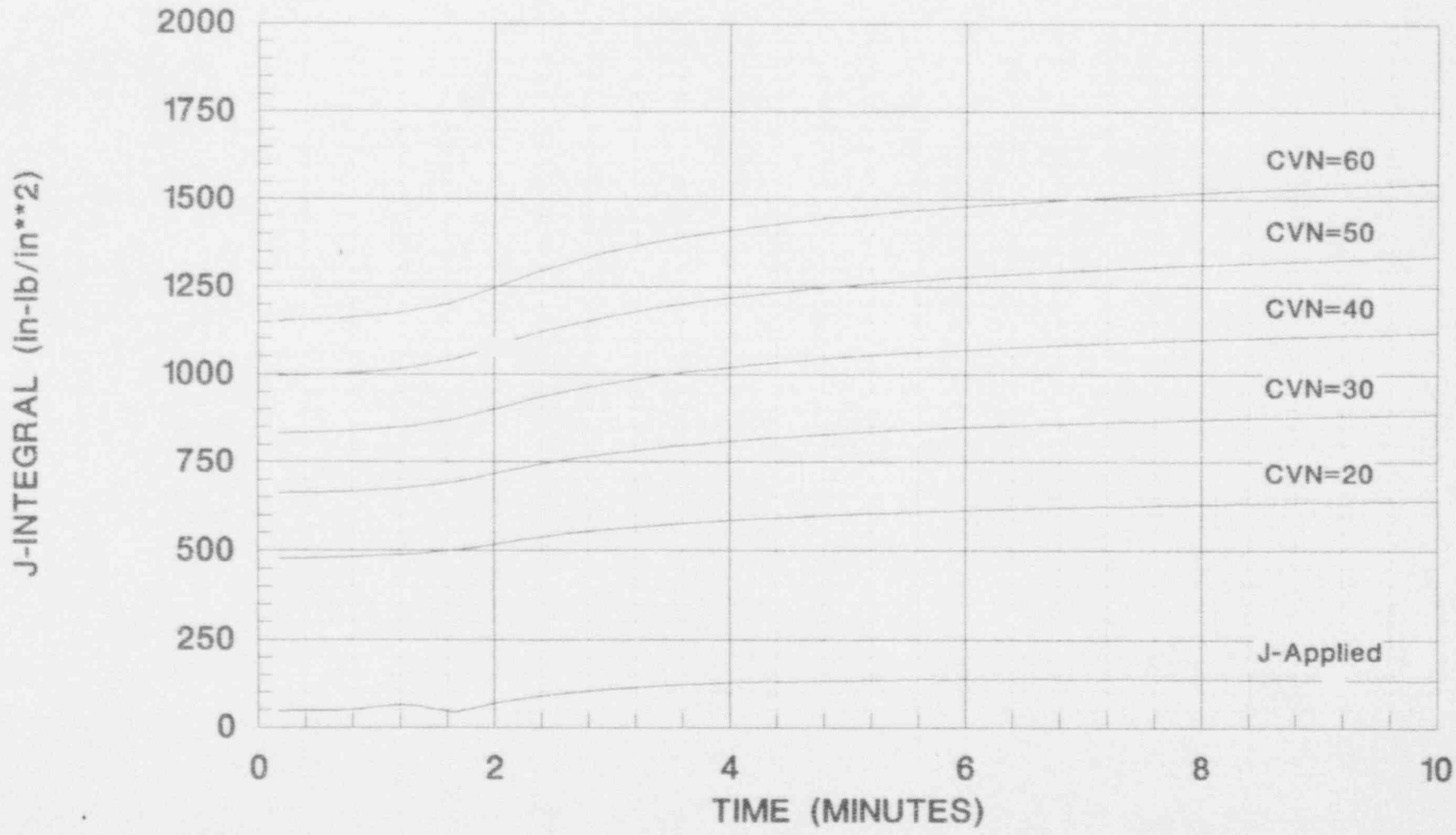

FIGURE 8.12B
J-INTEGRAL VS. TIME
STEAM LINE BREAK
CIRC. FLAW ORIENTATION, LEVEL D, PLATE MATERIAL

VESSEL SIZE: NOMINAL ID = 172 in, CLAD THICKNESS = 0.3125 in
BELTLINE THICKNESS = 8.625 in

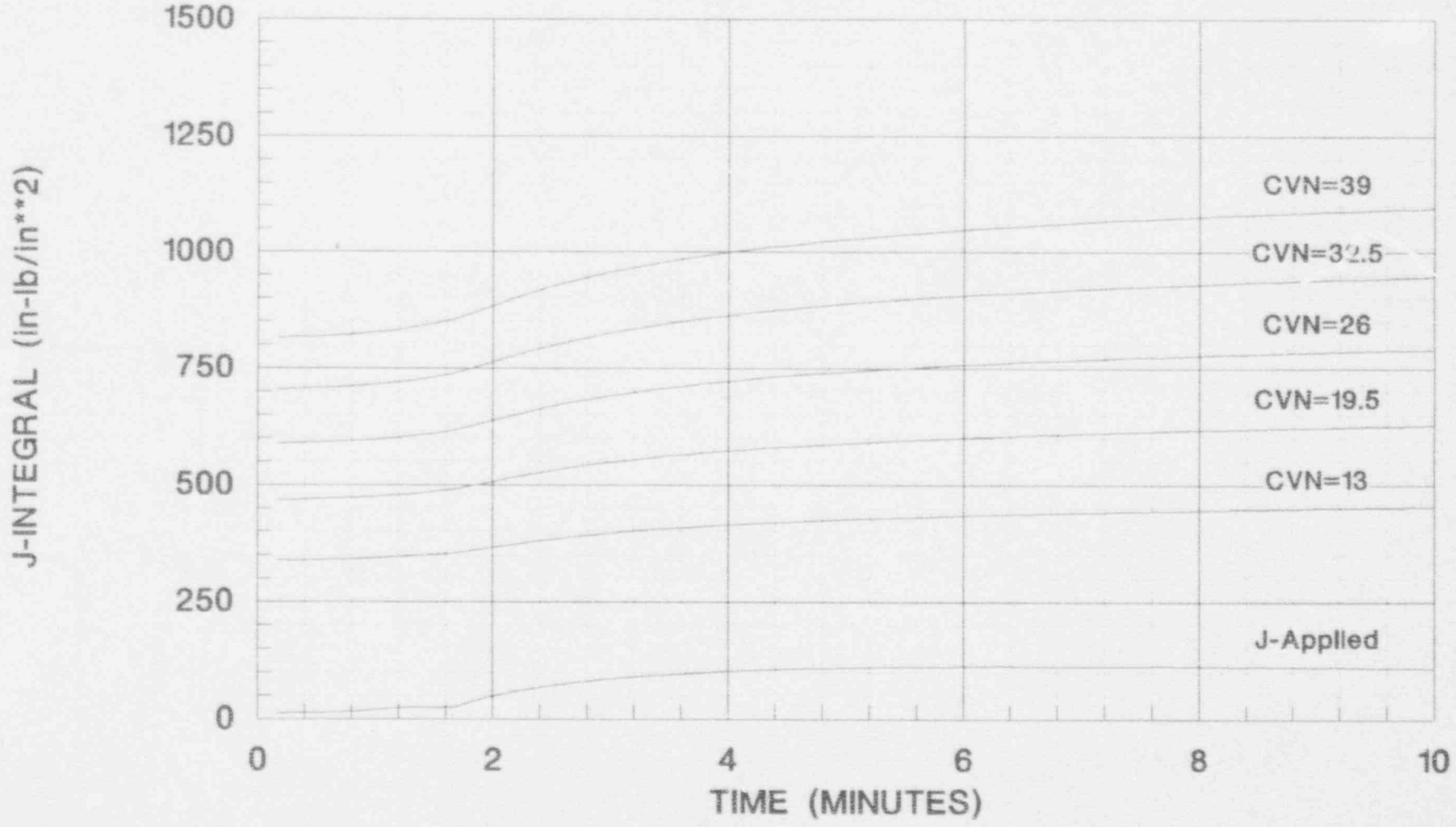

FIGURE 8.13A
J-INTEGRAL VS. TIME
STEAM LINE BREAK
AXIAL FLAW ORIENTATION, LEVEL D, PLATE MATERIAL

VESSEL SIZE: NOMINAL ID = 182 In, CLAD THICKNESS = 0.16 In
BELTLINE THICKNESS = 9.06 In

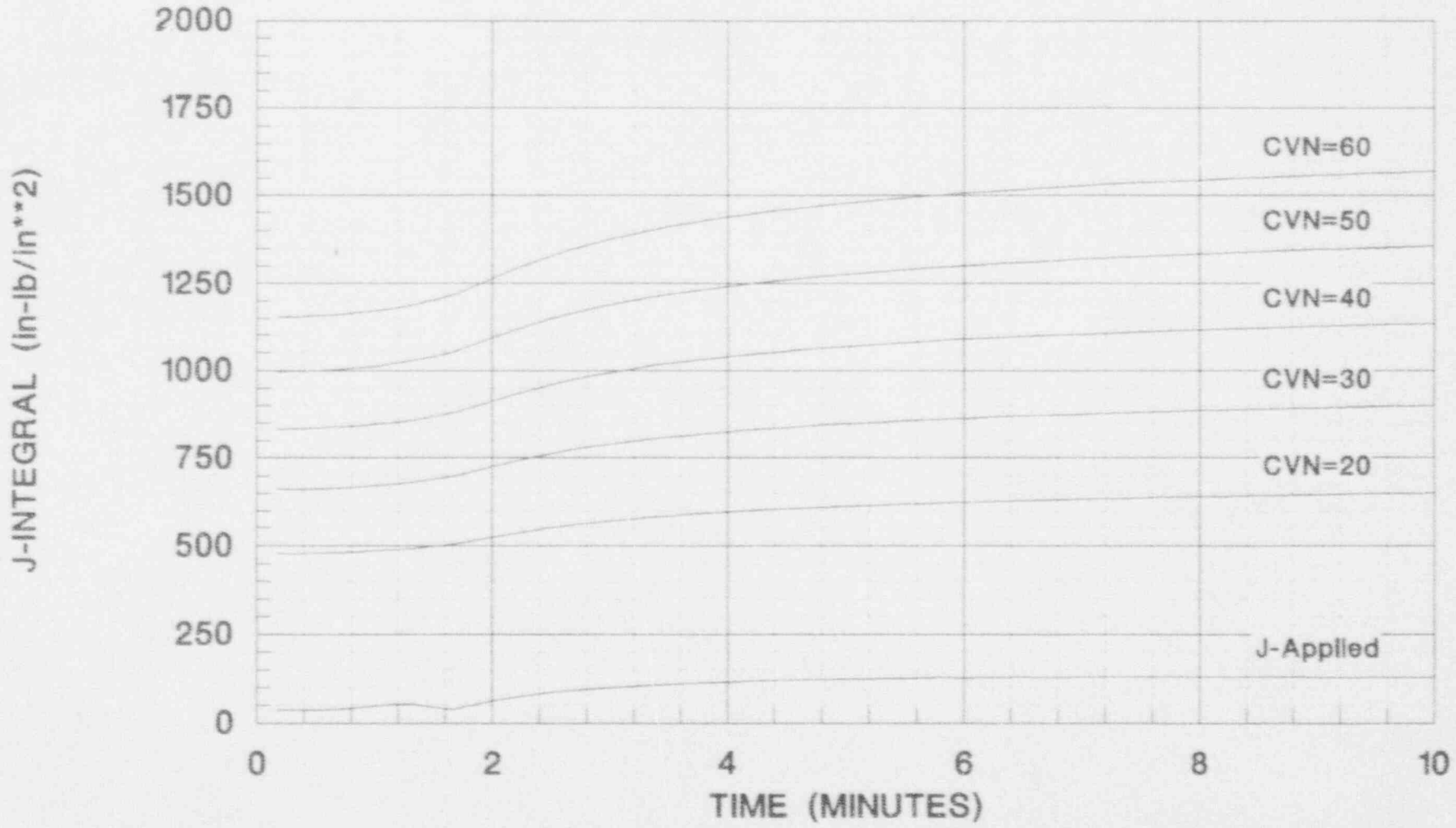

FIGURE 8.13B
J-INTEGRAL VS. TIME
STEAM LINE BREAK
CIRC. FLAW ORIENTATION, LEVEL D, PLATE MATERIAL

VESSEL SIZE: NOMINAL ID = 182 In, CLAD THICKNESS = 0.16 In
BELTLINE THICKNESS = 9.06 In

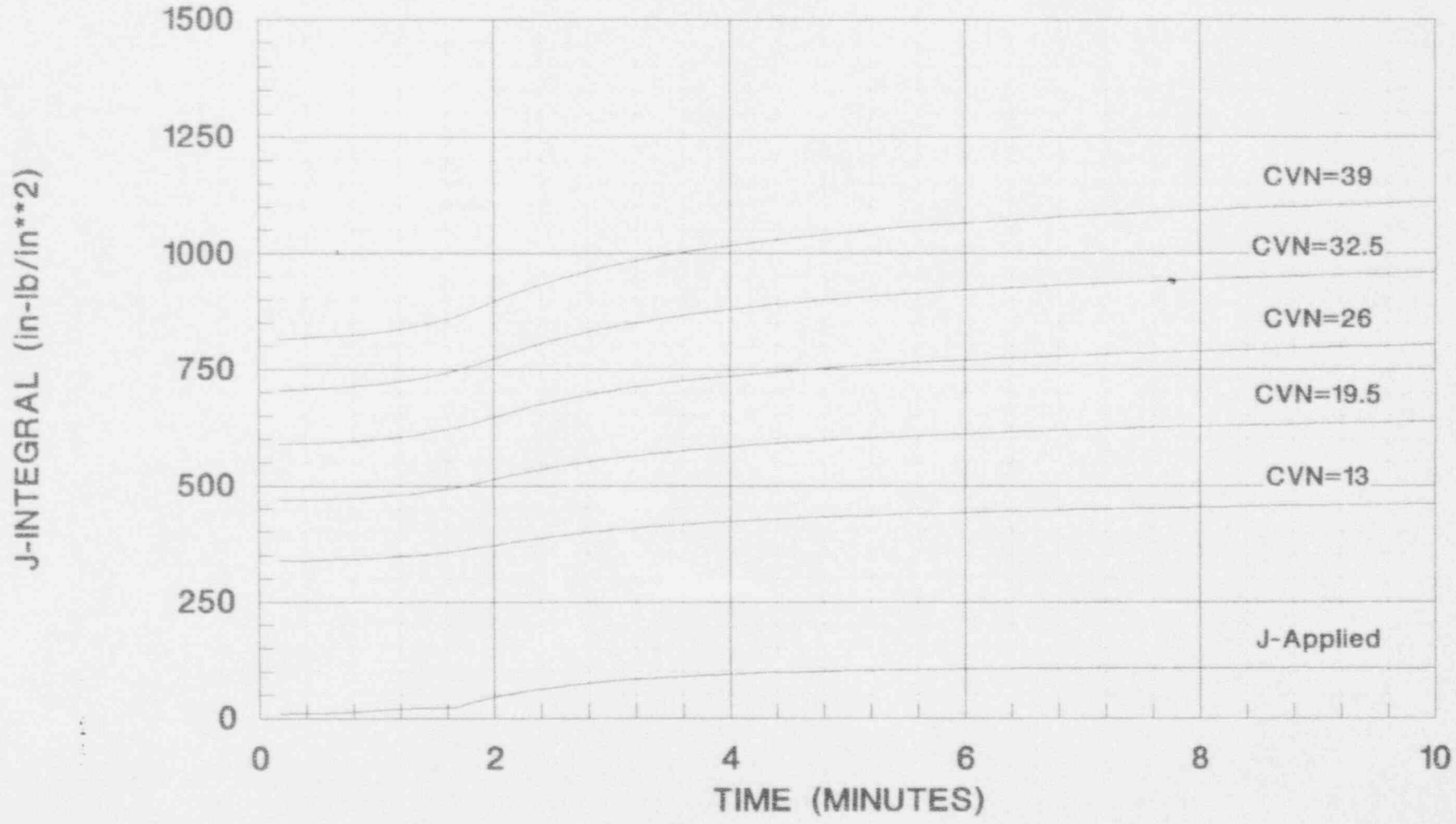

FIGURE 8.14A
J-INTEGRAL VS. TIME
FEEDWATER LINE BREAK
AXIAL FLAW ORIENTATION, LEVEL D, PLATE MATERIAL

VESSEL SIZE: NOMINAL ID = 140 in, CLAD THICKNESS = 0.2188 in
BELTLINE THICKNESS = 7.125 in

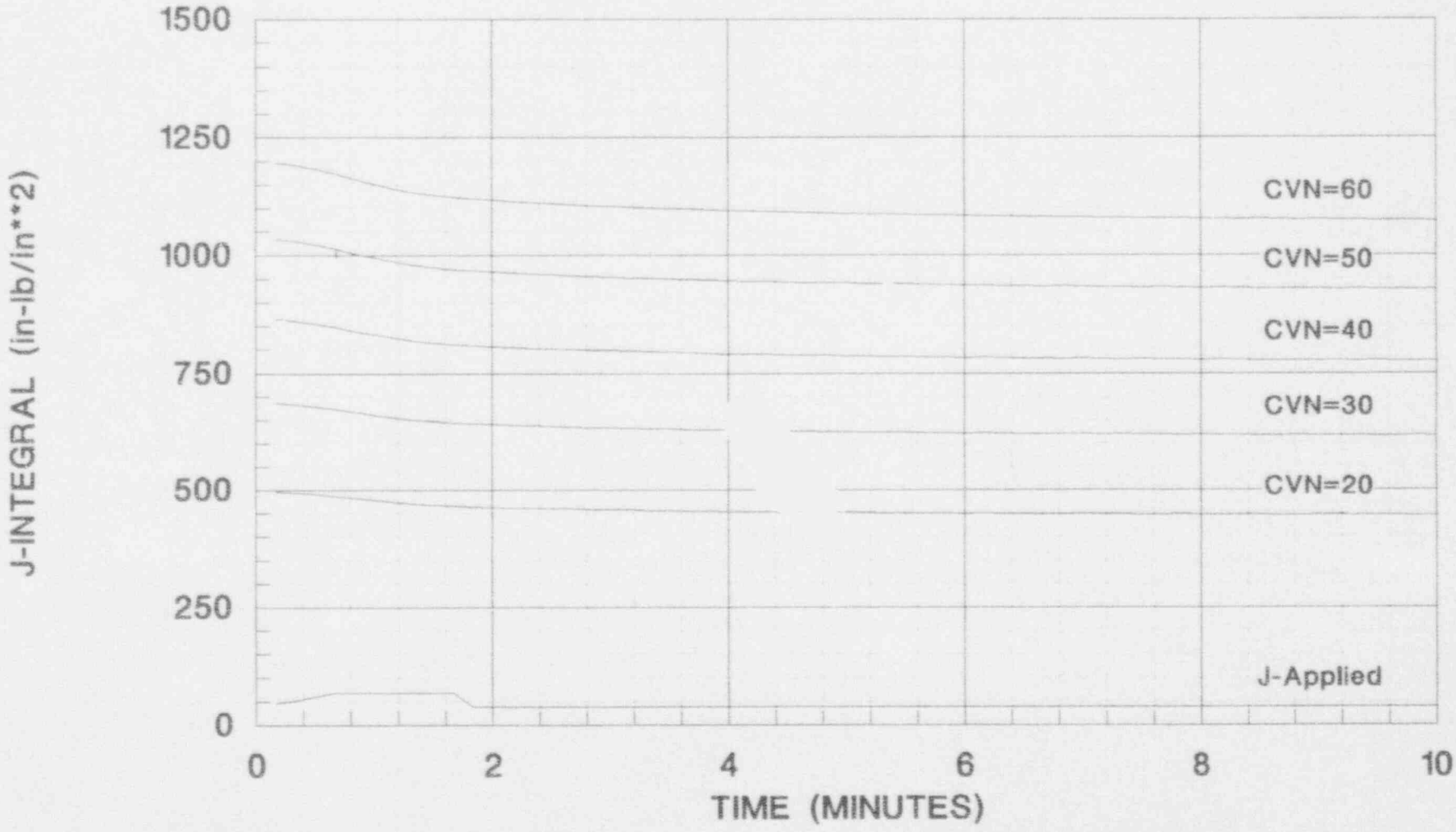

FIGURE 8.14B
J-INTEGRAL VS. TIME
FEEDWATER LINE BREAK
CIRC. FLAW ORIENTATION, LEVEL D, PLATE MATERIAL

VESSEL SIZE: NOMINAL ID = 140 In, CLAD THICKNESS = 0.2188 In
BELTLINE THICKNESS = 7.125 In

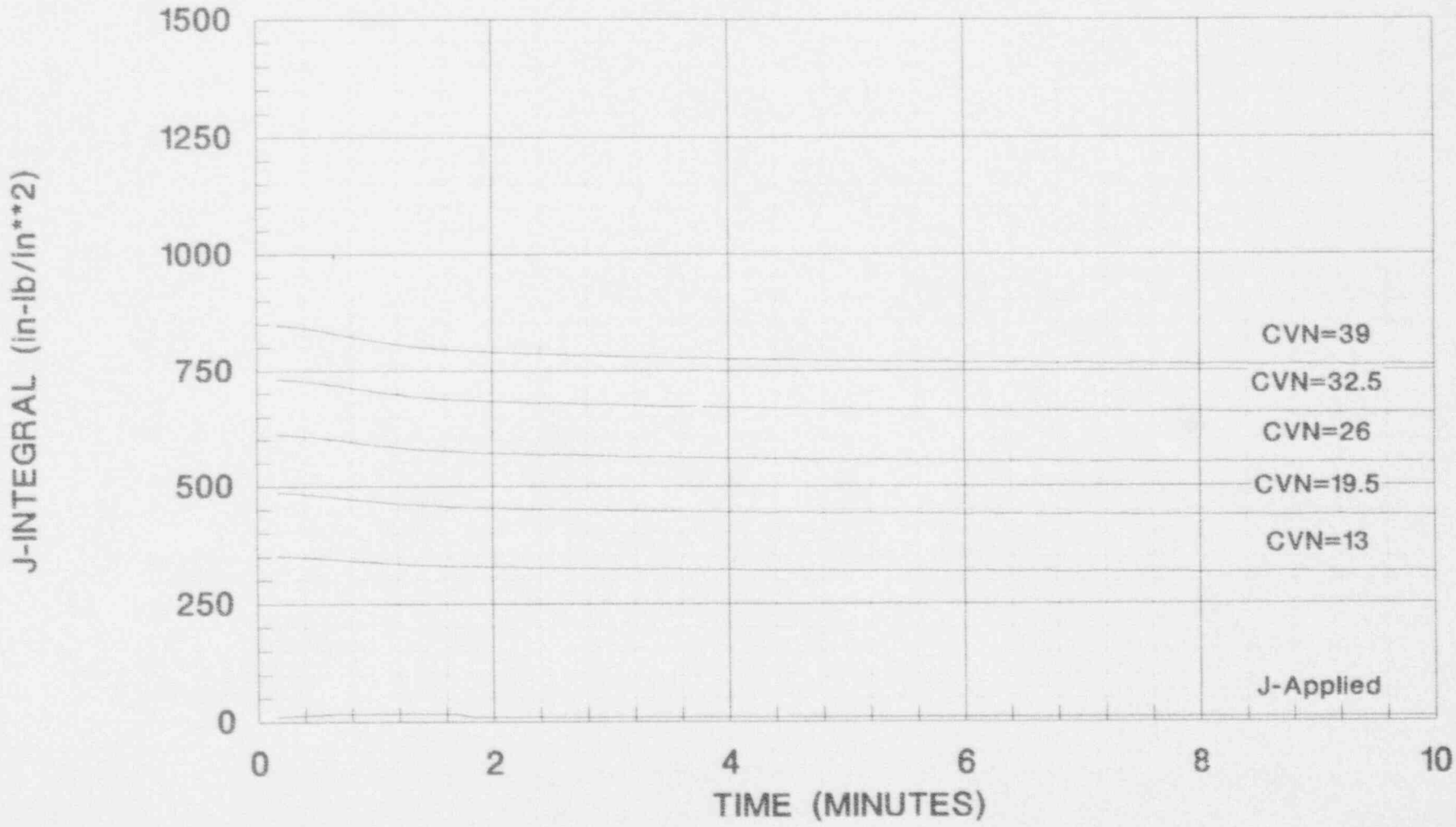

FIGURE 8.15A
J-INTEGRAL VS. TIME
FEEDWATER LINE BREAK
AXIAL FLAW ORIENTATION, LEVEL D, PLATE MATERIAL

VESSEL SIZE: NOMINAL ID = 172 in, CLAD THICKNESS = 0.3125 in
BELTLINE THICKNESS = 8.625 in

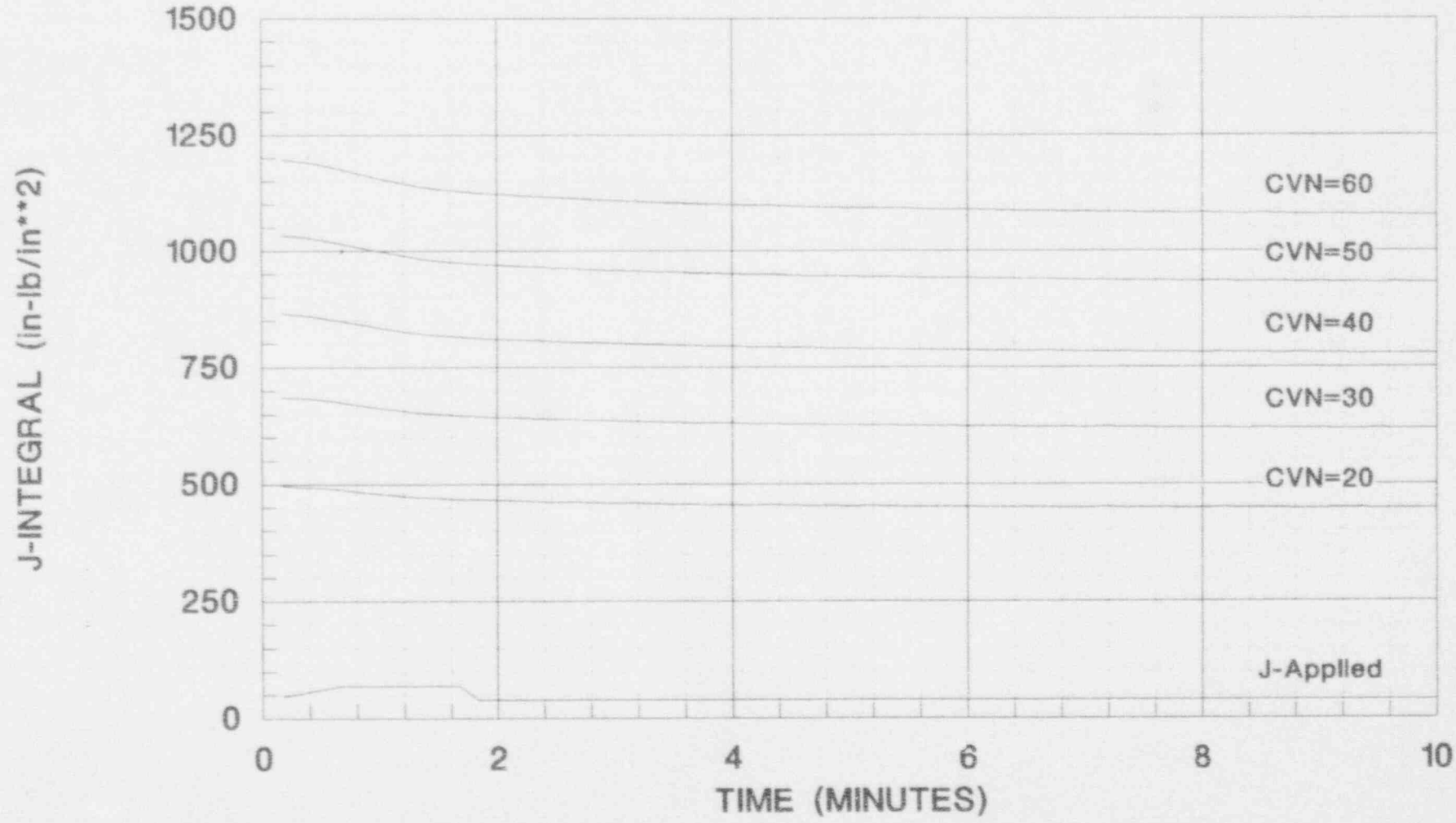

FIGURE 8.15B
J-INTEGRAL VS. TIME
FEEDWATER LINE BREAK
CIRC. FLAW ORIENTATION, LEVEL D, PLATE MATERIAL

VESSEL SIZE: NOMINAL ID = 172 In, CLAD THICKNESS = 0.3125 In
BELTLINE THICKNESS = 8.625 In

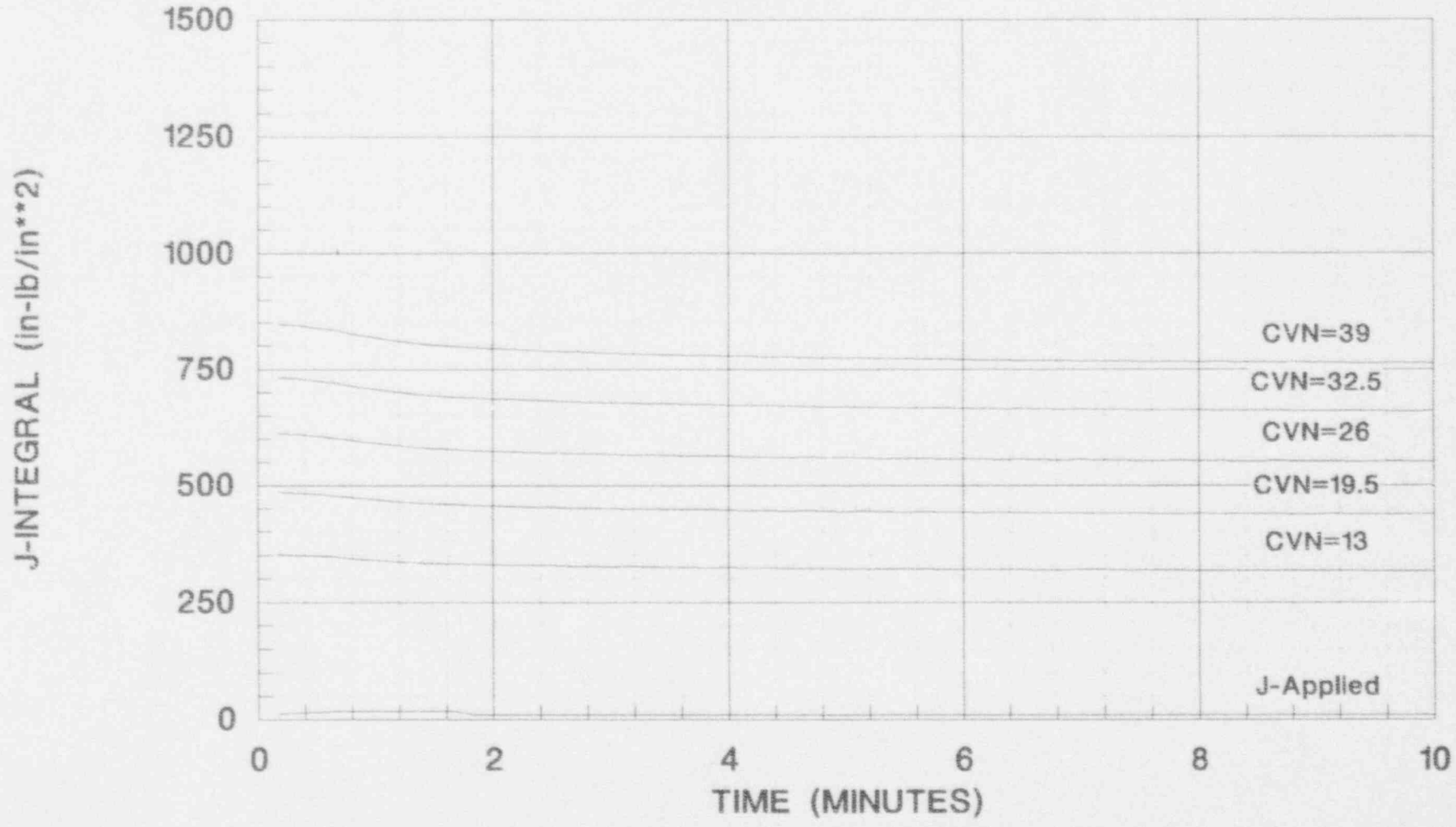

FIGURE 8.16A
J-INTEGRAL VS. TIME
FEEDWATER LINE BREAK
AXIAL FLAW ORIENTATION, LEVEL D, PLATE MATERIAL

VESSEL SIZE: NOMINAL ID = 182 in, CLAD THICKNESS = 0.16 in
BELTLINE THICKNESS = 9.06 in

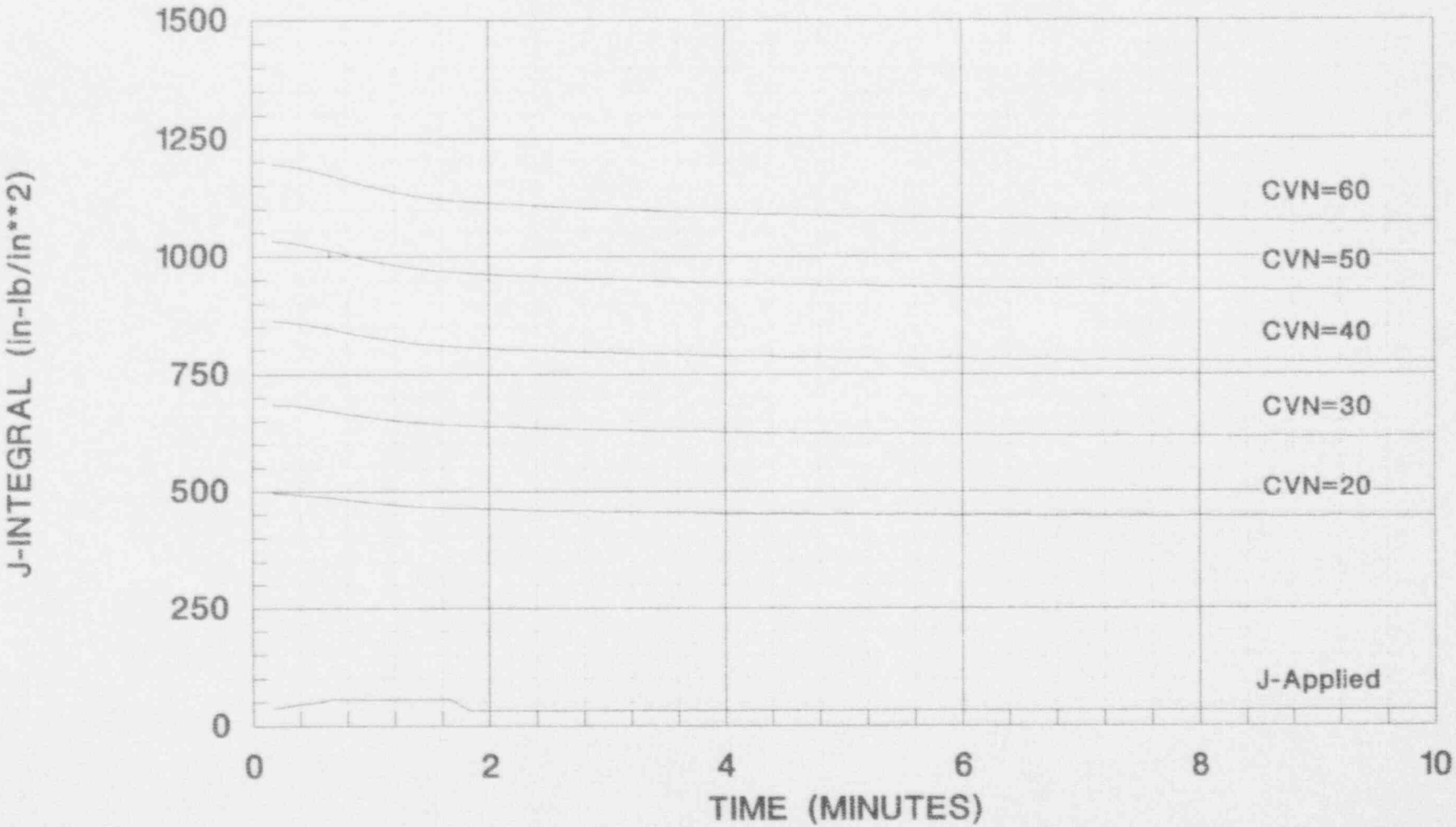

FIGURE 8.16B
J-INTEGRAL VS. TIME
FEEDWATER LINE BREAK
CIRC. FLAW ORIENTATION, LEVEL D, PLATE MATERIAL

VESSEL SIZE: NOMINAL ID = 182 In, CLAD THICKNESS = 0.16 In
BELTLINE THICKNESS = 9.06 In

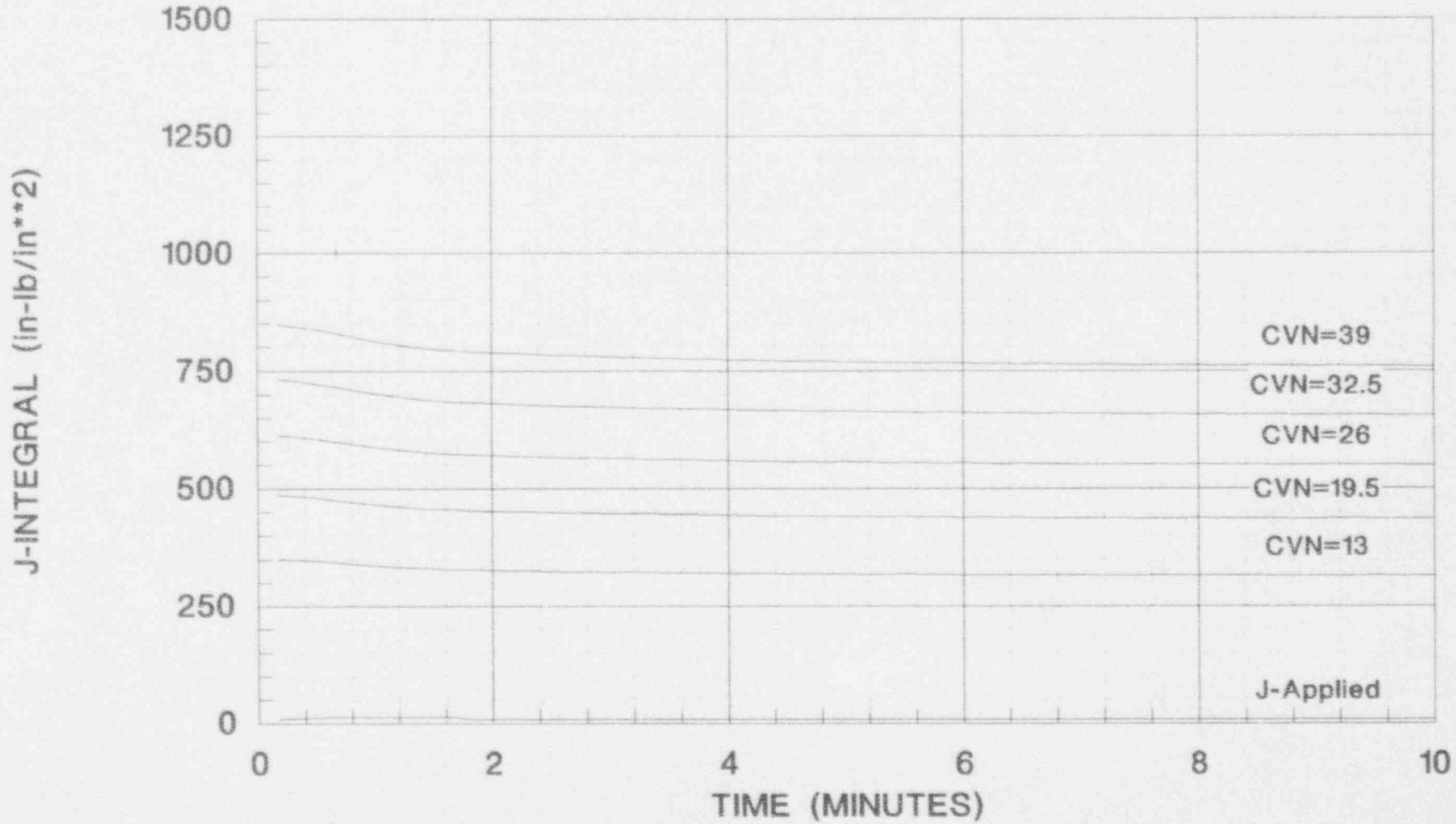

FIGURE 8.17A
J-INTEGRAL VS. CRACK DEPTH
STEAM LINE BREAK
AXIAL FLAW ORIENTATION, LEVEL D, PLATE MATERIAL

VESSEL SIZE: NOMINAL ID = 140 In, BELTLINE THICKNESS = 7.125 In
FLAW GROWTH

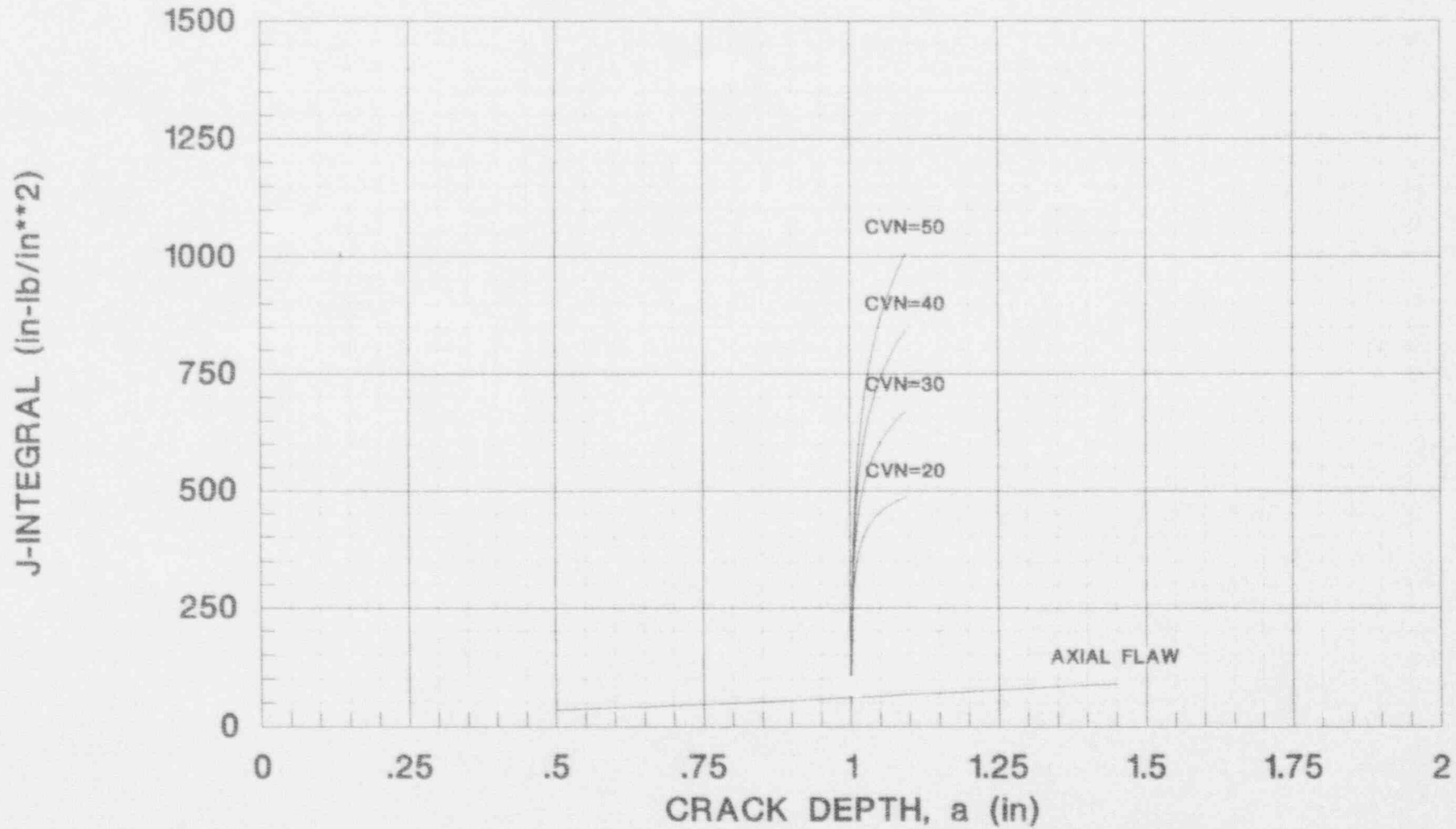

FIGURE 8.17B
J-INTEGRAL VS. CRACK DEPTH
STEAM LINE BREAK
CIRC FLAW ORIENTATION, LEVEL D, PLATE MATERIAL

VESSEL SIZE: NOMINAL ID = 140 In, BELTLINE THICKNESS = 7.125 In
FLAW GROWTH

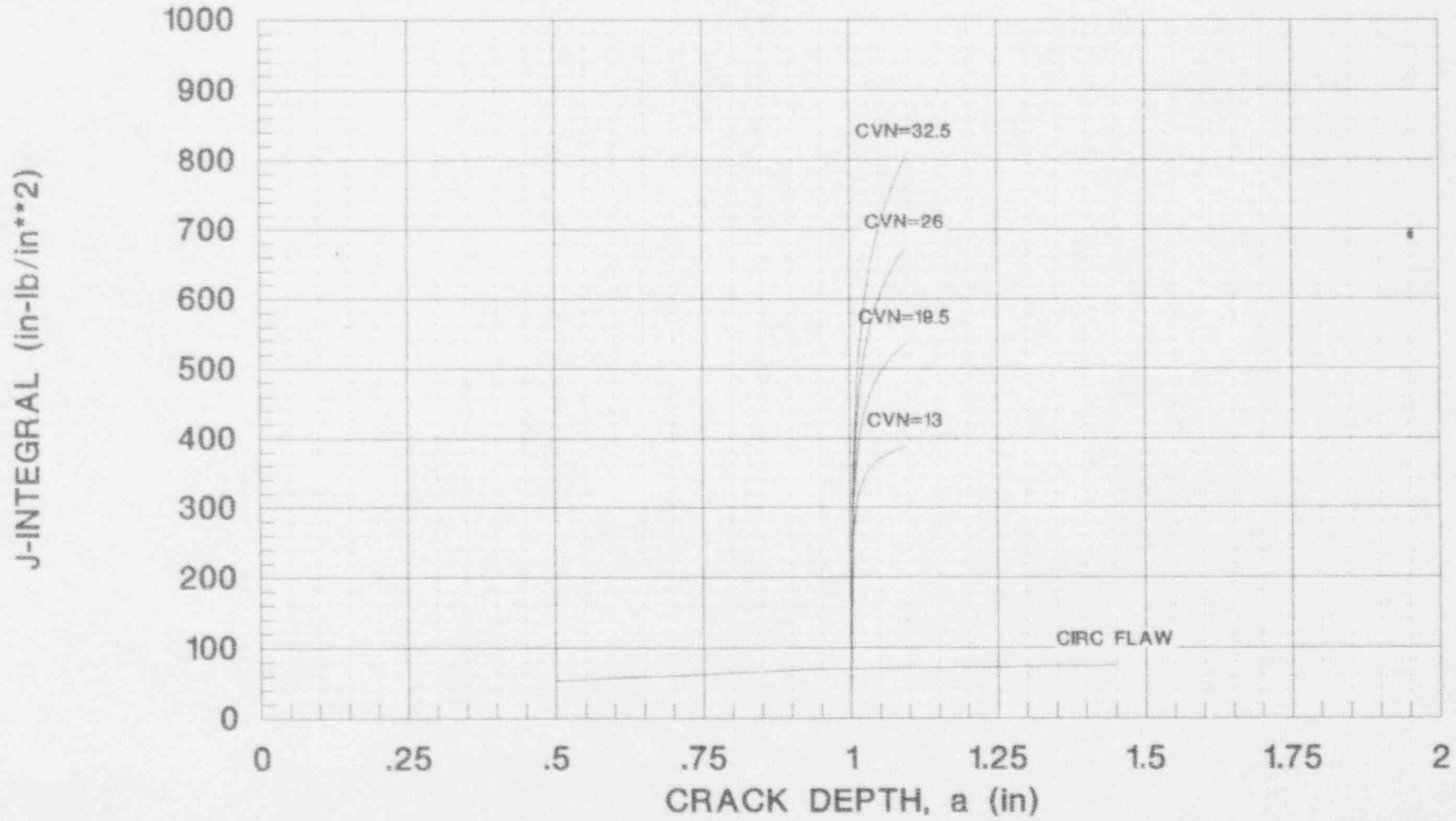

FIGURE 8.18A
J-INTEGRAL VS. CRACK DEPTH
STEAM LINE BREAK
AXIAL FLAW ORIENTATION, LEVEL D, PLATE MATERIAL

VESSEL SIZE: NOMINAL ID = 172 In, BELTLINE THICKNESS = 8.625 In
FLAW GROWTH

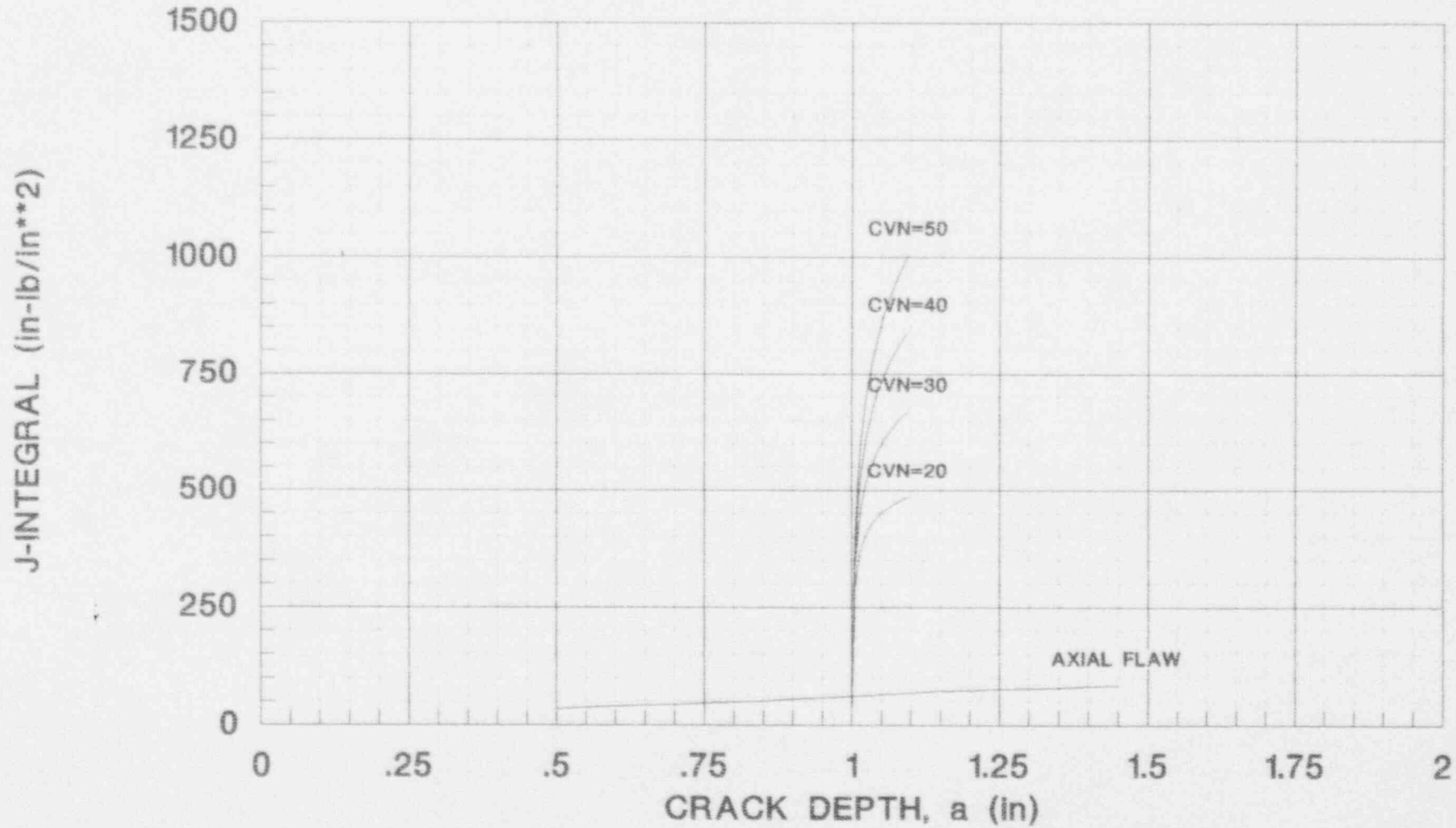

FIGURE 8.18B
J-INTEGRAL VS. CRACK DEPTH
STEAM LINE BREAK
CIRC FLAW ORIENTATION, LEVEL D, PLATE MATERIAL

VESSEL SIZE: NOMINAL ID = 172 in, BELTLINE THICKNESS = 8.625 in
FLAW GROWTH

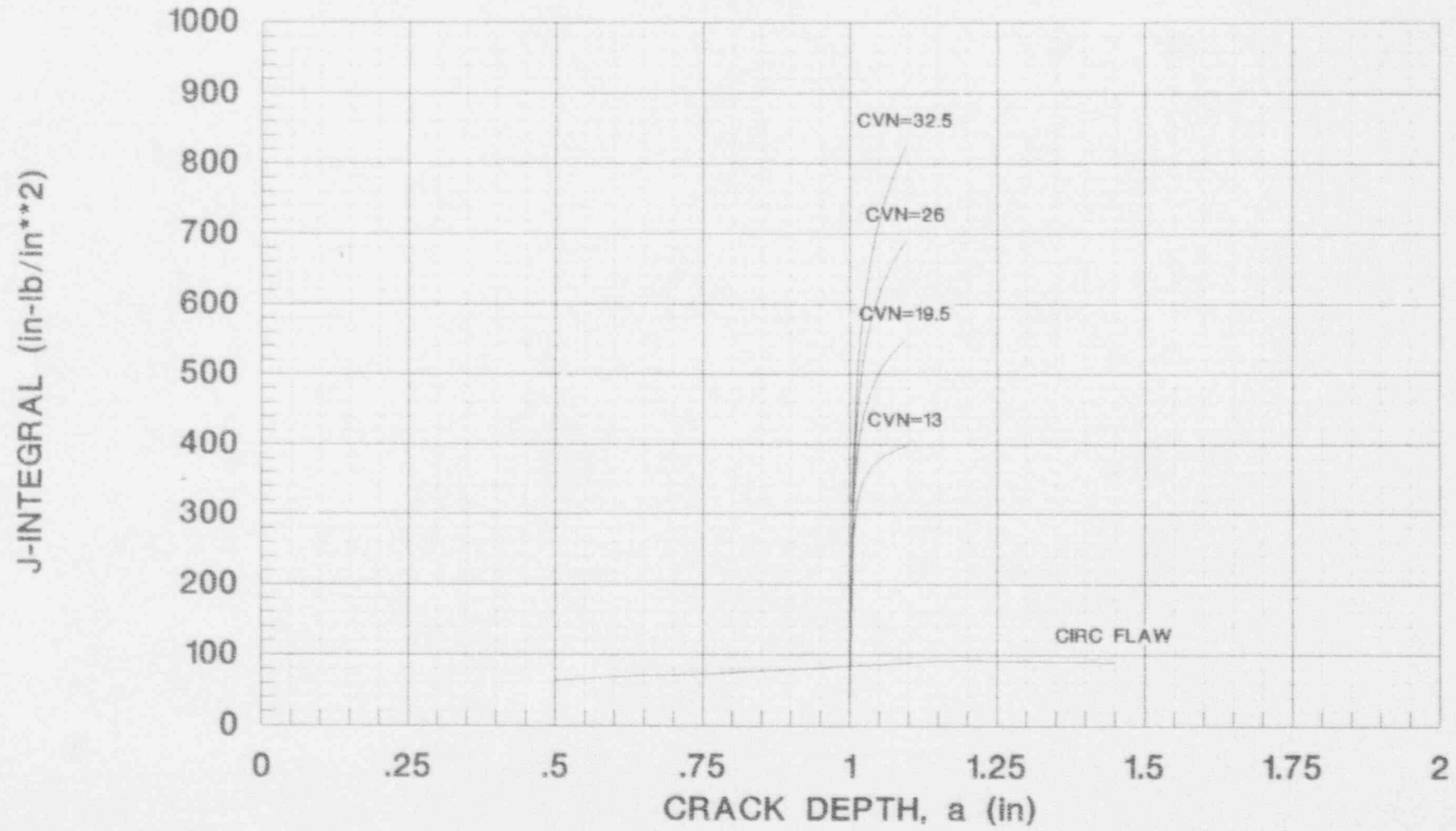

FIGURE 8.19A
J-INTEGRAL VS. CRACK DEPTH
STEAM LINE BREAK
AXIAL FLAW ORIENTATION, LEVEL D, PLATE MATERIAL

VESSEL SIZE: NOMINAL ID = 182 In, BELTLINE THICKNESS = 9.06 In
FLAW GROWTH

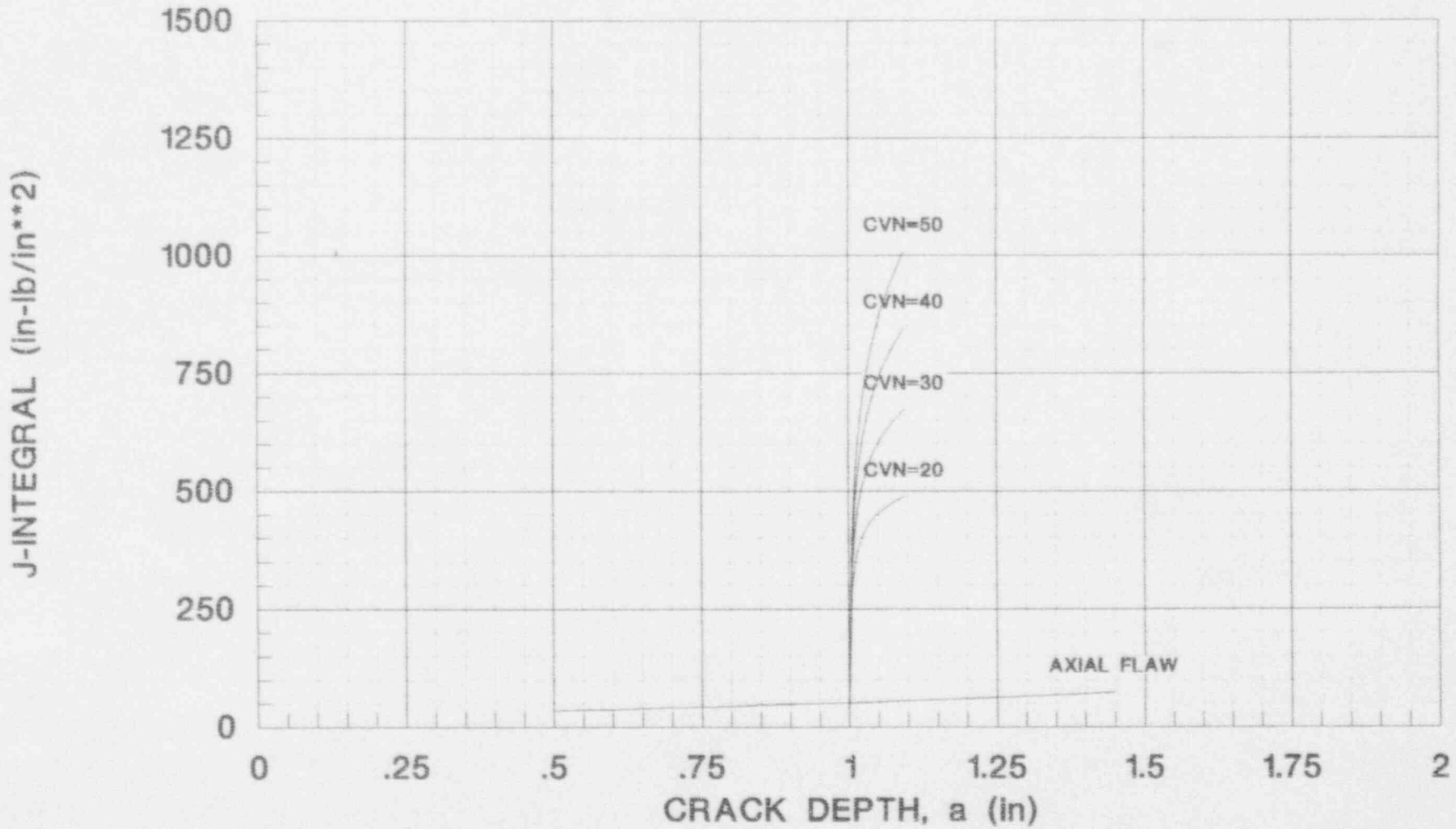

FIGURE 8.19B
J-INTEGRAL VS. CRACK DEPTH
STEAM LINE BREAK
CIRC FLAW ORIENTATION, LEVEL D, PLATE MATERIAL

VESSEL SIZE: NOMINAL ID = 182 In, BELTLINE THICKNESS = 9.06 In
FLAW GROWTH

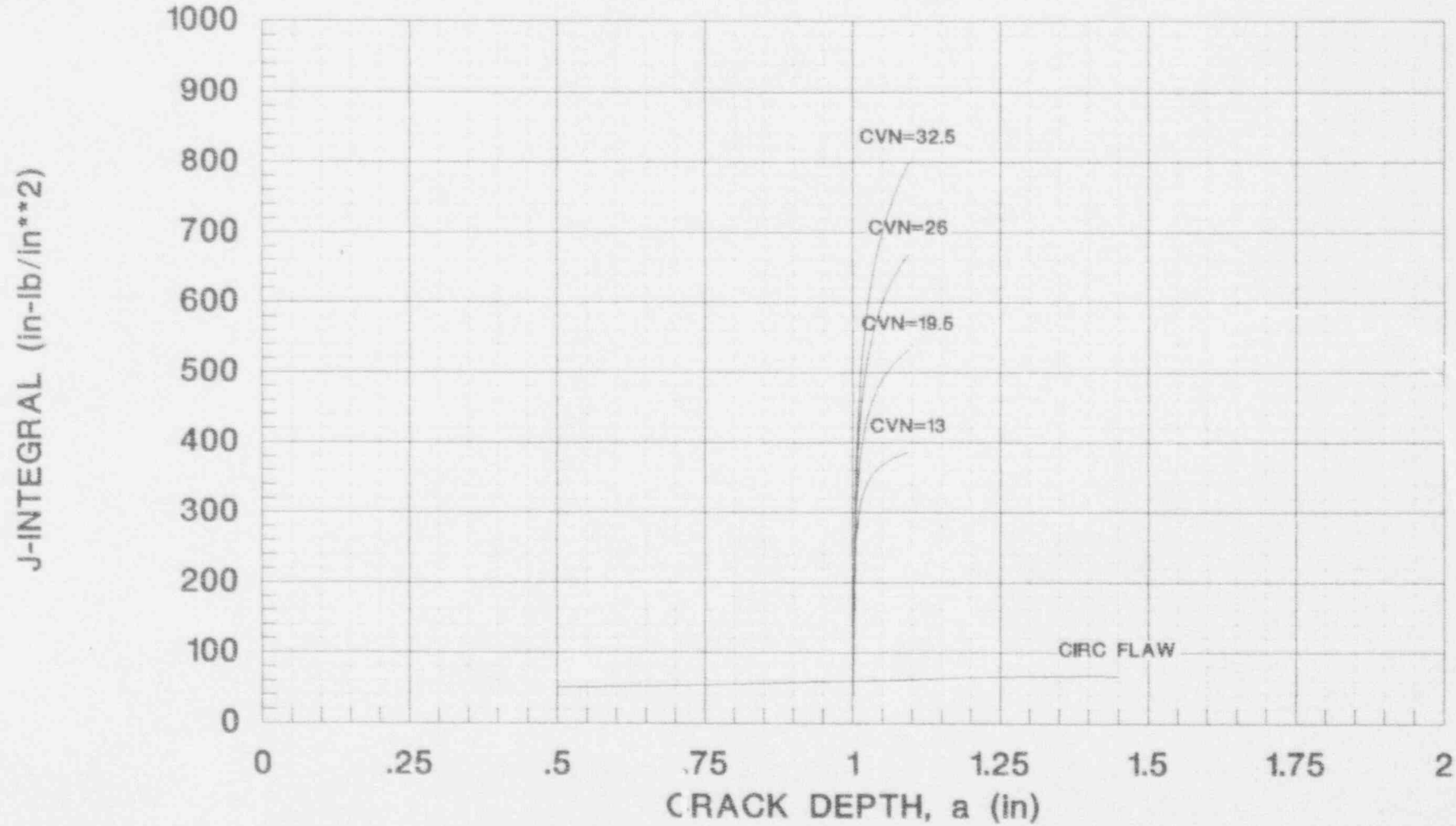

FIGURE 8.20A
J-INTEGRAL VS. CRACK DEPTH
FEEDWATER LINE BREAK
AXIAL FLAW ORIENTATION, LEVEL D, PLATE MATERIAL

VESSEL SIZE: NOMINAL ID = 140 In, BELTLINE THICKNESS = 7.125 In
FLAW GROWTH

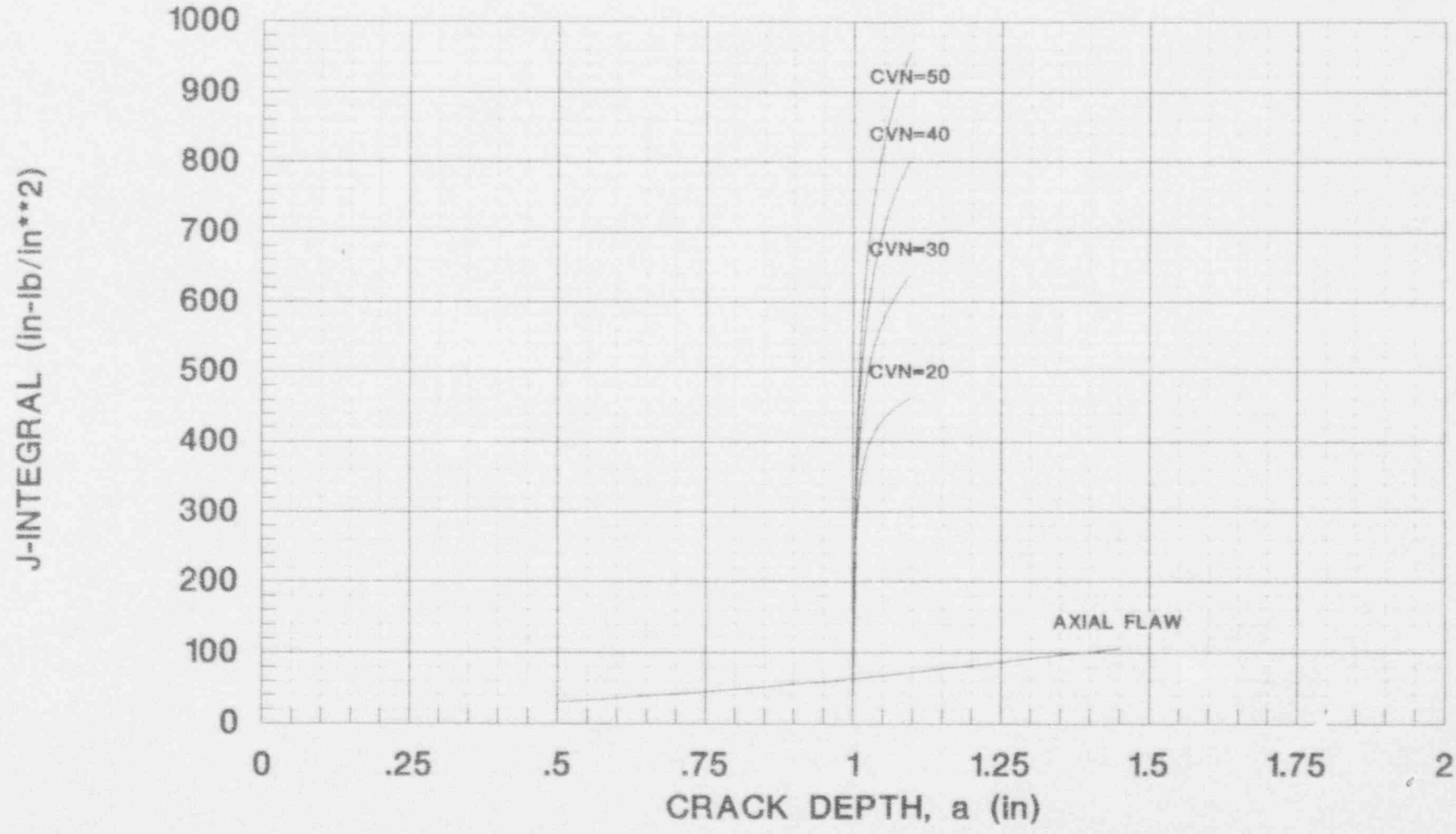

FIGURE 8.20B
J-INTEGRAL VS. CRACK DEPTH
FEEDWATER LINE BREAK
CIRC FLAW ORIENTATION, LEVEL D, PLATE MATERIAL

VESSEL SIZE: NOMINAL ID = 140 In, BELTLINE THICKNESS = 7.125 In
FLAW GROWTH

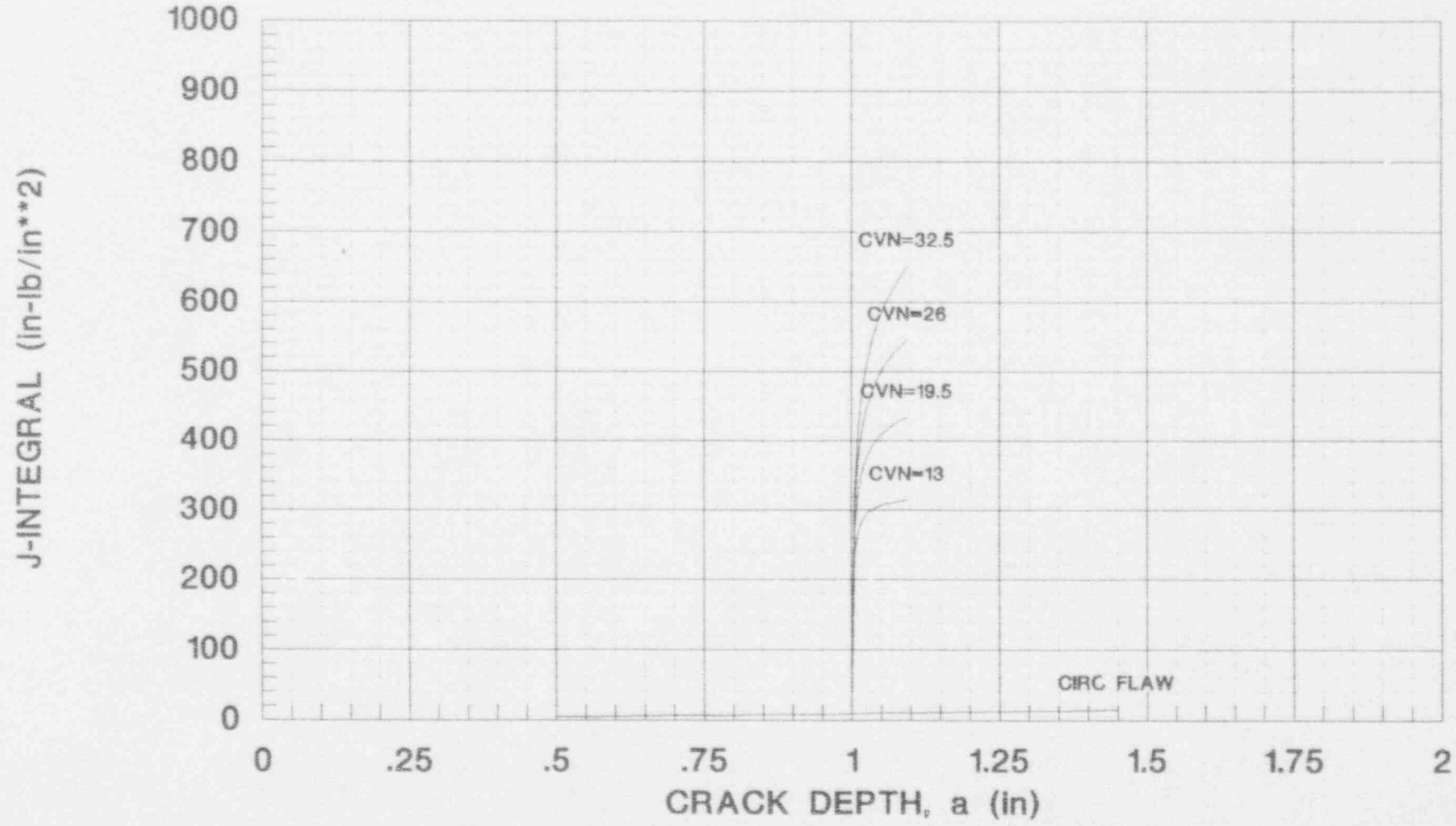

FIGURE 8.21A
J-INTEGRAL VS. CRACK DEPTH
FEEDWATER LINE BREAK
AXIAL FLAW ORIENTATION, LEVEL D, PLATE MATERIAL

VESSEL SIZE: NOMINAL ID = 172 In, BELTLINE THICKNESS = 8.625 In
FLAW GROWTH

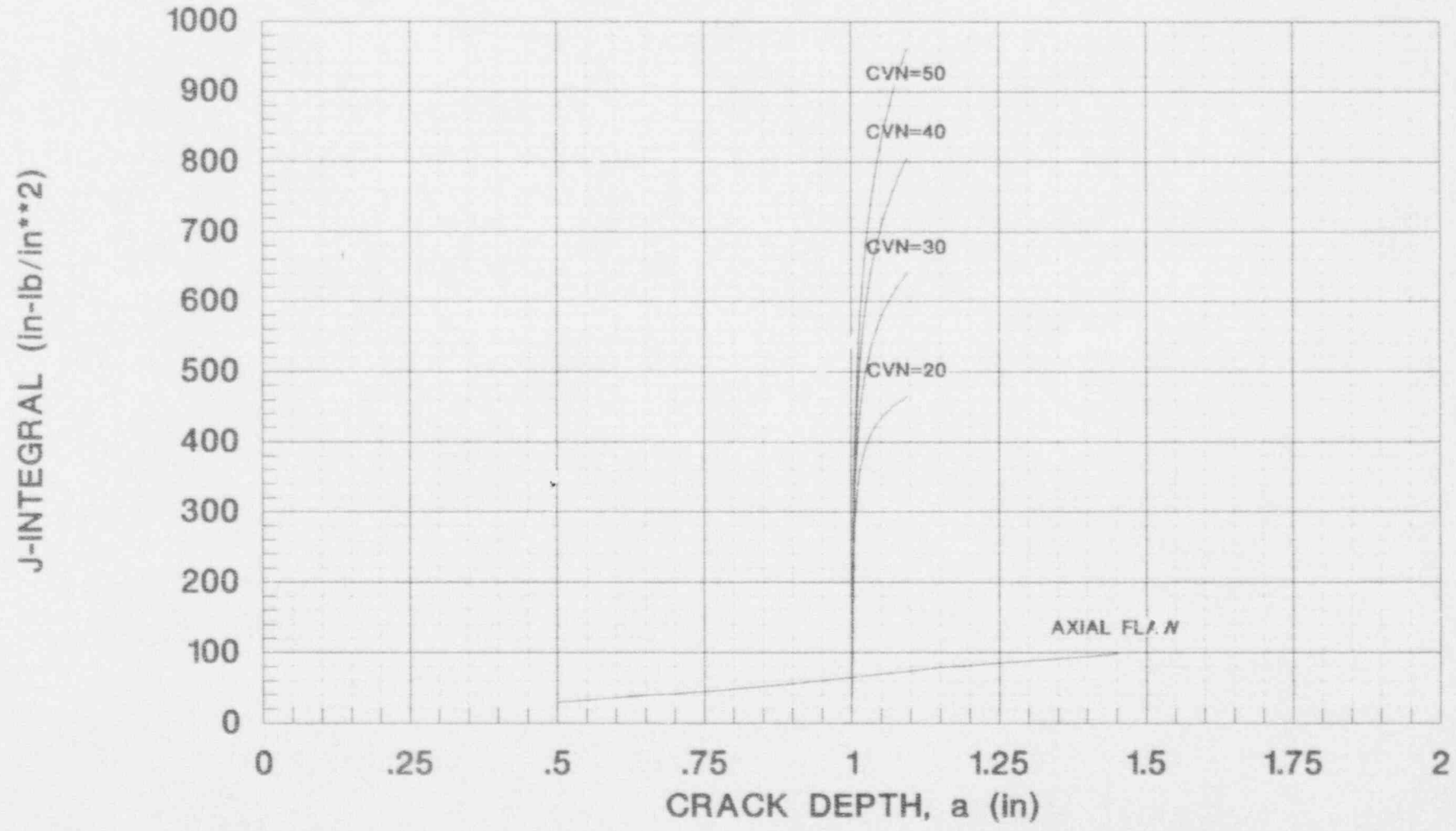

FIGURE 8.21B
J-INTEGRAL VS. CRACK DEPTH
FEEDWATER LINE BREAK
CIRC FLAW ORIENTATION, LEVEL D, PLATE MATERIAL

VESSEL SIZE: NOMINAL ID = 172 In, BELTLINE THICKNESS = 8.625 In
FLAW GROWTH

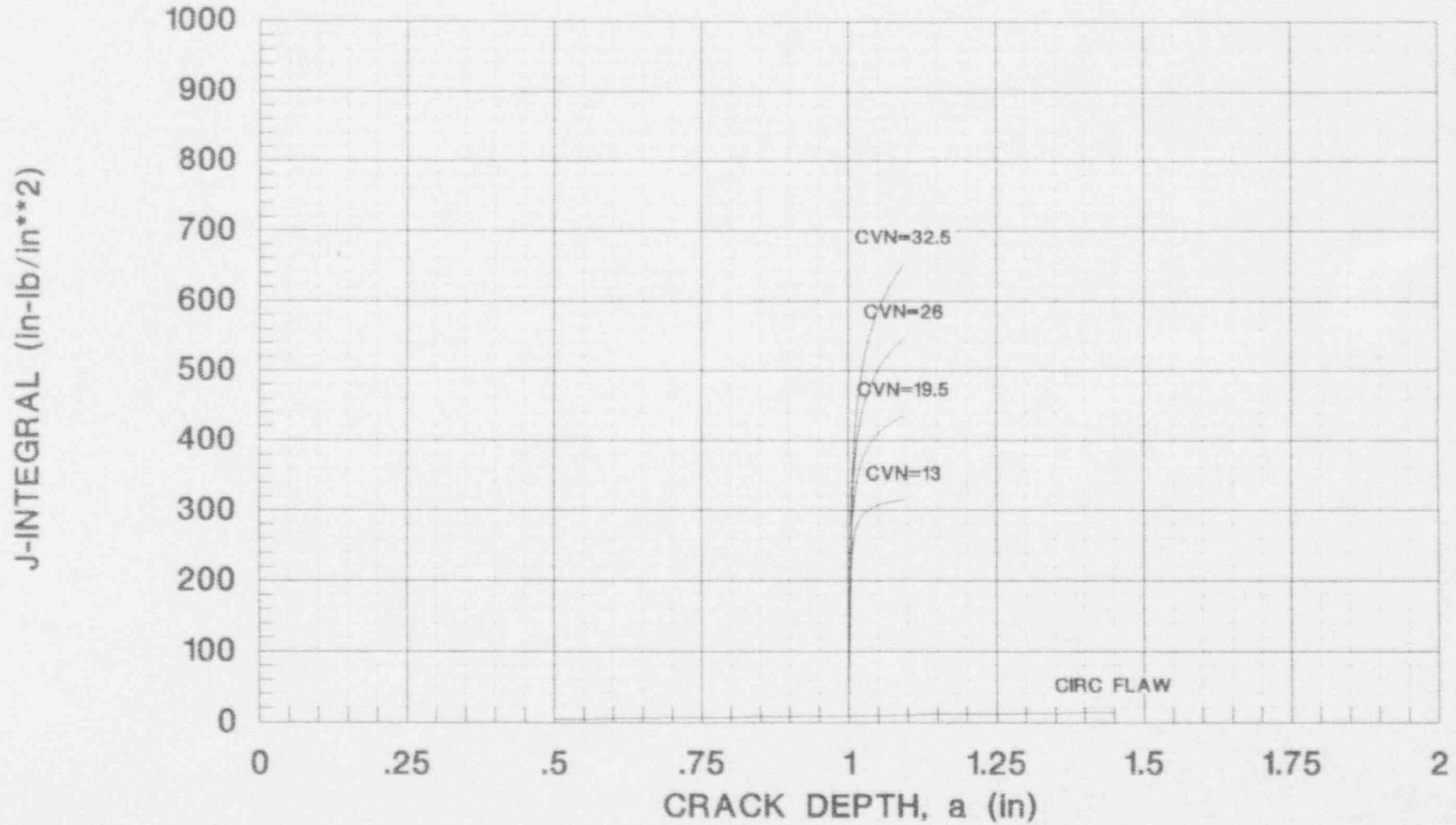

FIGURE 8.22A
J-INTEGRAL VS. CRACK DEPTH
FEEDWATER LINE BREAK
AXIAL FLAW ORIENTATION, LEVEL D, PLATE MATERIAL

VESSEL SIZE: NOMINAL ID = 182 In, BELTLINE THICKNESS = 9.06 In
FLAW GROWTH

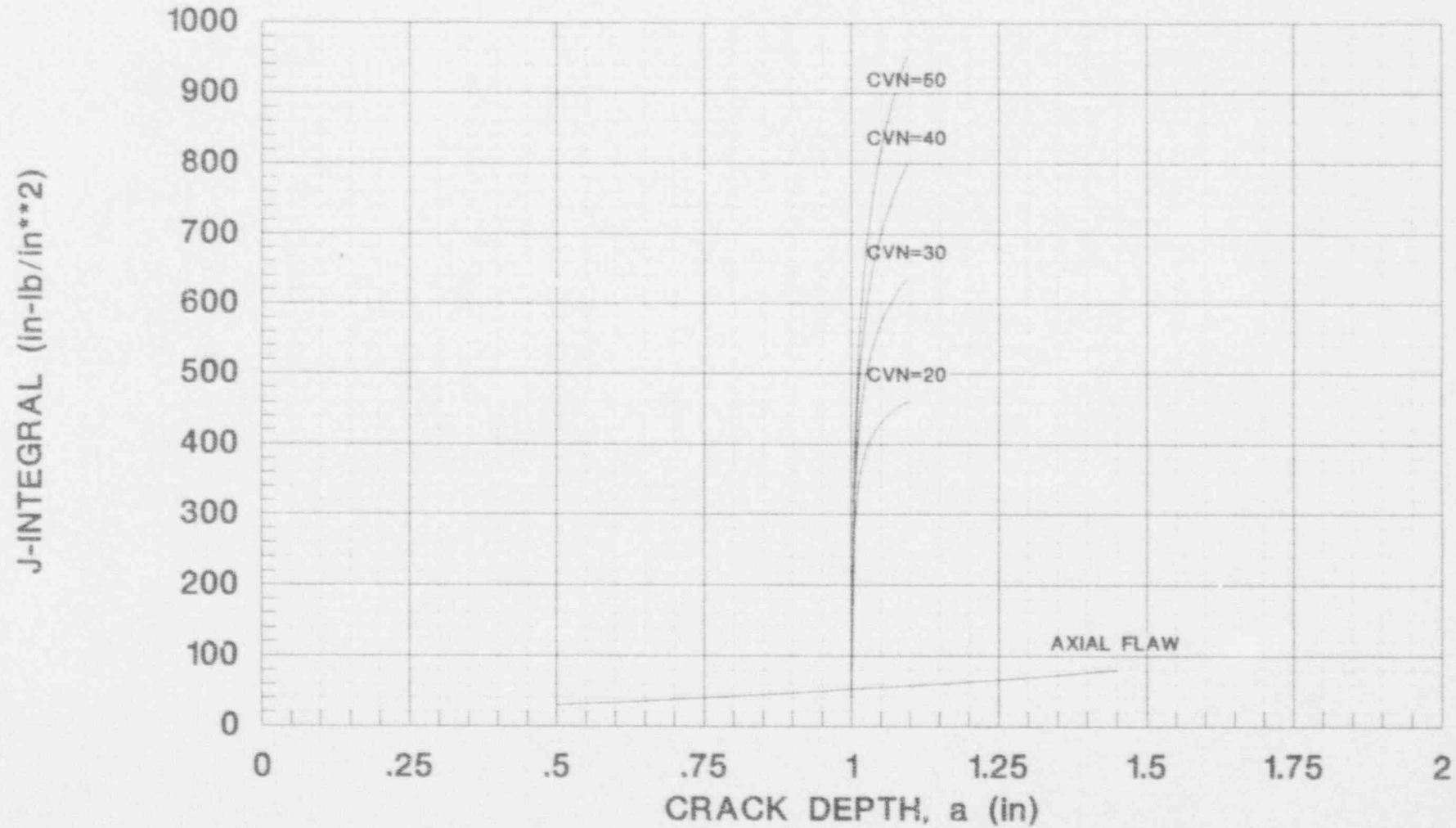

FIGURE 8.22B
J-INTEGRAL VS. CRACK DEPTH
FEEDWATER LINE BREAK
CIRC FLAW ORIENTATION, LEVEL D, PLATE MATERIAL

VESSEL SIZE: NOMINAL ID = 182 In, BELTLINE THICKNESS = 9.06 In
FLAW GROWTH

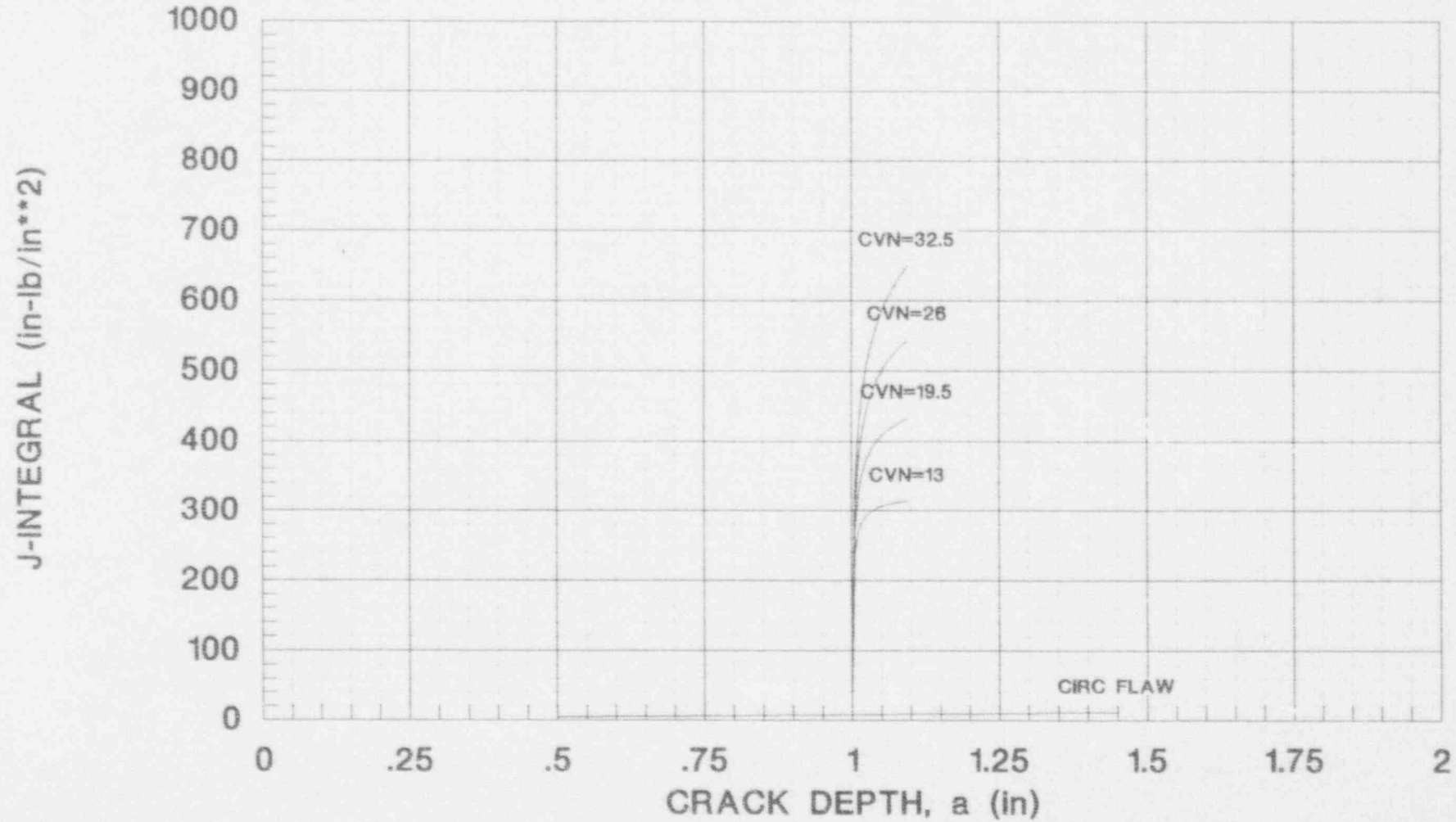

REFERENCES

1. Title 10 Code of Federal Regulations, Appendix G, Fracture Toughness Requirements, January 1992.

2. "Fracture Toughness and Surveillance Program Requirements," Federal Register, Vol. 38, No. 136, July 17, 1973 (19012 - 19016).

3. "Fracture Toughness Requirements for Light-Water Nuclear Power Reactors," Federal Register, Vol. 48, No. 104, May 27, 1983 (24008-24011).

4. Federal Register, Volume 45, No. 222, Friday, November 14, 1980, Proposed Rules, 10CFR Part 50.

5. ASTM E185-79, "Standard Practice for Conduction Surveillance Tests for Light-Water Cooled Nuclear Power Reactor Vessels," American Society for Testing and Materials, 1979 Annual Book of ASTM Standards, Part 45.

6. Reactor Vessel Structural Integrity, 10CFP50.54(f), (Generic Letter 92-01, Revision 1), NRR, dated March 6, 1992.

7. "Code Case N-512, Assessment of Reactor Vessels with Low Upper Shelf Charpy Energy Levels," Revision 12, ASME Boiler and Pressure Vessel Code Committee, Section XI Working Group on Flaw Evaluation, October 29, 1992. (Currently in Printing to be published as Code Case N-512, "Assessment of Reactor Vessels with Low Upper Shelf Charpy Impact Energy Levels," approved date March 11, 1993.)

8. "Development of Criteria for Assessment of Reactor Vessels with Low Upper Shelf Fracture Toughness," ASME Boiler and Pressure Vessel Code Committee, Section XI Working Group on Flaw Evaluation, December 1991.

9. U.S. NRC Regulatory Guide 1.99, Revision 2, Radiation Embrittlement of Reactor Vessel Materials, May 1988.

10. Branch Technical Position RSB 5-2, "Overpressurization Protection of Pressurized Water Reactors While Operating at Low Temperatures," Rev. 1, dated November 1988.

11. F. W. Stallman, F. B. Kam and B. J. Taylor, "PR-EDB: Power Reactor Embrittlement Data Base, Version 1," NUREG/CR-4816 (ORNL/TM-10328), Oak Ridge National Laboratory, Oak Ridge, TN, June 1990.

12. ASME Boiler & Pressure Vessel Code, Section III, Rules for Construction of Nuclear Plant Components.

13. "Evaluation of Upper Shelf Toughness Requirements for Reactor Pressure Vessels," Draft EPRI Report, Volume 1, Summary Report, March 1989, Electric Power Research Institute, Palo Alto, CA, March 1989.

14. "Evaluation of Upper Shelf Toughness Requirements for Reactor Pressure Vessels," Draft EPRI Report, Volume 2, Detailed Report, March 1989, Electric Power Research Institute, Palo Alto, CA, October 1989.

15. E. D. Eason and E. E. Nelson, "Improved Model for Predicting J-R Curves from Charpy Data, Phase I Final Report," NUREG/CR-5356 (MCS 890301), Modeling and Computing Services, Sunnyvale, CA, April 1989.

16. E.D. Eason, J. E. Wright and E. E. Nelson, "Multivariable Modeling of Pressure Vessel and Piping J-R Data," NUREG/CR-5729 (MCS 910401), Modeling and Computing Services, Newark, CA, May 1991.

17. R. Johnson, "Resolution of the Reactor Vessel Materials Toughness Safety Issue, Volumes 1 and 2", Nuclear Regulatory Commission Report NUREG 0744, 1982.

18. CE Report No. CEN-381-P, "Low Temperature Overpressurization Transient Pressure-Temperature Limit for Determination of Low Temperature Overpressure Protection Setpoints", Combustion Engineering, Inc., December 1988. (C-E Proprietary)

19. CE Report No. CEN-381-P Attachment 1-P, "Low Temperature Overpressure Protection Pressure-Temperature Limit Methodology Response to USNRC Inquiry", Combustion Engineering, Inc., August 1990. (C-E Proprietary)

APPENDIX A

Justification for the Use of Longitudinal Orientation Plate Upper Shelf Energy Data in the CEOG Equivalent Margins Analysis

Justification for the Use of Longitudinal Orientation Plate
Upper Shelf Energy Data in the CEOG Equivalent Margins Analysis

INTRODUCTION

The NRC Staff recently stated a concern regarding licensee compliance with the minimum Upper Shelf Energy (USE) requirements of 10CFR50 Appendix G, "Fracture Toughness Requirements". The request was made to address this issue by performing a generic bounding analysis which demonstrates equivalent margins of safety against fracture using the guidance provided by the ASME Code Section XI (Code Case N-512). The Combustion Engineering Owners Group (CEOG) submitted the results of its preliminary evaluation, CEN-604 dated November 1992, in which reactor vessel plates were determined to be the limiting material in the bounding analysis for the CEOG member reactor vessels. In this preliminary report, it was conservatively assumed that the postulated axial flaws should be analyzed using transverse orientation Charpy USE properties. In other words, the minimum plate toughness properties were used to analyze the maximum loadings.

The purpose of this report is to demonstrate that the transverse orientation USE properties should be used to analyze only the postulated circumferential flaws, whereas the longitudinal orientation USE properties should be used to analyze the postulated axial flaws. The following sections describe the manner in which reactor vessels were fabricated for CEOG member plants and how this was ascertained to be applicable to those reactor vessels.

ORIENTATION OF VESSEL PLATES

Reactor pressure vessels for CEOG members were fabricated at the ABB Combustion Engineering facilities in Chattanooga, Tennessee. A reactor vessel is made up of several shell courses, each of which was constructed by forming three plates and welding them together into a cylinder as shown in Figure 1. The circumferential and axial directions in the shell course are as shown. The circumferential direction is indicated to be coincident with

the direction of major rolling in the plate. The axial direction is shown perpendicular to the direction of major rolling.

Charpy impact specimens for ASME Code qualification were obtained from excess material from each plate as indicated in Figure 1. The orientation of the longitudinal and transverse Charpy specimens with respect to the shell course plate is shown in Figure 2. The major axis of the longitudinal Charpy specimen is parallel to the rolling direction; the major axis of the transverse specimen is perpendicular to the rolling direction. The root of the V-notch is perpendicular to the plate surface in both cases. The direction of crack front propagation is also indicated in Figure 2. The longitudinal Charpy specimens provide a measure of upper shelf toughness for cracking perpendicular to the rolling direction and parallel to the plate surface; i.e., in the axial direction shown in Figure 2. The transverse Charpy specimens provide a measure of upper shelf toughness for cracking parallel to the rolling direction and to the plate surface; i.e., in the circumferential direction shown in Figure 2.

APPLICABILITY TO CEOG MEMBER VESSELS

The preceding discussion concluded that USE data from longitudinal Charpy specimens is applicable to the analysis of a postulated axial flaw in a plate. The assumption was made that the direction of major rolling in the plate coincided with the circumferential direction is the reactor vessel shell course. The purpose of the following is to validate that assumption for the CEOG members' reactor pressure vessels listed in Table 1.

Fabrication records for each of the fifteen reactor vessels noted in Table 1 were researched to determine the relationship between the direction of major rolling for the plate and the circumferential direction in the reactor vessel beltline shell courses. The fabrication records consisted of shop drawings showing shell segment forming and test plate specimen layouts, material certification test reports, and plate material purchase orders. The major dimension of the plate coincided with the circumferential direction in the vessel shell and with the major rolling direction in the plate. (It should also be noted that rolling was used to attain the major plate dimension such that rolling direction and the greater plate length would logically

be coincident.) The test plate specimen layout drawing and the material test reports showed that the major axis of the longitudinal Charpy specimens was parallel to the plate rolling direction. Therefore, the fabrication records for each of the reactor vessels listed in Table 1 demonstrate that the vessel shell course plate and Charpy test specimens were oriented as shown in Figures 1 and 2.

CONCLUSIONS

1. Vessel beltline plates for CEOG member plants are oriented with their rolling direction parallel to the circumferential direction of the reactor vessel.
2. USE data obtained from longitudinally oriented Charpy specimens for those plates are applicable to the analysis of postulated axial flaws in the reactor vessel. USE data from transversely oriented Charpy specimens are applicable to the analysis of postulated circumferential flaws in the vessel.

TABLE A-1

Reactor Vessels for CEOG Member Utilities

Palisades

Ft. Calhoun

Calvert Cliffs Units 1 and 2

Maine Yankee

Millstone Unit 2

St. Lucie Units 1 and 2

San Onofre Units 2 and 3

Arkansas Nuclear One, Unit 2

Waterford Unit 3

Palo Verde Units 1, 2 and 3

FIGURE A-1
SHELL COURSE FORMING

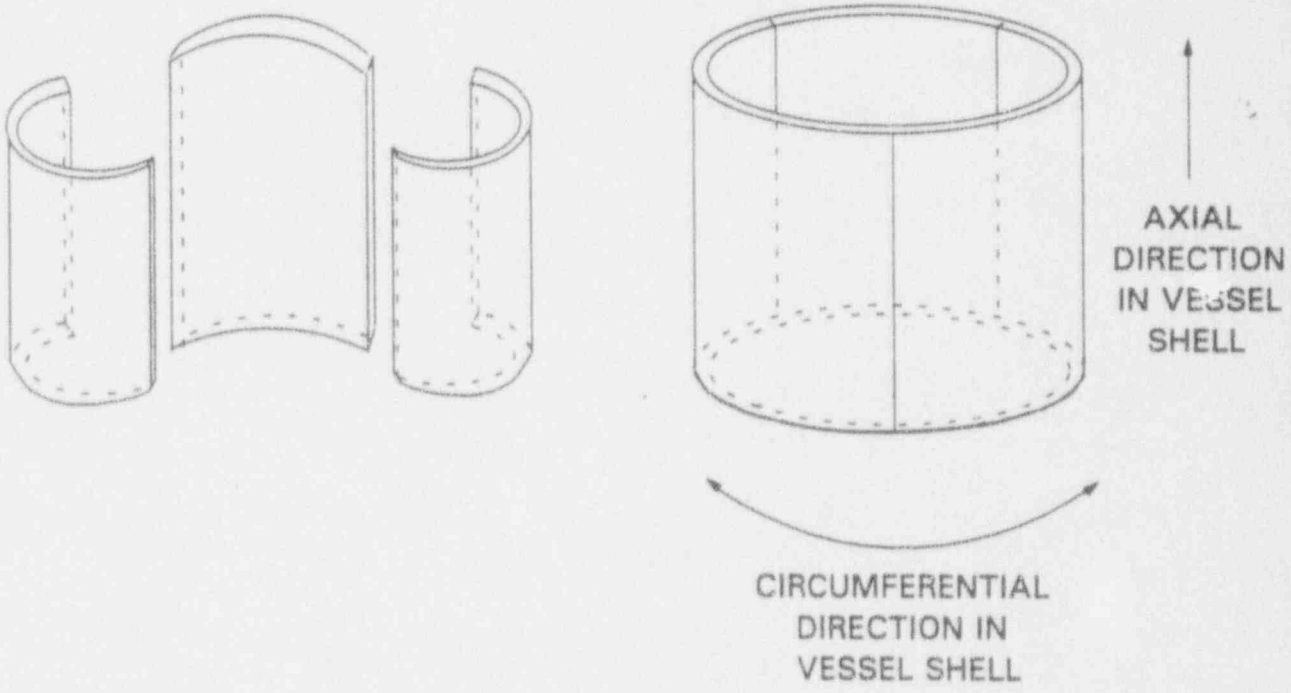

FIGURE A-2
TEST SPECIMEN ORIENTATION RELATIVE TO POSTULATED AXIAL AND CIRCUMFERENTIAL PLACES

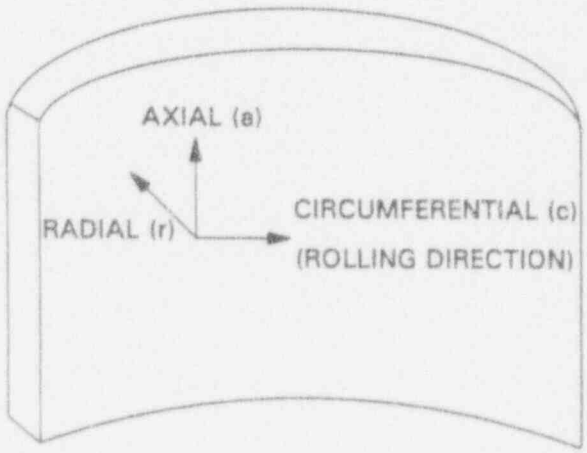

FORMED SHELL COURSE PLATE

LONGITUDINAL CHARPY SPECIMEN

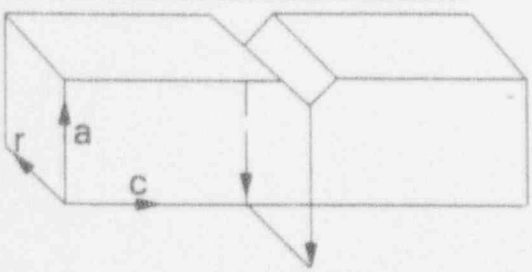

CRACK FRONT PROPAGATION AXIALLY

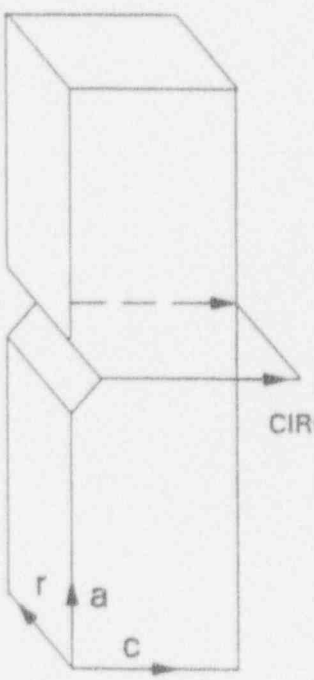

TRANSVERSE CHARPY SPECIMEN

CRACK FRONT PROPAGATION CIRCUMFERENTIALLY

APPENDIX B

Additional Steam Line Break Transient

Evaluation

INTRODUCTION

In addition to the steam line break (SLB) transient defined in Section 4.0, an additional SLB transient was provided for consideration. The inputs provided were both downcomer pressure and cold leg temperature as a function of time. No additional information pertaining to the system conditions was requested or provided. Upon review of the transient profile, it was concluded that the initial cooldown rate associated with the steam generator depressurization was greater than the analyzed cooldown rate. Consequently, this transient was evaluated within the scope of the CEOG Task 749 Phase 2 effort.

TRANSIENT PROFILE

The transient profile provided for evaluation was linearized and digitized and is presented in tabular form below and in graphical form in Figure B-1.

STEAM LINE BREAK PRESSURE AND TEMPERATURE TRANSIENT DATA

Time (sec)	Pressure (psia)	Temperature (F)
0	2250	535
250	156	240
350	312	320
450	500	310
600	400	305
910	2400	300
1500	2400	290

EVALUATION

The SLB transient described above would be classified as either a Level C or D transient. Lacking specific information regarding the break size, the transient was evaluated against the

Level C criteria in order to assure a conservative analysis. The analysis methodology is described in detail in Section 6. This evaluation was performed using the limiting reactor vessel geometry corresponding to an inside radius of 86.96 inches.

The transient profile depicts a rapid cooldown to a relatively low temperature followed by partial temperature recovery and subsequent repressurization. To evaluate this transient throughout its duration, the assumption that the material under consideration will remain on the upper shelf was made. Given CEOG reactor vessel material properties, this transient would likely result in material temperatures below the upper-shelf which would require further investigation to assure the employed methodology would be appropriate, as the methodology pertains to upper-shelf behavior.

RESULTS

The results of the transient evaluation are provided in Figures B-1 and B-2. These figures depict the applied J-Integral at 0.1 inch flaw extension throughout the duration of the SLB transient along with the J-Integral resistance of the material (J_d). This information was developed for both axial and circumferential flaw orientations.

Review of these figures show that the applied J-Integral values are sufficiently less than J_d given 0.1 inch ductile flaw extension meeting the first criteria necessary to show acceptability for the analyzed Charpy USE values.

Flaw stability, the second criteria, was assessed using the graphical procedure described in the report. Figures B-3 and B-4 depict the applied J-Integral for various crack depths versus J_d at the limiting time point during the transient for axial and circumferential flaws, respectively. The limiting time point varied as a function of Charpy USE, therefore the timepoint corresponding to the lowest analyzed USE value was utilized. This occurred at 910 seconds and 260 seconds for the axial and circumferential flaw, respectively. Review of the figures shows the slope of the applied J-Integral to be less than the slope of the J_d at the point of intersection. Hence, flaw stability has been verified.

DISCUSSION

The results of the evaluation show that the material is capable of providing equivalent margins of safety for Charpy USE values as low as 20 ft-lb and 13 ft-lb for transverse and longitudinal orientation specimens, respectively. These results are consistent with the results obtained for the Steam Line Break transient described in Section 4.0. Since the results of this analysis did not alter the results and conclusions of the report, the original Steam Line Break transient defined in Section 4.0 was not revised. In addition, these results provide additional information which support the conclusion that low Charpy USE values can be shown to provide adequate margins of safety from ductile flaw growth.

Figure B.1
Level C Transient
Steam Line Break with Repressurization

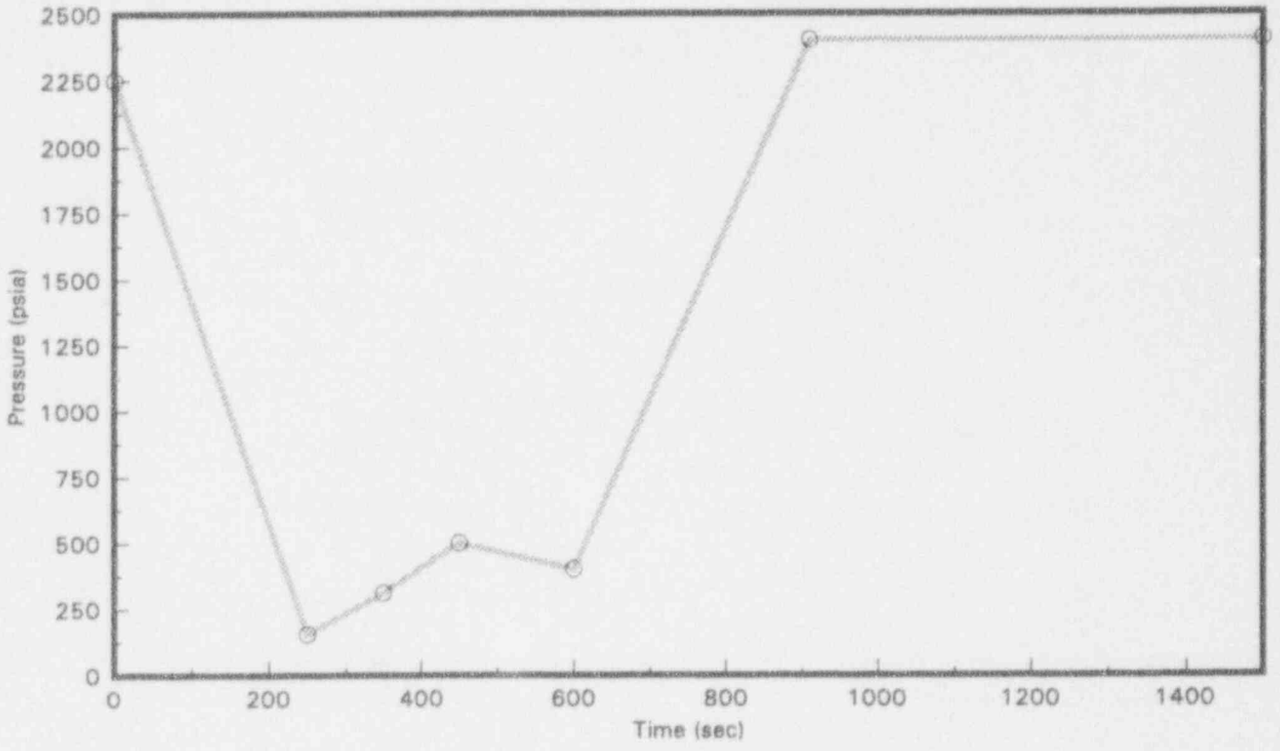

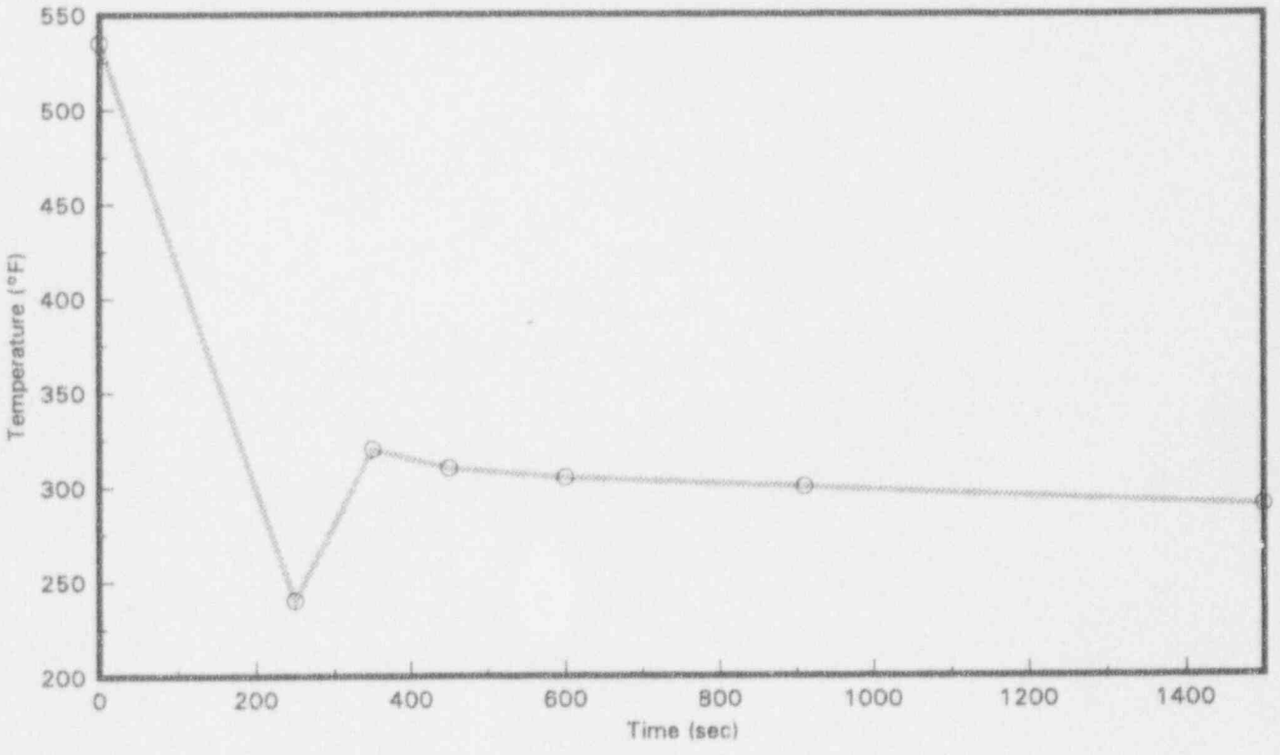

FIGURE B.2
J-INTEGRAL VS. TIME
STEAM LINE BREAK
AXIAL FLAW ORIENTATION, LEVEL C, PLATE MATERIAL

VESSEL SIZE: NOMINAL ID = 172 in, CLAD THICKNESS = 0.3125 in
BELTLINE THICKNESS = 8.625 in

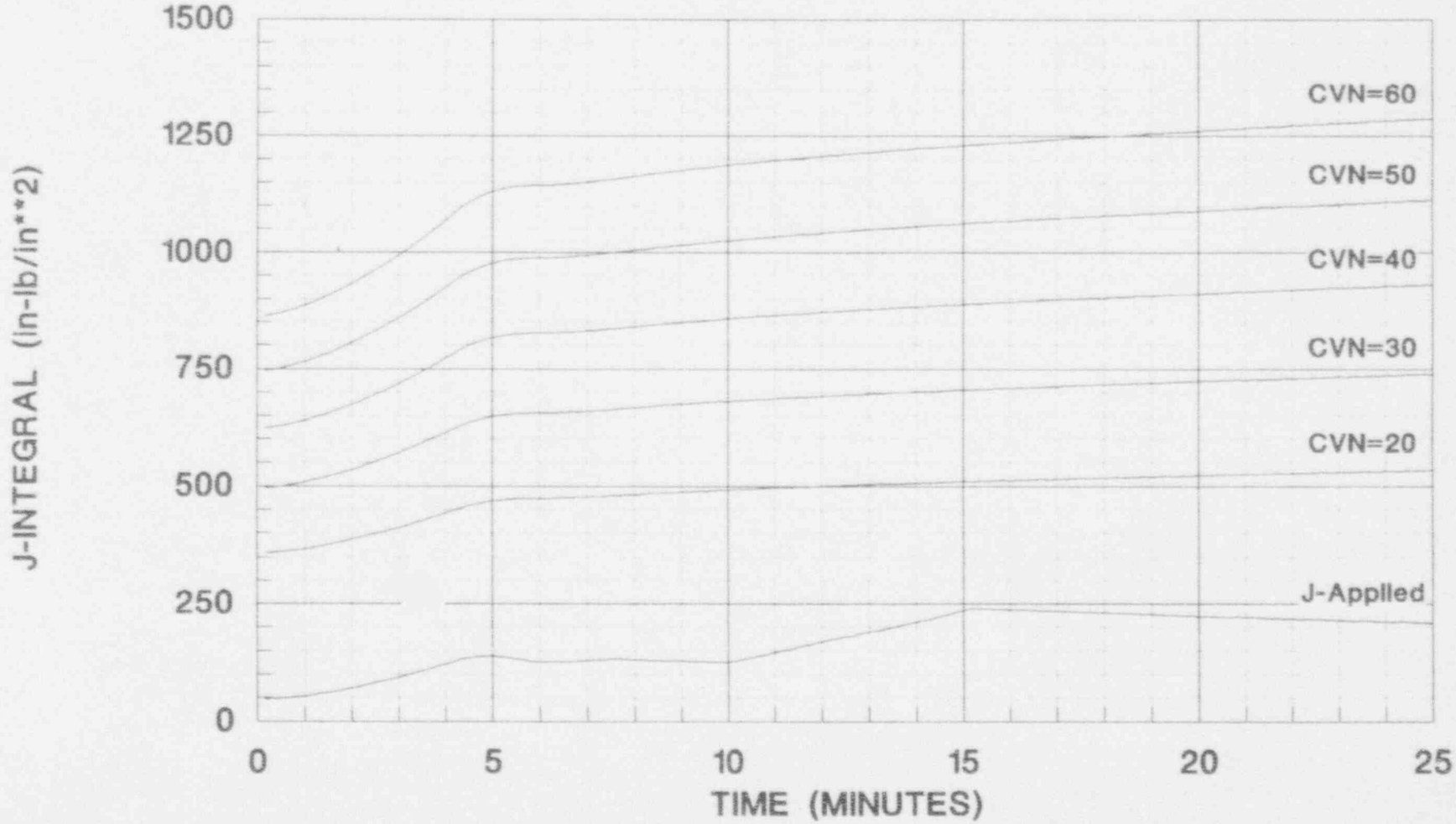

FIGURE B.3
J-INTEGRAL VS. TIME
STEAM LINE BREAK
CIRC. FLAW ORIENTATION, LEVEL C, PLATE MATERIAL

VESSEL SIZE: NOMINAL ID = 172 In, CLAD THICKNESS = 0.3125 In
BELTLINE THICKNESS = 8.625 In

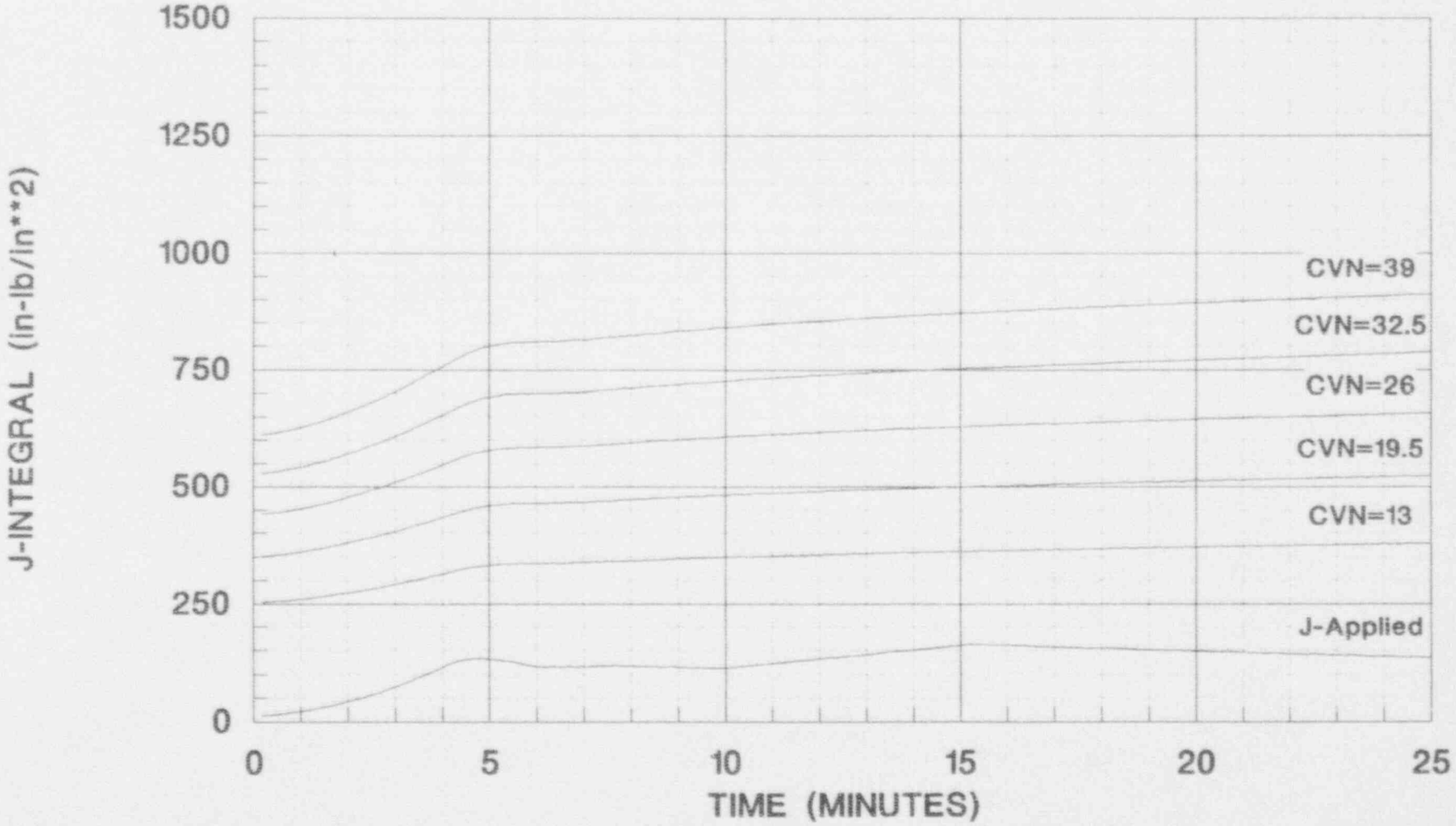

FIGURE B.4

J-INTEGRAL VS. CRACK DEPTH
STEAM LINE BREAK
AXIAL FLAW ORIENTATION, LEVEL C, PLATE MATERIAL

VESSEL SIZE: NOMINAL ID = 172 In, BELTLINE THICKNESS = 8.625 In
FLAW GROWTH

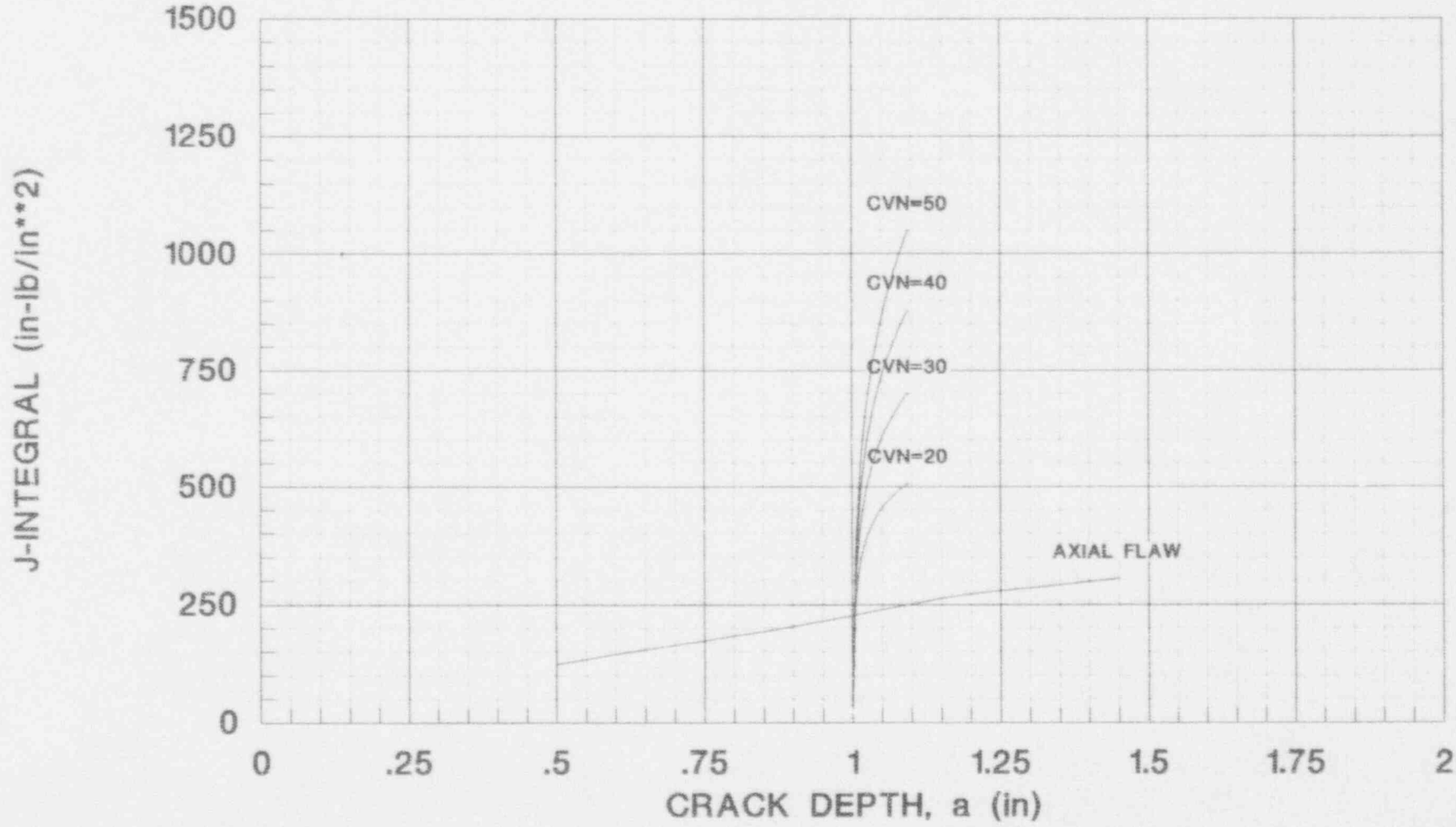

FIGURE B.5
J-INTEGRAL VS. CRACK DEPTH
STEAM LINE BREAK
CIRC. FLAW ORIENTATION, LEVEL C, PLATE MATERIAL

VESSEL SIZE: NOMINAL ID = 172 in, BELTLINE THICKNESS = 8.625 in
FLAW GROWTH

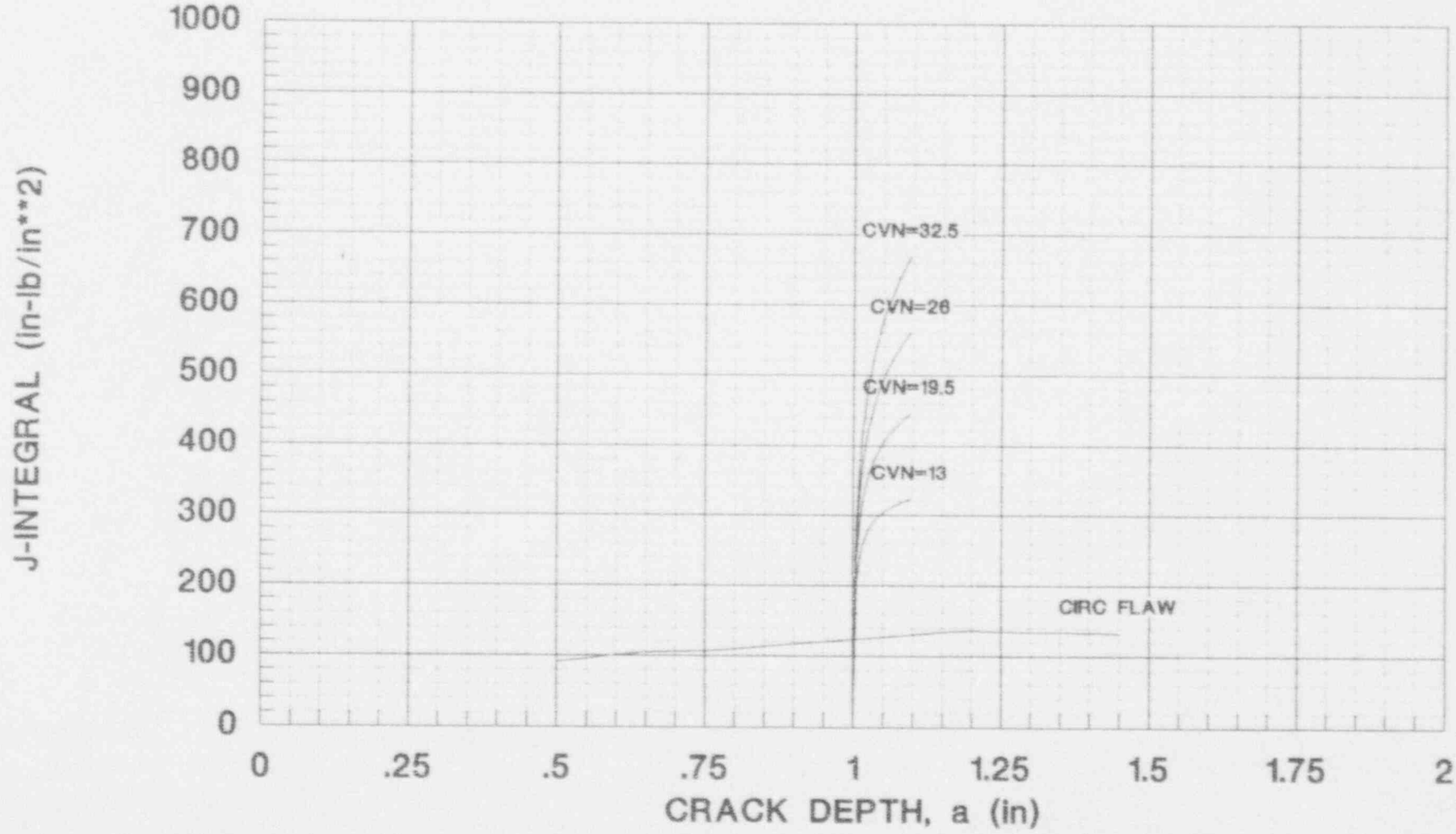

LIC-93-0270
Enclosure 2

Equivalent Margins Assessment of Low Charpy Upper-Shelf Energy Longitudinal Welds for the Fort Calhoun Reactor Vessel

O-MECH-ER-013, Revision 00

October 1993